Synchronisation and stability in nonautonomous oscillatory systems

Maxime Lucas, MSc

DEPARTMENT OF PHYSICS
LANCASTER UNIVERSITY
LANCASTER, UK

DEPARTMENT OF
PHYSICS AND ASTRONOMY
UNIVERSITY OF FLORENCE
FLORENCE, ITALY

October 2018

Acknowledgements

First and foremost, I would like to warmly thank my two supervisors, Prof. Aneta Stefanovska and Prof. Duccio Fanelli, for their constant support and for allowing me to undertake this adventure. You have guided me along the journey, and allowed me to grow as a scientist. Thank you, Aneta, for your passion, your exemplary perseverance, and for introducing me to the worlds of biological oscillations and nonautonomicity. Thank you, Duccio, for your passion, your availability, and your kindness.

Thanks to Prof. Peter V. E. McClintock for being there whenever was necessary, and for introducing me to Lancaster Helium Ltd. Thanks to Dr Julian Newman for our rich discussions, our new born collaboration, and his patient proofreading of this text. Thanks to Dr Martin Rasmussen for allowing me to visit him in London to learn about nonautonomous dynamical systems. Thanks to Prof. Arkady Pikovsky for the very insightful discussions about synchronisation, and for his inspiring presence. Thanks to Dr Yevhen Suprunenko for his help and the interesting discussions.

I would also like to my officemates and friends for our time together in and out of the office – in Lancaster – Ola, Federico, Bastian, Jean, Will, Valentina, Gemma, Miroslav, Yunus, Boštjan, Carlo, Mahmoud, Hala, Sultan, and Joe – and in Florence – Pau, Giulia, Leonardo, Niccolò, Sara, Ihusan, Francesca, and Giovanna. I would also like to very warmly thank all the other COSMOS students and PIs for making these three years stimulating and enjoyable. Thanks to Pierre and Francesca for proofreading parts of this thesis. Big thanks to my friends from back home for being there in the good and less good moments, even though I was often physically far away. Finally, thank you to all the wonderful people I have met and spent time with along the way and could not name here – I am sure you will recognise yourselves. I am proud to count you in my life.

Last but not least, I would like to thank my family for making me who I am and let them know I love them, no matter what. Knowing you have a united family there for you whenever you need them gives you the strength to face anything. Je pense à vous Mams, Micout, et Lul. Finally, thank you to our hairy companions Kali and Kajou for welcoming me home every time with such joy!

Declaration

This thesis is my original work and has not been submitted, in whole or in part, for a degree at this or any other university. Nor does it contain, to the best of my knowledge and belief, any material published or written by another person, except as acknowledged in the text. All quotations have been distinguished by quotation marks and the sources of information specifically acknowledged. This thesis is submitted for the degree of Doctor of Philosophy undertaken at Lancaster University (Lancaster, UK) and at the Università degli Studi di Firenze (Florence, Italy).

List of publications

Parts of the work presented in this thesis have been published in the following papers:

- LUCAS M., FANELLI D. & STEFANOVSKA A. Nonautonomous driving induces stability in network of identical oscillators. *Phys. Rev. E* **99**, 012309 (2019). (Work from Chapter 6).

- LUCAS M., FANELLI D., CARLETTI T. & PETIT J. Desynchronization induced by time-varying network. *Europhys. Lett.* **121**, 50008 (2018) (Work from Chapter 7).

- LUCAS M., NEWMAN J. & STEFANOVSKA A. Stabilization of dynamics of oscillatory systems by nonautonomous perturbation. *Phys. Rev. E* **97**, 042209 (2018) (Work from Chapter 4).

In addition, the following manuscript is currently under review:

- NEWMAN J., LUCAS M. & STEFANOVSKA A. *Limitations of the asymptotic approach to dynamics* submitted, preprint at arXiv:1810.04071. (2018) (Work from Chapter 5).

This work has also been presented at the following scientific conferences and workshops:

Oral presentations at conferences, workshops, and school

- LUCAS M. Synchronisation and stability in coupled oscillators with time-varying parameters. *COSMOS meeting. 24–27 September 2018. Dolenjske Toplice, Slovenia.*

- LUCAS M., FANELLI D., & STEFANOVSKA A. Synchronisation in coupled oscillators with time-varying parameters. *Workshop on Long-range Interactions and Synchronization. 28–31 June 2018. São Paulo, Brazil.*

- LUCAS M., FANELLI D., & STEFANOVSKA A. Stabilisation of dynamics of oscillatory systems by nonautonomous perturbation. *COSMOS toolbox laboratory. 8–13 October 2017. Brijuni, Croatia.*

- LUCAS M. & STEFANOVSKA A. Nonautonomous perturbation stabilises dynamics of complex system. *XXXVII Dynamics Days Europe. 5–9 June 2017. Szeged, Hungary.*

- LUCAS M., & STEFANOVSKA A. Nonautonomous perturbation stabilises dynamics of complex system. *COSMOS retreat. 26–31 March 2017. Wittenberg, Germany.*

- LUCAS M.. Time series: noise or determinism? *COSMOS workshop 2. 11–16 December 2016. Amsterdam, Netherlands.*

- LUCAS M., SUPRUNENKO Y., & STEFANOVSKA A. Non-autonomous limit-cycle oscillator. *COSMOS school 2. 27 June–6 July. 2016. Aberdeen, UK.*

List of publications

Invited seminars

- Lucas M.. Synchronisation in coupled oscillators with time-varying parameters. *Université Libre de Bruxelles. 3 April 2018. Brussels, Belgium.*

- Lucas M., Newman J., & Stefanovska A. Stabilisation of dynamics of oscillatory systems by non-autonomous perturbation. *University of Florence. 7 December 2017. Florence, Italy.*

Poster presentations

- Lucas M., Fanelli D., & Stefanovska A. Effect of time-varying parameters on stability in coupled oscillators systems. *Analysis and Modelling of Complex Oscillatory Systems (AMCOS). 19–23 March 2018. Barcelona, Spain.*

- Lucas M., Suprunenko Y., & Stefanovska A. How to characterise non-autonomous dynamics? *STATPHYS26. 18–22 July 2016. Lyon, France.*

- Lucas M. & Stefanovska A. Why do we need non-autonomous models and methods? *International conference on biological oscillations (ESGCO 2016). 10–14 April 2016. Lancaster, UK.*

- Lucas M. & Stefanovska A.. Living systems and chronotaxicity. *Lancaster University Christmas Conference. 15 December 2015. Lancaster, UK.*

Abstract

Many natural and artificial systems can be modelled by ensembles of coupled oscillators. These types of systems can exhibit various synchronisation phenomena, where the interaction between the oscillators leads them to some kind of coherent behaviour, despite heterogeneities in the system. Moreover, many such systems are subject to a time-variable environment which effectively drives them. Many examples can be found in living systems, e.g., the dynamics of a cell is strongly dependent on the ever-changing intra- and extra-cellular ionic concentrations.

Motivated by these considerations, this thesis investigates the effect of time-varying parameters on synchronisation and stability in ensembles of coupled oscillators. Time-variability is a crucial ingredient of the dynamics of many real-life systems, and interest in it is only recently starting to grow. Such systems are in general described by nonautonomous equations, which are hard to treat in general. This present work aims at answering questions such as: Can time-variability be detrimental/beneficial to synchronisation? If so, under which conditions? Can time-variability seed new dynamical phenomena? How can one best treat nonautonomous systems?

The systems studied can be divided into two categories. First, the effect of a driving oscillator with a time-varying frequency is investigated. It is shown that increasing the amplitude of the frequency modulation can increase the size of the stability region in parameter space, under general assumptions. Short-term dynamics and stability properties are also investigated, and their dynamics is shown to be of importance. Second, the effect of time-varying couplings between the oscillators is considered. This is shown to be able to make the synchronous state unstable and yield oscillation death.

Overall, the thesis illustrates that time-variability can be either beneficial or detrimental to synchronous dynamics, and investigates in detail and gives insight about cases of both. It argues towards the general fact that short-term dynamics is often crucial to a physically relevant understanding of nonautonomous systems.

Glossary, abbreviations, and notations

Glossary and abbreviations

Adjacency matrix Matrix that encodes the coupling of pair of oscillators in a network

Arnold tongue Region of synchronisation in parameter space

Asymptotic Lyapunov exponent (ALE) Lyapunov exponent defined in the limit $t \to \infty$

Autonomous dynamical system Dynamical system of which the evolution does *not* depend explicitly on time

Chronotaxic system Nonautonomous system with time-varying frequency and amplitude, yet that is stable against external perturbations

Circadian rhythms Rhythms of about 24 hours, involved in many biological oscillatory processes

Finite-time Lyapunov exponent (FTLE) Lyapunov exponent defined over a finite time (long or short)

Frequency mismatch Frequency difference between a driving and a driven oscillator

Instantaneous Lyapunov exponent (ILE) Lyapunov exponent defined over an infinitesimal time

Limit-cycle (LC) Mathematical realisation of a self-sustained oscillator

Nonautonomous dynamical system Dynamical system of which the evolution does depend explicitly on time

Ordinary differential equation (ODE) Mathematical framework used to model a dynamical system

Phase oscillator Oscillator described only by a phase

Quasiperiodic (QP) A quasiperiodic function is a function of two independent phases

Runge-Kutta 4 (RK4) Fourth order Runge-Kutta scheme for numerical integration of ODEs

Self-sustained oscillator (SSO) System that oscillates even without external influence

Suprachiasmatic neurons (SCN) Neurons in the brain responsible for the synchronisation of circadian rhythms in the body

Synchronisation Adjustment of rhythms of interacting oscillators

Watanabe-Strogatz (WS) Type of network with identical phase oscillators

Wavelet transform (WT) Algorithm for time-frequency analysis of a time series

Notations

θ	Phase
ψ	Phase difference
$\lambda^{(\infty)}$	Asymptotic Lyapunov exponent
λ	Lyapunov exponent
$\lambda(t)$	Instantaneous Lyapunov exponent
$\mathbf{x}$	Vector
$\mathbf{M}$	Matrix
$\mathbf{J}$	Jacobian matrix
$\mathbf{A}$	Adjacency matrix
$\mathbf{L}$	Laplacian matrix
$\xi(t)$	Noise

Contents

List of figures

List of figures

List of tables

1. Introduction

The human body is an incredibly complex – yet beautifully working – machine. Let us try, just for a minute, to imagine the thousands of structures and processes, at all scales, working together to keep the body alive and well. At all scales in space: from the heart cells beating simultaneously to pump blood and bring nutrients and oxygen to the entire body, and the neurons in the brain firing in a coordinated way so as to think and direct the limbs, to the heart, the brain, and the lungs working together to maintain essential functions. And at all scales in time: from the fast beating of the heart, to the daily rhythms of body temperature, and the ovarian monthly cycles. All these processes, and many more, work in an extraordinarily coordinated way for life to be maintained. As if that was not an exceptional enough feat, they do so in the face of ever-changing external conditions: every living person has had their heart beat too fast out of excitement, or beat slower when asleep at night – and yet is still alive. This example illustrates the two main elements of this thesis: the orderliness in time of interacting oscillatory units – synchronisation – and their maintaining stability, notwithstanding the time-variable influence of the environment.

Order is often found in nature, although the second law of thermodynamics seems to indicate that nature should tend to a state of greater disorder. This seems like a contradiction and has puzzled scientists for a long time, such as the eminent E. Schrödinger in his book "What is life?" [138]. Structures arise from the complex interaction of many units, and not only in the living body. As S. H. Strogatz beautifully writes it [146]: "At the heart of the universe is a steady, insistent beat: the sound of cycles in sync. It pervades nature at every scale from the nucleus to the cosmos." Investigating these questions in the 20th century, I. Prigogine, with his work on self-organisation in dissipative structures [109], and H. Haken, with synergetics [52], were probably among the pioneers

of what is now called "complexity science".

Synchronisation is the timely order that arises from interacting oscillatory units; it is the type of order considered in this thesis. Rhythms, or equivalently oscillatory dynamics, abound in nature [45, 46]. Theoretical biologist A. Winfree started to model processes such as circadian rhythms mathematically as an ensemble of coupled oscillators [166]. However, his model was hard to treat mathematically. It was only in 1975, when Y. Kuramoto simplified it [80], that the field attracted more attention and inspired many more studies [1, 5, 136]. The model was simple and mathematically tractable, and yet displayed the emergence of order: synchronisation of all coupled phase oscillators. What is now known as the "Kuramoto model" became a paradigm in the study of synchronisation and inspired a whole field of research. Synchronisation has been applied to physics, but also to chemistry, biology, medicine, neurosciences, engineering, and many other fields. Examples include diverse aspects of nature [32, 45, 46], circadian rhythms [40, 50, 90], cardio-respiratory dynamics [22, 98, 149], metabolic oscillations [85], the brain [153, 161], and climate dynamics [33, 42]. Synchronous dynamics can be crucially needed, such as for the beating of the heart, but can also be severely detrimental, such as in epileptic seizures [4, 101]. Phenomena such as ageing [62] and anæstesia [143] are known to alter synchrony of dynamics. The early globally-coupled-oscillators setting of Kuramoto was later extended to *complex networks* of oscillators [5], representing structures also found in, e.g., sociology, the brain, or the internet. Coupled oscillators exhibiting synchronisation are the first ingredient of the systems in this thesis.

Most of the literature to date effectively models systems as *thermodynamically closed*, i.e. using *autonomous* models [147]. By definition, an autonomous dynamical system obeys a time-independent evolution law, and its future state only depends on its own present state. Hence, in such a model, it is assumed that all variables needed to determine the state of the system are known, and any external influence is negligible. Very often, however, systems in nature do depend on the interaction with their environment. Strictly speaking, the only truly autonomous system is the entire universe. Finally, experimentalists often do not have access to measure all processes at hand, but can only measure a few of them. Nonetheless, autonomous modelling has proven successful since its advent first with I. Newton and then its crucial developments with H. Poincaré and A. Lyapunov. Newton's

gravitational force model is an example of a time-independent law. In fact, autonomous dynamical system theory was originally developed by Newton and later Poincaré with celestial mechanics in mind. In a sense, autonomous modelling is related to the approach of *reductionism.* Starting in ancient Greece with Democritus and his atomist theory, reductionism in science is the approach that seeks to understand a whole system by understanding its elementary subparts. Taking this approach as far as possible led to the development of the successful field of particle physics. However, this approach often does not work in complex systems, where "the whole is more than the sum of its parts" and a more *holistic* approach needs to be applied.

Many systems in nature are thermodynamically *open*: they exchange energy and matter with their environment. This is especially true of living systems: how long would one survive without eating and breathing? Such systems are modelled mathematically by *nonautonomous* dynamical systems [72], i.e. dynamical systems which obey a time-dependent evolution law. To determine the future state of the system, not only is its own current state needed, but so is the current time. For example, the firing of a neuron and the metabolism of a cell both strongly depend on the intra- and extra-cellular ionic concentrations [121]. These concentrations are ever-changing and depend on multiple other complex processes, and yet neurons keep firing. The heart too (fortunately!) maintains its function – beating – but is constantly adapting its frequency to external and internal events. The theory of nonautonomous dynamical systems started being developed only in the last two decades by the mathematics community [72], but its importance is only recently starting to be recognised in other communities, such as in physics. Its importance is especially clear for the life sciences [40, 73, 85], but nonautonomous theory is also being applied in other fields such as climate dynamics [26, 33, 37, 42, 118], and fluid dynamics [55, 100, 134, 154, 163]. Such time-variability implies that, often, macroscopic properties such as synchrony or stability will also be time-varying [14, 20]. This was observed, e.g., for fish communities in Japan [160]. It is then clear that a finite-time approach is crucially needed in such cases, and especially in nonautonomous systems. Nonautonomicity, i.e. for the systems considered to be nonautonomous, is the second ingredient in this thesis.

Two main realisations of nonautonomicity are considered in this thesis, both motivated

by clear experimental evidence of their presence in real systems.

First, evidence shows that many oscillatory systems in nature have time-varying frequencies. This is also common knowledge. The heart is a striking example of a stable system exhibiting an ever-changing frequency. Evidence of this type of oscillations has also been found in other examples including in cell metabolism [85], cardio-respiratory dynamics [22, 98, 149], and the brain [153, 161]. The stable yet time-varying oscillations of such systems seems to be the result of a mechanism of great importance in the maintaining of life. For this reason, systems with the aforementioned properties were coined *chronotaxic* [149–151], and their stability started to be investigated. Time-series analysis methods have also been developed to resolve in time the dynamical characteristics of time-varying-frequency oscillators (e.g., wavelet-based spectrum, coherence and bispectrum [29] as well as Bayesian inference of coupling functions [142]) rather than analyse them in a statistical sense (e.g. calculating power-spectrum density) and thereby miss noteworthy time-dependent dynamical features. Part of the work presented here was initiated with a view to building on some of these developments.

Second, time-varying networks [57, 58], i.e. networks for which the topology changes over time, are ubiquitous. Examples include the network of social interactions – people make new friends – the internet – new pages are created and link to each other – or scientific collaborations – new collaborations start while others finish with the end of a common project. Time-varying networks, sometimes also called temporal networks, is a rapidly growing field, and yet, to date, little is known about synchronisation on this type of network setting.

This thesis focuses on the two aforementioned cases of time-variability: time-varying driving frequency, and time-varying network topology. Can time-variability be detrimental/beneficial to synchronisation? If so, under which conditions? Can time-variability seed new dynamical phenomena? How can one best treat nonautonomous systems? Those are the type of questions this thesis aims to answer.

1.1. Outline of the thesis

Chapter 2 introduces the theoretical concepts and tools used in – and needed for the understanding of – the subsequent chapters of the thesis. General concepts of dynamical systems and stability are presented, as well as a review of the relevant literature about synchronisation in networks of oscillators.

Chapter 3 investigates a quasiperiodically forced nonlinear oscillator. The various dynamical regimes are described and characterised, over parameter space. In this chapter, we confirm results obtained for similar systems in the literature. This chapter serves as a complement to chapter 2.

Chapter 4 introduces time-varying-frequency driving, in a pair of unidirectionally coupled oscillators. Stability of the driven oscillator, and synchronisation to the driving oscillator, are investigated via long- and short-term Lyapunov exponents. The growth of the stability region in parameter space with the frequency modulation amplitude is established, and explained by the apparition of a regime of intermittent synchronisation.

Chapter 5 investigates a one-dimensional nonautonomous phase equation, generalising the system and the results of chapter 4. That system is then used to illustrate the limitations of the traditional asymptotic approach to stability, and how it can differ from a more physically relevant long-but-finite-time approach.

Chapter 6 considers a model that is a direct generalisation of that in chapter 4 to a network of identical oscillators driven by a common external driving with a time-varying frequency. The stability of the synchronous solution is assessed. In the case of attractive network couplings, results are a direct generalisation of those in chapter 4. In the case of repulsive network couplings, stability also depends on the topology, and strategies based on topological changes and time-variability are proposed to stabilise the system.

Chapter 7 investigates the stability of the synchronous state in a network of nonlinear oscillators where the network connections can change over time. It is shown that the time-variability in the network topology can induce the instability of synchrony, and even lead to oscillation death.

Finally, chapter 8 summarises the work presented in this thesis and discusses possible directions for future research.

2. Theoretical background

In this chapter, we introduce concepts, terminology, and results from the literature that are relevant to the understanding and self-consistency of the thesis. This chapter is not intended as an exhaustive presentation of the topics considered, and the interested reader will be referred to the relevant literature for more details.

The chapter is organised as follows. Section 2.1 introduces autonomous and nonautonomous dynamical systems, as well as related concepts. In particular, self-sustained oscillators are introduced, which will serve as the basic dynamical unit for the whole thesis. Then, Sec. 2.2 introduces the concept of stability of a dynamical system, together with Lyapunov and Floquet exponents, and the numerical methods to compute them. The first two sections allow Sec. 2.3 to introduce synchronisation, the main topic of the thesis. Finally, Sec. 2.4 introduces networks of oscillators and provides additional background information about synchronisation in such networks, including relevant results from the literature.

This chapter is heavily based on [5, 72, 125, 127, 136, 146]. More specifically, the interested reader is referred to: [147] for autonomous dynamical systems and their stability, [72] for nonautonomous dynamical systems theory and their stability, [125] for Lyapunov exponents, [127] for synchronisation in general, and finally [5, 136] for synchronisation more specifically in complex networks.

2.1. Dynamical systems

Dynamical systems theory studies the evolution over time of the state of a system under a given law. For a d-dimensional system, the evolution of state $\mathbf{x}$ is typically formalised

by a set of *ordinary differential equations* (ODEs)

$$\dot{\mathbf{x}} = \mathbf{f}(\mathbf{x}), \tag{2.1}$$

where $\mathbf{x}$ is a d-dimensional vector, $\mathbf{f}$ is the constant function encoding the evolution law, and the dot denotes the time derivative, $\dot{\mathbf{x}} \equiv \frac{\mathrm{d}\mathbf{x}}{\mathrm{d}t}$. Here, and throughout the text, we consider time as a *continuous* variable. We thus only consider *continuous dynamical systems*, which we will simply refer to as dynamical systems. Discrete dynamical systems, for which time is a discrete variable, are described by difference equations. Finally, we only consider *deterministic* systems, for which no randomness is part of the evolution, as opposed to, e.g., random dynamical systems.

In Eq. (2.1), the state of the system at future time t only depends on its evolution law and its current state. The evolution law is constant in time: it is an *autonomous* dynamical system. Newton's law of gravitation is a physical example of such a law: given two masses at a given distance, Newton's law states that the attraction between the two has been, is, and always will be the same. This assumption of *time-homogeneity* is also made for most fundamental forces in physics.

For future use, we now briefly define a few standard concepts. The *state space* of system (2.1) is the space of all possible states $\mathbf{x}$. Often, it is also called *phase space* but we avoid this terminology and reserve the word *phase* to denote the phase of an oscillator. The dimension of the state space is denoted by d. Finally, the *Jacobian matrix* of system (2.1) at $\mathbf{x}^*$ is defined as $\mathbf{J}(\mathbf{x}^*) = \partial_{\mathbf{x}}\mathbf{f}(\mathbf{x}^*)$, and its eigenvalues are measures of the linear stability of the state considered.

Note on terminology: we use the word *system* in the sense of a physical system being studied, sometimes including its evolution law; but not in the sense of a set, for example, of linear equations.

Since the evolution of system (2.1) does not depend on time, the system is defined over infinite time. In fact, the study of the dynamics of an autonomous system can be turned into the geometric analysis of static flows in state space. This approach was first introduced by H. Poincaré when he was studying celestial mechanics. When studying the dynamics of a system, a very important concept is that of *attractors*. An *attractor*

is, in simple terms, a solution of system (2.1) that attracts other nearby trajectories. Typical types of solutions include steady states, periodic solutions, or chaotic solutions, which correspond to the following geometrical objects in state space: a fixed point, a closed orbit, and a strange attractor, respectively. When studying a given dynamical system, the study of its attracting solutions (or attractors) is of prime importance. Here, all attractors are static dynamical objects. Methods such as Poincaré sections, and delay-embedding for the reconstruction of state space from data, all make the important assumption that the flow and its attractors are static, and time can go to infinity. Another crucial concept is that of *bifurcation*. A bifurcation refers to a qualitative change in the dynamical behaviour of a system as a parameter value is changed. Such change typically is the appearance, disappearance, or change in stability of attractors.

In autonomous systems, the stability of an attractor is typically defined by *asymptotic* stability: a forward-time trajectory is asymptotically stable if there is a neighbourhood of its initial condition that contracts in diameter to zero under the flow as time tends to ∞. This definition does not mention any condition on the trajectories diverging before reaching infinite time, only that they must converge in the limit of infinite time. More details about stability will be given in the next section.

As mentioned in chapter 1, an autonomous model implicitly assumes that all variables needed to determine the state of the system are known by the modeller, and any external influence is negligible. In many real-life systems, however, this assumption is not realistic. For example, experimentalists often do not have access to measure all processes at hand, but can only measure a few of them. Strictly speaking, the only truly autonomous system is the entire universe. To take the external influences into account, nonautonomous models are needed, which we describe in the next chapter. Autonomous dynamical systems theory has been very successful and virtually used in all fields of science and beyond. Despite evidence to suggest that the understanding of real-life systems may greatly benefit from nonautonomous dynamical systems, such ideas have started to attract attention from the community only recently, see [28, 149].

For a more detailed presentation of autonomous dynamical systems theory, the interested reader is referred to the classical textbook [147] and references therein.

2.1.1. Nonautonomous dynamical systems

When the evolution law of a system explicitly depends on time, the system is *nonautonomous* and written in general

$$\dot{\mathbf{x}} = \mathbf{f}(\mathbf{x}, t). \tag{2.2}$$

The future of an initial condition of system (2.2) not only depends on the initial condition itself, but also on the initial time, contrary to autonomous systems – such a solution is denoted by $\mathbf{x}(t; t_0)$. Nonautonomous systems such as (2.2) are in general hard to treat mathematically. Indeed, the flow is not a fixed geometrical object anymore, but one that evolves with time, and hence many techniques and concepts of autonomous dynamical systems theory are either not applicable or can be misleading. Moreover, new concepts are needed to describe such systems. As defined above, the attractor of an autonomous system attracts close trajectories as time goes to $+\infty$. In nonautonomous systems, two different types of (asymptotic) attractors need to be defined: forward and pullback. An attractor, i.e. here a nonautonomous invariant set [72], $\mathbf{x}_*(t)$, is said to be *forward*, similarly to the autonomous case, if it satisfies

$$\lim_{t \to +\infty} |\mathbf{x}(t; t_0) - \mathbf{x}_*(t)| = 0, \tag{2.3}$$

and *pullback* if it satisfies

$$\lim_{t_0 \to -\infty} |\mathbf{x}(t; t_0) - \mathbf{x}_*(t)| = 0, \tag{2.4}$$

where the initial time t_0 tends to infinity. Such a distinction is clearly not possible for autonomous systems. If a pullback attractor exists, it is unique. On the contrary, forward attractors are intrinsically nonunique. Pullback and forward attractors are independent concepts. This can be seen by considering the two following simple systems. On the one hand, the nonautonomous system $\dot{x} = 2xt$ has no forward attractor, but $\mathbb{R} \times \{0\}$ is a pullback attractor. On the other hand, the nonautonomous system $\dot{x} = -2xt$, has no pullback attractor, but has an infinity of forward attractors (see [72]).

Note that in nonautonomous systems, the attractor is an object that evolves in time. Pullback attractors have been used in climate dynamics and oceanography, in driven

systems, and were often visualised as *ensemble snapshots* [42, 43, 137]. An ensemble snapshot is obtained by evolving a set of initial conditions covering the state space, and showing their positions at a given time t. Ensemble snapshots allow to visualise the pullback attractor at time t. Nonautonomous systems also offer new bifurcation scenarios, investigated for example in [3, 8, 9, 87].

A common misconception is that standard autonomous dynamical systems theory automatically covers the need to understand nonautonomous dynamics, since the introduction of time into the state space as a variable τ with $\dot{\tau} = 1$ makes the nonautonomous system autonomous. However, the qualitative behaviour of this autonomised version of a nonautonomous system is trivial from the point of view of autonomous theory: all solutions simply move towards ∞. Autonomous theory generally focuses on bounded objects – attractors – such as fixed points, periodic orbits, and associated Lyapunov exponents; but none of these exist for a system involving a component $\tau = 1$ [72, Remark 2.5].

In some simple cases, however, it can be useful to consider an autonomised extended-state space when analysing a nonautonomous system. In particular, when the system is driven by a periodic or quasiperiodic system, as will be discussed in chapter 3. In those cases, one (periodic case) or 2 or more (quasiperiodic case) phase variables are used to represent time, instead of extending the state space with a linearly growing variable. In that case, the extended state space is bounded, and so are solutions. Attractors exists in the extended state space in the sense of autonomous systems. This situation will be discussed in the next chapter in more detail. Note however, that this applies only in simple cases, and is only practical when the number of additional variables needed is very small.

In the rest of the text, we use the word *nonautonomicity* as the noun form of "nonautonomous". For example, when saying "we investigate the effect of nonautonomicity in oscillatory systems" we mean "we investigate the effect of being nonautonomous rather than autonomous, for oscillator systems". The word nonautonomicity has already been used in this way in some texts, e.g. [29, 73, 149].

For a more detailed presentation of nonautonomous dynamical systems theory, the interested reader is referred to the classical textbook [72] and references therein.

2.1.2. Self-sustained oscillators

Among all dynamical systems, we are most interested in oscillatory ones, and in particular in self-sustained oscillators (SSO), which abound in nature [127]. Such oscillators have the following main properties. First, they are self-sustained: they keep on oscillating even if isolated. Second, the shape of the oscillation is independent of the system parameters, and of the initial state. Third, the oscillation is stable against (small) perturbations: after being perturbed, the system will go back to oscillating identically.

Such systems are described formally as *limit-cycle oscillators*, where the limit-cycle is the curve in state space associated to the oscillation. The limit-cycle is the attractor of the system, and any initial condition ends up rotating on it. Specifically, the direction perpendicular to the limit-cycle – the *amplitude* – is stable: if pushed away in that direction, the perturbation decays and the oscillator goes back to the limit-cycle. Note, however, that the position on the limit-cycle – the *phase* – is only *neutrally stable*: if the oscillator is pushed away along that direction, the perturbation neither grows nor decays. The latter property allows this type of systems to synchronise, as we will see in the next section. In Fig. 2.1, we show the dynamics of the Brusselator as an example of a nonlinear SSO. The Brusselator is a two-dimensional system (x, y) satisfying $\dot{x} = 1 - (b+1)x + cx^2y$ and $\dot{y} = bx - cx^2y$, where b and c stand for free parameters. For $b > c+1$, the Brusselator model displays a limit-cycle.

Limit-cycle oscillators are typically modelled by an autonomous system $\dot{\mathbf{x}} = \mathbf{f}(\mathbf{x})$ with a stable periodic solution $\mathbf{x}(t) = \mathbf{x}(t + T)$ of period T.

Self-sustained oscillators are the base unit for all systems considered in thesis, just as cells are the base unit for living systems in biology.

Phase oscillators

When self-sustained oscillators are weakly nonlinear and interact weakly, only one scalar variable is necessary to describe their behaviour: their phase. Such a one-dimensional description is called a *phase oscillator*. As the single most basic oscillatory dynamical unit, they have been used extensively in the literature to understand the basic mechanism
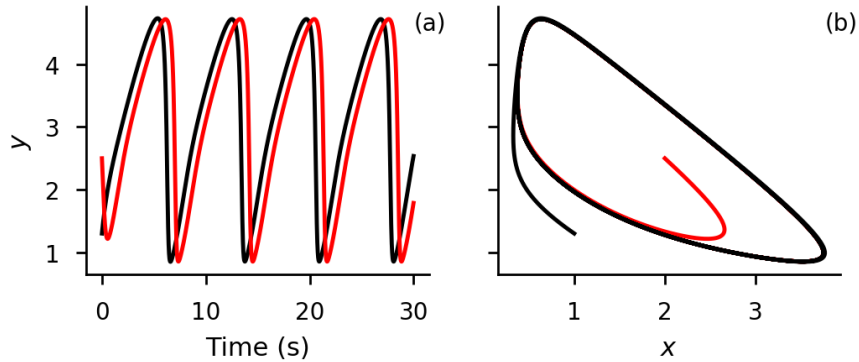
Figure 2.1.: Dynamics of the Brusselator. The trajectories of two initial conditions are shown (one black, one red). (a) Dynamics of the y-component over time. (b) Trajectory of the oscillation in state space (y vs. x). Even though the phase is only neutrally stable – constant shift between the trajectories in (a) – the direction perpendicular to the LC is stable – all trajectories end up on the limit-cycle in (b). Parameters are $b = 3$ and $c = 1$.

of synchronisation phenomena. The phase oscillators considered in this thesis have a linearly growing phase

$$\dot{\theta} = \omega, \tag{2.5}$$

with solution $\theta(t) = \theta(0) + \omega t$. Its period is fixed, $T = 2\pi/\omega$. The frequency f, is related to the angular frequency $\omega = 2\pi f$ simply by a factor 2π. The latter is often more practical to deal with in the context of synchronisation, and we refer to it simply as the *frequency*, and omit "angular", unless state otherwise.

In nature, however, many oscillators have a time-varying frequency. Simply extending definition (2.5) yields a *nonautonomous self-sustained oscillator*

$$\dot{\theta} = \omega(t), \tag{2.6}$$

where the explicit form of $\omega(t)$ can be anything: periodic, or aperiodic. The solution is now formally $\theta(t) = \theta(0) + \int_0^t dt' \omega(t')$. In the context of Eq. (2.6), there is no fixed period anymore: the time taken to complete a period of 2π changes with time. The definition of a period itself needs, in general, careful thinking.

As mentioned previously, phase oscillators models can often be obtained as good approximations of nonlinear LCs. The transformation to go from one description to the other is called *phase reduction*, for which various methods exist [104, 105] for autonomous LCs, and more recently for nonautonomous LCs [83, 84, 115].

2.1.3. Chronotaxic systems

To highlight the importance of, and draw attention to, open but stable oscillatory systems, *chronotaxicity* was first introduced in [149]. Coming from the Greek *chronos* – time – and *taxis* – order, the term was coined to describe their defining property: the ability to maintain stable but time-varying frequencies (and amplitude) against ongoing external influences. Chronotaxicity was introduced as a new class of nonautonomous oscillatory systems and realised mathematically as a time-dependent oscillating point attractor. As explained in chapter 1, such systems are very common in real-life – and in particular living – systems, and those properties could be key to their maintaining stability and function (and thus life) in the face of external events.

The theory of chronotaxicity was further developed [150] and later generalised in [151]. In the latter work, to avoid the need of an *a priori* knowledge of a point attractor, chronotaxicity was defined in terms of a time-dependent region of contraction in state space. One of the goals of these work was also to argue for the importance to the physics community of nonautonomous models and methods when dealing with real-life open systems. Chronotaxicity was also used to model and tackle inverse approach problems from biological data, see for example [29, 30, 85, 86]. Finally, chronotaxicity can also be related to *generalised synchronisation* [127]. The link between the two will be discussed in Sec. 2.3 where synchronisation is introduced.

2.2. Stability

A key concept in the study of dynamical systems is their stability: their ability to be resilient against small external perturbations. Indeed, it is much needed if one wants to understand the effective dynamics of the system. Merely knowing a trajectory exists without knowing if the tiniest perturbation will send it to a completely different type of solution, or if all other trajectories are attracted to it, is not enough to have a comprehensive understanding of the system. Stability analysis is thus a tool of prime importance to the dynamical systems scientist.

Many notions of stability can be defined and found in the literature. In the case of small perturbations, one can study the linear regime of the system very close to the original

system. Such analysis more precisely studies *linear stability*, which is the only concept of stability that we use in this text. We will refer to it as just "stability" unless stated otherwise.

In that context, an equilibrium, or more generally a trajectory, is said stable or unstable if, after it is kicked away from its original state, it comes back to, or goes away from the original solution, respectively. If the perturbation does not grow nor decay, the trajectory is said *neutrally stable*. This concept is typically formalised by the concept of Lyapunov exponent (LE). Stability is traditionally understood *asymptotically*, meaning that stability/instability is decided by the fate of the perturbation after an infinite time. However, notions of finite-time stability can also be defined. A first reason to do so, is that when dealing with experimental or numerical data, one does not have access to infinite times. Moreover, finite-time – short or long – stability can also be relevant in systems, and especially nonautonomous ones as will be discussed in the remainder of this thesis.

2.2.1. Lyapunov exponents

The asymptotic Lyapunov exponent (ALE) of a trajectory is a measure of the exponential rate of divergence (or convergence) of two initially close initial conditions [125]. For a one-dimensional system $\dot{x} = f(x)$, the ALE of a trajectory with initial condition x_0 is defined as

$$\lambda^{(\infty)} = \lim_{t \to \infty} \frac{1}{t} \ln \left\| \frac{\delta x(t)}{\delta x(0)} \right\|, \tag{2.7}$$

where $\delta x(0) \equiv x_0 - x_0'$ is the initial distance that separates x_0 and another infinitesimally close initial condition x_0', and $\delta x(t)$ that same distance after a time t. A positive asymptotic LE indicates instability in the sense of exponential divergence of nearby trajectories and is traditionally accepted as a necessary condition for chaotic behaviour. Similarly, a negative or zero ALE means stability or neutral stability, respectively. Note that, in the literature, asymptotic LEs are often referred to simply as LEs; here, however, we reserve the term LE for (long but) finite-time LEs, as will be discussed below.

For a d-dimensional system, a set of d ALEs exists, called the *Lyapunov exponent spectrum*. Each ALE is associated to a one-dimensional subspace, the set of ALEs is

typically ordered in decreasing order

$$\lambda_{max} = \lambda_1 \geq \lambda_2 \geq \cdots \geq \lambda_d. \tag{2.8}$$

The largest ALE is sufficient to determine the stability in a higher dimensional system. Indeed, only one unstable direction in state space is sufficient to make the whole trajectory unstable. Hence, $\lambda_{max} > 0$ is a sufficient condition for instability. Additionally, a negative maximum ALE guarantees all ALEs in the spectrum are negative, and hence guarantees stability. The existence of such set of exponents is the subject of the Oseledets theorem, also called Multiplicative Ergodic Theorem [111]. Symmetries in the dynamical system considered typically yield zero ALEs. For example, symmetry under time-shifts of autonomous continuous-time dynamical systems implies the existence of a zero ALE in the spectrum. The zero ALE in the case of an autonomous limit-cycle described above is due to that symmetry.

Lyapunov exponents also have the powerful property of being *dynamical invariant*: they are coordinate-invariant – i.e. independent of the choice of variables – and metric-invariant – i.e independent of the metric chosen to measure the distance between states. This makes them an objective and fundamental characterisation of the system.

It is important to point out that the ALE depends on the trajectory considered; there is in general not a single ALE for a given system. Typically, in systems with multiple attractors, or more generally to each invariant set, a different ALE will correspond to each invariant set. Imagine a system defined by a phase with an attracting point and its repelling counterpart (as will be the case in some chapters of this thesis). Almost all initial conditions will converge to the attracting point and have a negative ALE. A trajectory starting exactly on the repelling will however have a positive ALE. Moreover, different initial conditions in the basin of attracting of the same attractor may even converge to varying values of ALE; this depends on the existence of an ergodic invariant measure. Finally, even in autonomous systems, there exist cases for which the ALE does not exist, i.e. there is no convergence [113].

Note that ALEs need not exist for nonautonomous systems – in fact, nonautonomous systems need not even be well-defined over infinite-time. However, even if they can be

defined, ALEs may not necessarily be physically relevant for the limited timescales on which a system is considered in practice. Finite-time LEs will be discussed below.

In general, the analytical derivation of the Lyapunov spectrum for a given set of ODEs is a hard problem, and in most cases the spectrum is not analytically known. So then, it is often necessary to have numerical methods to determine the spectrum. Note that for phase oscillators systems, it is often possible to have an analytical formula. We discuss such numerical methods below.

To measure stability, it is also possible to define *instantaneous* Lyapunov exponents (ILE). Instantaneous LEs measure the instantaneous rate of growth or decay of two nearby initial conditions. Such exponents will be used and derived analytically for the system discussed in chapter 6.

Numerical methods

Various algorithms exist in the literature for the computation of LEs [125]. Algorithms can be separated into those aiming at computing ALEs from time series (obtained from numerical or experimental data) without prior knowledge of the underlying system, and those computing ALEs for a given set of ODEs (or other mathematical realisation of dynamical systems). Each of these two classes of algorithms can then be subdivided in two based on whether the algorithm computes the whole Lyapunov spectrum or just the maximum LE.

The canonical algorithm by Wolf [167] computes the whole spectrum of ALEs from time series. It is based on the reconstruction of state space from time series, using techniques such as the Takens-Mañé theorem of delay-embedding [96, 152]. While this algorithm has been used, it is notorious that extracting reliable ALEs from experimental data is a hard problem: indeed, ALEs measure sensitivity to initial conditions, and the inherent noise in experimental data adds effective sensitivity to the data. In the context of this thesis, only the second kind – which computes ALEs from ODEs – is used, and hence is the one that we will discuss below.

Although the computation of the sole maximum ALE often has advantages in terms of computational resources and time needed, the computation of the whole spectrum allows

for more precision and consistency checks. Here, we describe the general principles of the canonical algorithm by Benettin [17, 18], which computes the whole spectrum, and was used in the subsequent chapters of the thesis.

Benettin's algorithm computes the Lyapunov spectrum associated to a generic system of ODEs, under fairly general conditions. We now describe the main principles of the algorithm, of which a pseudocode can be found in [125, Appendix B, Algorithm 1]. The algorithm is based on the numerical computation of the values defined by the d-dimensional version of (2.7). To do so, the algorithm numerically integrates a trajectory of both an initial condition $\mathbf{x}$ in state space and d initial perturbation vector $\delta\mathbf{x}^{(k)}$ in the so-called *tangent space*. Vectors in tangent space are also called *tangent vectors*, and obey the system of ODEs linearised around the trajectory. Moreover, the algorithm needs to compute the growth rates in tangent space associated to each of the d ALEs. The underlying mathematical idea is the following: the sum of the n first ALEs is related to the growth rate of a volume of a generic n-dimensional parallelepiped, which can in turn be computed as the product of the n different lengths of its edges.

Practically, during the integration of the system over a (long) time $T = m\tau_\perp$ with integer m, every $\tau_\perp$ s, the set of tangent vectors is orthonormalised, the growth rate of each direction k stored as $\alpha_k^{(i)}$ (for the i-th orthonormalisation), and the k-th ALE is computed via the formula

$$\lambda_k = \frac{1}{m\tau_\perp} \sum_{i=1}^{m} \ln \|\alpha_k^{(i)}\|. \tag{2.9}$$

When applying the algorithm, care should be taken when choosing the value $\tau_\perp$. Indeed, if too large, tangent vectors align along the most expanding direction and orthonormalisation becomes numerically impossible; if too small, computational resources are not used efficiently since the orthonormalisation has a relative high computational cost compared to other operations, and it might become very slow.

There exist more than one numerical procedure to carry out the orthonormalisation. The most popular is the Gram-Schmidt (GS) method, which was used in this thesis and for which a pseudocode can be found at [125, Appendix B, Algorithm 2]. In this thesis, unless stated otherwise, $\tau_\perp = 0.1$ s for numerical computations. For more details about the numerical subtleties involved, see [17, 18, 125].

Note that when computing ALEs numerically, the infinite-time limit of the definition (2.7) can never be attained formally, and numerical exponents are thus all strictly speaking finite-time exponents. We discuss finite-time LEs in the next section.

2.2.2. Finite-time Lyapunov exponents

Finite-time Lyapunov exponents (FTLE) are a measure of stability over finite timescales. They are defined similarly to ALEs, but over a finite time-window of length τ and initial time t, $[t, t + \tau]$.

When τ is taken very small, FTLEs tend to the instantaneous LEs – in fact, that is how ILEs can be computed numerically. We will refer to them as *time-localised Lyapunov exponent* or just FTLE when clear from the context. When τ is taken very large, FTLEs tend to the asymptotic LEs for autonomous dynamical systems – in fact, as mentioned earlier, any numerical computation of ALEs are practically FTLEs. By contrast with time-localised LEs, we will use the term *long-term Lyapunov exponent* to refer to a Lyapunov exponent taken over a long time-interval $[0, T]$; when clear from the context, we will sometimes drop the word "long-term". Technically, a long-term LE is still a finite-time Lyapunov exponent, but it plays a similar role to asymptotic LE for autonomous systems. Finally, in nonautonomous dynamical systems where no ALEs can be well-defined, FTLEs are the only measure of long-term stability. Additionally, sometimes FTLEs will be computed for intermediate timescales, as in chapter 4 and 6. In those cases, the FTLEs will be proxies for Lyapunov exponents obtained via an adiabatic approach, which will be eplxained in the aforementioned chapters.

Note that, unlike ALEs, FTLEs are not metric-invariant. They prove to be, however, a useful tool, as shown by their use in existing literature. Examples include the study of SNAs [39, 124, 131, 141], metabolic control [38], or in many diverse contexts involving fluid flows data [55, 64, 88, 100, 134, 140, 154, 156, 163]. In the latter case, coherent structures within the body of fluid are studied, such as the Red Spot on Jupiter [54]. These structures are typically identified in terms of FTLEs, and exist completely independently of whether temporal variations follow an infinitely extendible pattern over time – which, typically, they do not. Very recently, the distribution of FTLEs in chimera-states was also investigated [21].

For the sake of clarity: an asymptotic LE is denoted by $\lambda^{(\infty)}$, a long-term FTLE is denoted by λ, an instantaneous and a short FTLE is denoted by $\lambda(t)$. Only in chapter 5, where long-term FTLEs are computed for different long times windows, the length T of the time-window will be written explicitly to avoid confusion: λ_T.

Numerical methods

Various methods exist for the computation of FTLEs [125]. In this thesis, FTLEs over a time-window τ are computed by computing growth rates $\alpha_k^{(i)}$ every time $\tau_\perp$, as described in the previous section for ALS, and then performing a moving average with a time-window τ (MA$_\tau$) over all computed growth-rates values as follows

$$\lambda_k(t;\tau) = \mathrm{MA}_\tau\left(\left\{\frac{1}{\tau_\perp}\ln\|\alpha_k^{(i)}\|\right\}_i\right). \tag{2.10}$$

When computing long-term LEs, τ is the (large) total time of integration, the moving average is just an average over all values, in which case formula (2.10) is identical to formula (2.9). When computing time-localised LEs, τ is taken very small; note that τ can only be taken as small as $\tau_\perp$, which in turn cannot be smaller than the step of integration used in the RK4 scheme.

2.2.3. Floquet exponents

Floquet analysis provides another way of assessing stability [132], but only for linear systems of the type

$$\dot{\mathbf{x}} = \mathbf{A}(t)\,\mathbf{x}, \tag{2.11}$$

where $\mathbf{A}(t)$ is a periodic function with period T.

For the sake of clarity and simplicity, we restrict the presentation to the application of Floquet theory to the stability analysis of limit-cycle solution. Let us consider a two-dimensional autonomous limit-cycle $\dot{\mathbf{x}} = \mathbf{f}(\mathbf{x})$ with T-periodic solution $\tilde{\mathbf{x}}(t)$. Let $\delta\mathbf{x} = \mathbf{x} - \tilde{\mathbf{x}}$ be a small perturbation to the limit-cycle. Linearising the governing equation yields $\delta\dot{\mathbf{x}} = \mathbf{J}(t)\,\delta\mathbf{x}$, where $\mathbf{J}(t)$ is the Jacobian matrix, periodic of period T as well. Let us label with $\mathbf{\Phi}(t)$ a *fundamental matrix* of the system, i.e., a matrix that satisfies

$\dot{\boldsymbol{\Phi}} = \mathbf{A}(t)\,\boldsymbol{\Phi}$ and is non-singular. Then, for all t, there exists a non-singular, constant matrix $\mathbf{B}$ such that

$$\boldsymbol{\Phi}(t+T) = \boldsymbol{\Phi}(t)\,\mathbf{B}. \tag{2.12}$$

Moreover, $\det \mathbf{B} = \exp\left[\int_0^T \operatorname{tr} \mathcal{J}(t)\,\mathrm{d}t\right]$. The matrix $\mathbf{B}$ depends in general on the choice of the non-unique fundamental matrix $\boldsymbol{\Phi}(t)$. Its eigenvalues, ρ_i with $i = 1, 2$, however, do not. These are called the *Floquet multipliers* and yield the *Floquet exponents*, defined as

$$\mu_i = T^{-1} \ln \rho_i. \tag{2.13}$$

Solutions of the examined linear system can then be written

$$\mathbf{x}(t) = a_1\,\mathbf{p_1}(t)\,e^{\mu_1 t} + a_2\,\mathbf{p_2}(t)\,e^{\mu_2 t}, \tag{2.14}$$

where the $\mathbf{p_i}(t)$ functions are T-periodic, and the a_i are constant coefficients determined by the initial conditions.

When the system is linearised around a limit-cycle solution, the maximum Floquet exponents is identically equal to zero, $\mu_1 = 0$, whereas the second exponent is negative, $\mu_2 < 0$. This is also the case for LEs. Here, similarly to LEs, the first exponent is associated with perturbations along the longitudinal direction of the limit-cycle: these perturbations are neither amplified nor damped as the motion progresses. The second exponent, μ_2 is negative, meaning that perturbations in the transverse direction are bound to decay in time, and any initial conditions ends up rotating on the limit-cycle.

For periodic systems, LEs are the real part of the Floquet exponents [125].

2.3. Synchronisation

Synchronisation is the timely adjustment of interacting self-sustained oscillators. In order to introduce the concept more formally, we consider the simplest example: a uni-directionally coupled pair of phase oscillators. Let us denote $\theta_0(t)$ and $\theta(t)$ the driving and driven oscillators with constant frequency ω_0 and ω, respectively. The dynamics of the driven oscillator is

$$\dot{\theta} = \omega + \gamma \sin[\theta - \theta_0(t)], \tag{2.15}$$

where γ is the coupling strength, and the driving oscillator simply obeys

$$\dot{\theta}_0 = \omega_0. \tag{2.16}$$

Now, physically, two types of dynamics can occur: either the two oscillators synchronise, or they do not. *Synchronisation* is when both oscillators end up oscillating at the same frequency (or at commensurate frequencies in the case of higher-order synchronisation, see below) due to their interaction, although their natural frequencies are different. In this setting, their common frequency will be that of the driving. Note that *coherent* oscillations are synchronised only if they interact: two swings oscillating coherently in two different countries do so only as the result of chance, and it is very unlikely to happen over a long period of time. For two synchronisation oscillators, since their effective frequencies are identical – phenomenon known as *frequency entrainment* – the difference between their phases is constant – phenomenon known as *phase-locking*. Frequency entrainment and phase-locking are in general independent phenomena, although they are equivalent in the simple case of fixed-frequency driving (2.15) – chapter 4 discusses the relation between the two in more details.

The *phase difference* $\psi = \theta - \theta_0$ obeys

$$\dot{\psi} = \Delta\omega + \gamma \sin\psi, \tag{2.17}$$

where $\Delta\omega \equiv \omega - \omega_0$ is the frequency mismatch. It is a one-dimensional autonomous equation, and has two types of solutions: a fixed point, and a monotonically growing solution (or decreasing). Synchronisation corresponds to existence of a stable fixed point, where the phase difference stays constant – phase-locked. The condition for synchronisation is $\gamma \geq |\Delta\omega|$, in which case the stable fixed point is

$$\psi = \pi - \arcsin(\tfrac{-\Delta\omega}{\gamma}), \tag{2.18}$$

and attracts all initial conditions but the coexisting unstable fixed point $\psi = \arcsin(\tfrac{-\Delta\omega}{\gamma})$. If the condition for synchronisation is not fulfilled, $\gamma < |\Delta\omega|$, solutions monotonically grow, $\dot{\theta} > 0$, or decay, $\dot{\theta} < 0$. The region in parameter space where synchronisation occurs is called *Arnold tongue*, and is shown in Fig. 2.2.
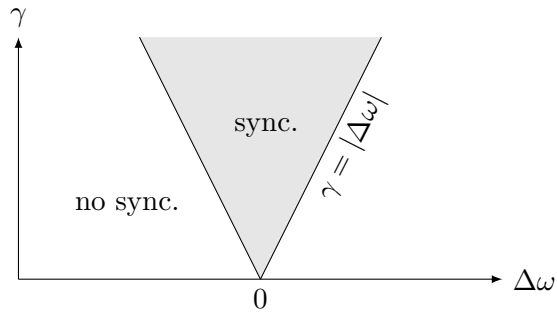
Figure 2.2.: Arnold tongue: region of synchronisation. The region of synchronisation is associated with a negative LE whereas the non-synchronised has zero LE.

In terms of ALEs, the driven oscillator has $\lambda^{(\infty)} < 0$ if it is synchronised, and $\lambda^{(\infty)} = 0$ if not. In other words, in the case of synchronisation, there is *phase-locking* between the driven and the driving phase: almost all initial conditions of the driven oscillator end up rotating with the same phase, and any perturbation decays exponentially. Only one rotating point attracts almost all solutions. On the other hand, in the non-synchronised case, no phase-locking occurs, the driven phase is neutrally stable, and different initial conditions end up with different phases, covering the whole attracting circle.

Solutions of (2.17) have period T, formally given by

$$T = \left| \int_0^{2\pi} \frac{\mathrm{d}\psi}{\Delta\omega + \gamma \sin\psi} \right|, \tag{2.19}$$

which is finite in the non-synchronisation region, and tends to ∞ close to the synchronisation region. Very close to the border, in the no synchronisation region, the dynamics of ψ is highly non-uniform, and stay for very long epochs quasi-constant, and then effectuates a quick rotation of 2π: this phenomenon is called *phase slip*.

Another important quantity is the frequency difference, often called *beat frequency*, defined as

$$\Omega_\psi = 2\pi \left[\int_0^{2\pi} \frac{\mathrm{d}\psi}{\Delta\omega + \gamma \sin\psi} \right]^{-1}. \tag{2.20}$$

As show, in Fig. 2.3, a zero beat frequency corresponds to frequency entrainment, in the autonomous case. Finally, the mean observed frequency of the driven oscillator thus reads

$$\langle \dot{\theta} \rangle = \omega + \Omega_\psi. \tag{2.21}$$
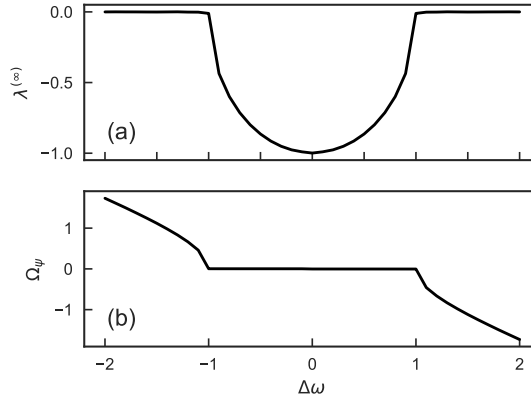
Figure 2.3.: Synchronisation region for a fixed $\gamma = 1$. The region of synchronisation corresponds to that of negative LE (phase stability) and plateau of zero beat frequency (frequency entrainment).

In the literature, often for networks of oscillators, *frequency entrainment*, when all oscillators of the system end up oscillating at the same frequency, is sometimes referred to as *frequency synchronisation*. This is to contrast with what is sometimes called *phase synchronisation*: when all oscillators of the system oscillate with the same phase. Phase synchronisation implies frequency synchronisation, but the reverse is not true. Note that, in the literature, the term *phase synchronisation* is also used with a different meaning when talking about the synchronisation of chaotic oscillators. In that context, *phase synchronisation* – here referring to phase locking and frequency entrainment – is specified to distinguish it from *complete synchronisation* – where all chaotic oscillators follow the exact same trajectory. To avoid confusion, we will in general not use the terms *phase synchronisation* and *frequency synchronisation* but will specify what is used if not clear from the context.

So far, we have only considered synchronisation where the driving and the driven oscillators complete one cycle in the same time period, also known as 1:1 phase-locking. Higher order phase-locking dynamics is possible. In general, one calls $n\!:\!m$ phase-locking, or synchronisation, a solution where the driving oscillator complete n cycles while the driven oscillators completes m cycles, where m and n are integers. The condition on parameters to have $n\!:\!m$ phase-locking, is that the phase difference $\psi_{n:m} = m\theta - n\theta_0$, which obeys

$$\dot{\psi}_{n:m} = (m\omega - n\omega_0) + \gamma \sin \psi_{n:m}, \tag{2.22}$$

has a stable fixed point. Subtongues of higher order phase-locking can be computed in

some cases, and decrease in size as the order is increased. Such phase-locking is also directly linked to multistability, see [33]. For mode details about $n:m$ phase-locking, see [127].

More broadly, one can speak of *generalised synchronisation* when the state of the driven system is determined by the state of the driving system. This definition also includes synchronisation by quasiperiodic forcing (see chapter 3) and other types of synchronisation not considered, that can occur, e.g., with coupled chaotic oscillators.

The traditional concepts in this section are presented as in the literature [127] for two coupled fixed-frequency SSOs, and will be revisited in the different chapters of this thesis for SSOs with time-varying frequency. The first few studies considering synchronisation between time-varying oscillators include [41, 65, 149–151]. In [149–151], the above-mentioned concept of chronotaxicity was introduced to describe a class of nonautonomous oscillatory systems with time-varying yet stable frequency and amplitude. Chronotaxic systems were defined in terms of a moving point attractor, and can be seen as an important type of generalised synchronisation. In [65], a nonautonomous version of system (2.17) was studied, the same equation considered in chapter 4. It provides a description of solutions, and in particular derives a condition on the slowness of the nonautonomicity needed for the solutions to be valid. This work will be discussed in further details in chapter 4. Finally, in [41], a similar nonautonomous version of Eq. (6.4) was considered, and rich Canard solutions were found, for which trajectories were going to and staying on unstable branches for long transients. Other existing work on the topic but considering networks of oscillators will be presented in the next section.

2.4. Networks and synchronisation

Synchronisation can also occur in large ensembles of coupled oscillators. Such oscillators can be coupled in simples ways – globally, like in the Kuramoto model, or locally to their nearest neighbour in lattice structures, for example – and in more intricate ways. In general, such ensembles can be referred to as *networks of oscillators*, and the network – the structure of the couplings – can be simple or complex. Network structure are ubiquitous [108], as argued in chapter 1. Networks of oscillators have been used in

many diverse fields from neurosciences to ecology and social sciences. In this section, we define relevant concepts relative to networks of oscillators and synchronisation in such networks.

Historically, the paradigmatic model for synchronisation in network of oscillators is the Kuramoto model for phase oscillators [1, 81]. Such network, for N oscillators, reads

$$\dot{\theta}_i = \omega_i + D \sum_{j=1}^{N} A_{ij} \sin(\theta_j - \theta_i), \qquad (2.23)$$

with $i = 1, \ldots, N$, and where ω_i is the frequency of oscillators i, D is a coupling constant, A_{ij} are the elements of the adjacency matrix $\mathbf{A}$, and oscillators are coupled with a sine function vanishing for identical phases. The important idea in this model is that, above a certain critical coupling strength, all oscillators synchronise, i.e. they behave in a coherent way, despite their different frequencies. This synchronisation can be measured by an order parameter R defined in terms of the complex mean field

$$Z = Re^{i\Phi} = 1/N \sum_j e^{i\theta_j}. \qquad (2.24)$$

When all oscillators have the same phase, $R = 1$; when they are spread maximally, $R = 0$. In (2.23), the order parameter R undergoes a bifurcation from zero – small coupling strength D – to positive (tending to one) values – for large coupling strength D. In 2008, E. Ott and T. M. Antonsen found a low-dimensional description of system 2.23 in the thermodynamic limit $N \to \infty$, sometimes called the Ott-Antonsen (OA) manifold [112]. Moreover, they showed that this manifold is the only attractor, as long as the natural frequencies are drawn from a continuous distribution.

Before describing the dynamics in further details, we define and describe in more details the concept of network and adjacency matrix. In general, some of these oscillators are coupled and influence each other's dynamics directly, and some are not. Two coupled oscillators are also said to be *connected* or *linked*. The connexions in such ensemble can be represented by a mathematical *graph* or in this context more often called *network*. A network is composed of *nodes* and *links*. Each node represents an oscillator, and each link between two nodes represents a link, or coupling, between two oscillators. The information about the topology of the network, i.e., which pairs of oscillators are

coupled, is stored in the $N \times N$ *adjacency matrix* **A**. The value of each element A_{ij} is either 1 if oscillators i and j are connected, or 0 if they are not. In this thesis, we only consider *undirected* networks, in which connections are symmetric such that the adjacency matrix is symmetric: $A_{ij} = A_{ji}$. In *undirected* networks, connections are asymmetric, and oscillator j can drive oscillator i without the reciprocal being true. An important quantity is the connectivity of each node, i.e., the number of other oscillators node i is coupled too, which is defined as $K_i = \sum_{j=1}^{N} A_{ij}$. Finally, in *weighted* networks, the entries A_{ij} can take real values. In this thesis, we only consider unweighted undirected networks.

Different classes of networks exist, based on the properties of their adjacency matrix. We briefly describe the types used in this thesis. The simple case is that of a *globally coupled* network, also called *all-to-all* coupling, where, as the name indicates, $A_{ij} = 1$ for all pairs of oscillators. Global coupling was initially used by Y. Kuramoto in his study. *Nearest neighbour* coupling refers to a lattice structure where only neighbouring are coupled. On the other extreme, in *random networks*, connexion are drawn at random from a chosen distribution. Finally, intermediate cases include scale free networks, which are defined by their connectivity following a power-law distribution. A notorious example of scale-free network is the Barabási-Albert type which builds an adjacency matrix following an algorithm based on preferential attachment. More details as well as other types of networks can be found in [5, 108, 136] and references therein.

Note that all types of networks described so far are *static* networks: their adjacency matrix is constant. Most of the literature to date deals with static networks [5, 108, 136]. Evidence for *time-varying* networks, sometimes called *temporal* networks, exists [57, 58] and the topics has very recently started to attract the attention of the community, see for example [66, 119].

2.4.1. Watanabe-Strogatz

In this thesis, we only consider networks of identical oscillators, for which $\omega_i = \omega$ for all i. Such networks of identical frequency phase oscillators are often called Watanabe-Strogatz (WS) networks in reference to the results by the authors of the same name [164, 165],

who originally studied the following system in the global coupling setting, $A_{ij} = 1$,

$$\dot{\theta}_i = \omega + D \sum_{j=1}^{N} A_{ij} \sin(\theta_j - \theta_i). \tag{2.25}$$

In system (2.25), a fully-synchronous solution always exists, where all oscillators have exactly the same phase. It is a condition of utmost coherence that can only be achieved because the oscillators are identical. In contrast, the Kuramoto model (2.23) can never achieve such perfect synchrony: oscillators can at most be very coherent and their phase distributed in a small cluster. Here, in system (2.25), and in the rest of the thesis, we study the stability of the fully synchronous state. Discussions on the links between the WS and the OA theories as the distribution of natural frequencies tends to a Dirac delta can be found in [126] and references therein.

Originally, [164] considered a globally coupled network, and showed that the dynamics of (2.25) could be reduced to a low-dimensional system consisting of 3 macroscopic variables. Moreover, they were the first to show that the synchronous solution was a global attractor: almost all initial conditions converge to it. In fact, they studied the system with the more general coupling $g(\theta_j, \theta_i) = \sin(\theta_j - \theta_i - \delta)$, with a time-lag $\delta \in [-\pi/2, \pi/2]$. For $\delta = \pm\pi/2$, the coupling is effectively a cosine, yielding a conservative kind of coupling, and no dissipation to the synchronous state. For intermediate values, attractiveness of the synchronous solution depends on the sign of the derivative of the effective coupling $D\sin(\theta_j - \theta_i - \delta)$ at the origin. If the derivative is negative, the synchronous solution is attractive, and the coupling is referred to as *attractive*. If the derivative is positive, the synchronous solution is repulsive, and the coupling is referred to as *repulsive*. In fact, almost all initial conditions then converge to attractive incoherent states. For more complex configurations, the master stability function formalism was introduced in [116], based on the computation of the eigenvalues of a specific matrix evaluated on the synchronisation manifold.

2.4.2. Beyond Watanabe-Strogatz networks

The WS system has been extended in many diverse directions – complex topologies, different coupling functions – and new types of dynamics were observed. The synchronous

2. Theoretical background

solution always exists, however, as long as the coupling function $g(\theta_i, \theta_j) = g(\theta_i - \theta_j)$ vanishes at the origin. Nonetheless, its local stability depends on the sign of $Dg'(0)$.

T.-W. Ko and G. B. Ermentrout studied the coupling function $g(\theta) = \sin(\theta - \alpha) + \sin\alpha$, which is zero but not anti-symmetric at the origin. They approximated the system by simplifying the topology $DA_{ij} \to K_i/N$ with weights depending on the connectivity degrees. They observed *partially locked states* [74], where a subpopulation is phase-locked, but the rest drifts independently, like in chimera states [82, 114]. Such heterogeneity was surprising for identical frequency oscillators, but was explained by the distribution of couplings K_i. It was also noticed that the asymmetry in the coupling function g combined to the heterogeneous couplings K_i could stabilise *incoherent states* [74], and even yield bistability with the synchronous state. A bit earlier, Y. Kuramoto [82] discovered *chimera states*, which are possible even in identical oscillator networks [114]. These phenomena show that even identical oscillators can have rich dynamics, despite their apparent simplicity compared to networks with distributed frequencies.

In [10], *splay-states* – rotating states that consist of a number of equidistant clusters of oscillators – were investigated. More complicated configurations of clustered states exist, for example [75], and [110] which discussed how to design clustered states in globally coupled oscillators by tuning the coupling function. In [7], the role of additional types of coupling functions is investigated. For a more focused study on the role of coupling functions in general, see [142]. The effect of topology has also been investigated, e.g., in [157] for small-world networks.

In 2011, H. Hong and S. H. Strogatz (HS) studied [59] a "conformists and contrarians" of the WS system

$$\dot{\theta}_i = \omega + \frac{1}{N}\sum_{j=1}^{N} K_i \sin(\theta_j - \theta_i), \qquad (2.26)$$

with both K_i both positive and negative, i.e. attractive and repulsive links – or in their words, conformists and contrarians. Using the WS approach and the OA ansatz, they observed and described 4 types of dynamics: a 2-cluster state, travelling waves, incoherence, and a so-called blurry state. Surprisingly, they found that this system has richer dynamics than its counterpart with non-identical frequencies. Many studies followed in the direction and extended the HS model, e.g. [24, 168].

Although all the above-mentioned studies consider static networks of fixed-frequency oscillators, it is still possible to observe time-varying macroscopic properties. An example of this is the work in [20] where chaotic dynamics of the order parameter was observed in a symmetric system of identical phase oscillators.

2.4.3. Nonautonomicity in networks

A category of nonautonomous networks is that of static network driven by an external oscillator. Such a system was studied in for the Kuramoto model (heterogeneous frequencies) in [112] for a fixed-frequency driving. More recently, the dynamics of order parameter in the Kuramoto model was derived for a nonautonomous version of Kuramoto model in [120]. The cases of time-varying coupling and time-varying frequencies were considered, in an adiabatic and an non-adiabatic limit. Finally, the stability of the low-dimensional manifold of the Kuramoto model was also considered and proven for various general parameter variations in [122].

Little work has been done on driven networks. For networks of identical oscillators driven by a constant frequency, the effect of driving a selected subset of nodes was investigated for regular [133] and multiple complex topologies [76, 77]. H. Kori [76] investigated directed networks of identical oscillators presenting a hierarchical structure, which were driven by a pacemaker with a heterogeneous strength, and a more general coupling function depending on the phase differences. It was shown that the Arnold tongue (region of synchronisability) becomes increasingly narrow for networks with higher hierarchical organisation. To the best of our knowledge, the very few studies investigated time-varying parameters and time-varying driving are for network with heterogeneous frequencies are those cited above.

As mentioned earlier, time-varying networks [57, 58] have been attracting attention recently, e.g., in epidemic spreading [102] or in statistical physics [117]. However, despite evidence for the importance and the presence of time-varying networks, little research has been done on time-varying networks of oscillators. One of the few is [119] where time-variability was shown to induced instability of the homogeneous steady state.

2.5. Summary

In this chapter, basics of dynamical systems theory were introduced. Autonomous and nonautonomous models were compared, and concepts such as attractors and bifurcations were discussed in both cases. Notions of self-sustained oscillators, the base unit of all systems considered in this thesis, and chronotaxic systems, were introduced. The need for nonautonomous models for realistic modelling of living-systems was argued. Then, a detail discussion about stability was provided. In particular, Lyapunov and Floquet exponents were defined, and numerical methods for their computation were presented in detail. Different types of Lyapunov exponents were introduced, to assess stability over different time scales. Finite-time stability was discussed, and compared to the traditional notion of asymptotic stability which cannot always be applied to nonautonomous systems. Synchronisation was subsequently introduced for a pair of coupled oscillators with fixed-frequencies, and related concepts were presented. Finally, the presentation of synchronisation was extended to networks. The current and relevant literature on the topic was reviewed, and the context of the work of this thesis made clear. As we saw, little is yet known about nonautonomous systems of coupled oscillators, despite much evidence for the existence and the importance of such systems, which motivates the work in this thesis.

3. Attractors and multistability for a quasiperiodically driven oscillator

3.1. Introduction

Often, and especially in living systems, assuming that the external influence driving the system is periodic is too simplistic for a realistic model, as argued in chapter 1. In this chapter, we consider the simplest kind of (autonomous) aperiodic driving: a quasiperiodic driving. A quasiperiodic function can be defined as a function of two or more independent phases. Quasiperiodic driving has been used, e.g., to model the influence of the atmosphere on climate [33, 39, 42].

This chapter introduces concepts and numerical techniques that will be useful in the subsequent chapters of the thesis. Here, the different types of dynamics exhibited by the considered quasiperiodically forced oscillator are characterised, and the double-tongue structure of parameter space is shown. The focus is put on that structure. Quasiperiodically forced systems are known to exhibit strange nonchaotic attractors (SNA), which are stable object but with a strange structure and interesting finite-time properties. The strange attractors – chaotic and nonchaotic – are only briefly discussed and their interesting properties described, as they do not serve the rest of the thesis.

Note that the topic of quasiperiodically forced oscillators has been extensively studied for the last ten years, and further details about this type of systems can be found in [39].

The chapter is organised as follows. Section 3.2 introduces the model and defines quasiperiodicity. Section 3.3 illustrates the different types of dynamics exhibited by the system. Section 3.4 then provides theoretical analysis to characterise the different

regimes, and understand the stucture of the phase diagram in parameter space. Section 3.5 confirms numerically the analysis, and finally a summary is given in Sec. 3.6.

3.2. Model

We consider a Poincaré limit-cycle oscillator [29], of which the y variable is quasiperiodically forced with forcing $f(t)$. In cartesian coordinates, the system reads

$$
\begin{aligned}
\dot{x} &= \epsilon \left(r_p - \sqrt{x^2 + y^2} \right) x - \omega_0 y, \\
\dot{y} &= \epsilon \left(r_p - \sqrt{x^2 + y^2} \right) y + \omega_0 x + \gamma f(t),
\end{aligned}
\tag{3.1}
$$

where r_p and ω_0 are the radius and the frequency of the unforced oscillator, respectively, and ϵ is the attraction coefficient to that radius in the radial direction. This system is borrowed from [29]. The quasiperiodic driving drives the y-variable with strength denoted by γ, and its explicit form given by

$$
f(t) = \sin \omega_1 t + \sin \omega_2 t,
\tag{3.2}
$$

where the two frequencies ω_1 and ω_2 are incommensurate, i.e. there are no two integers n, m such that $\omega_1 / \omega_2 = m/n$. If – on the contrary – the two frequencies were commensurate, then $f(t)$ would simply be periodic. As mentioned earlier, such quasiperiodic function is aperiodic.

In polar coordinates, the system is rewritten

$$
\begin{aligned}
\dot{r} &= \epsilon (r_p - r) r + \gamma f(t) \sin \theta, \\
\dot{\theta} &= \omega_0 + \gamma f(t) \frac{\cos \theta}{r},
\end{aligned}
\tag{3.3}
$$

which makes the amplitude-phase coupling explicit.

In the unforced oscillator, $\gamma = 0$, however, the radius and the phase are uncoupled. The system present an attracting linear limit-cycle oscillator with radius r_p and frequency ω_0 centred at the origin, and a repelling fixed point at the origin. The limit-cycle solution is stable along the radial direction, but only neutrally stable along the angular direction. In terms of LEs, this corresponds to a negative and a zero LE for the radial and angular

directions, respectively. This means any initial condition will end up rotating on the limit-cycle with its own different phase, which depends on the initial condition.

When $\gamma \neq 0$, the forcing can in general be expected to synchronise the driven oscillator, or to alter its limit-cycle.

3.3. Types of dynamics

Before analysing the system in further details, we illustrate the different types of dynamics exhibited by system (3.1) in the (γ, ω_0)-parameter space, by means of numerical integration. All numerical integration in this chapter are carried out using a 4th-order Runge-Kutta scheme, with integration times step of 0.01 s, and we set $r_p = 1$, $\epsilon = 5$, $\omega_1 = 4$, and $\omega_2 = 2\pi$, unless stated otherwise.

Just as in periodically driven oscillators, synchronisation phenomena and an Arnold tongue-like structure of parameter space are expected. In addition to these features, it is known that quasiperiodically forced oscillators can exhibit chaotic and strange nonchaotic (SNA) attractors [39]. Here, we describe quantitatively the different behaviours, which will be characterised more formally in the subsequent sections. To the naked eye, three main types attractors are observed, which will be analysed in more details in the next section: a moving limit-cycle (MLC), a (or multiple) moving point attractor(s) (MPA), and a moving one-dimensional attractor exhibiting folding (1DA). The MLC corresponds to a non-synchronised regime.

3.4. Theoretical analysis

3.4.1. 4-dimensional autonomous formulation

Nonautonomous systems such as (3.1) are hard to treat mathematically in general [72]. As explained in chapter 1, one can always turn a nonautonomous system into an autonomous one by adding variable τ accounting for time in the state space. Such new variable thus has time derivative $\dot{\tau} = 1$. Such a description, even if mathematically equivalent, is in general of not much use since trajectories in such an *extended state space* are all
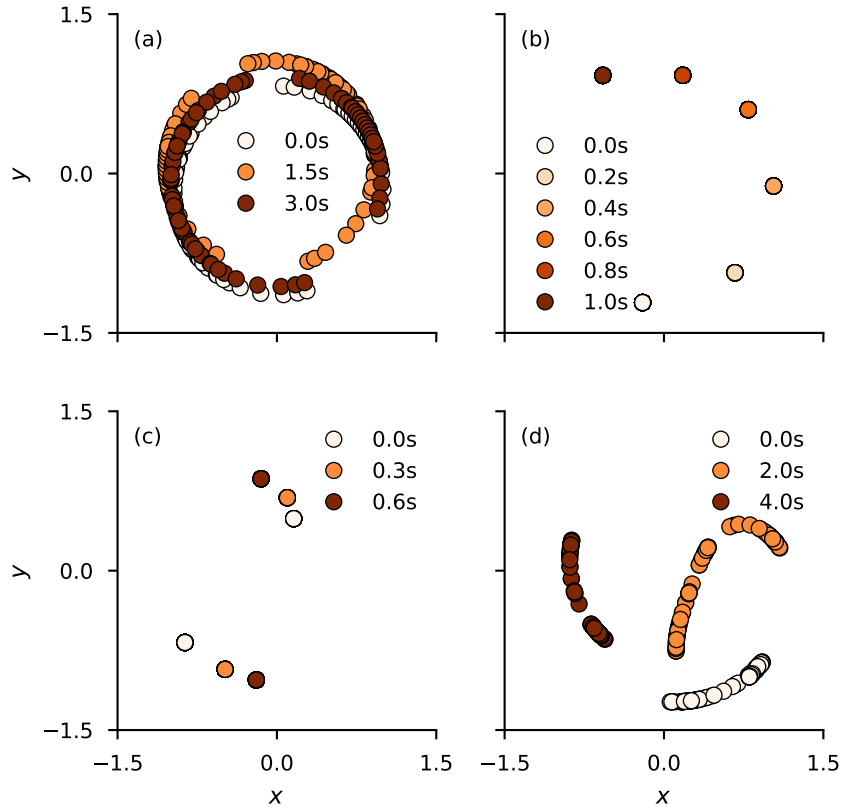
Figure 3.1.: Ensemble snapshots of system (3.1) for different regimes: (a) Moving limit-cycle, (b) single moving point attractor, (c) double moving point attractor, and (d) chaotic attractor. The snapshots are the results of the evolution of 100 random initial conditions, and are shown for different times, after a transient of 100 s. Each colour represents a different time as indicated by the legends.

unbounded. Indeed, they all grow to infinity together with τ, which grows monotonically. Autonomous dynamical system theory deals with bounded objects – attractors – and study their properties, e.g, stability. Such attractors do not exist in such extended state space.

In some specific cases, a useful autonomous description exists for nonautonomous systems. This is the case for periodic or quasiperiodic external driving for example. Indeed, in such systems, time can be described by one or more periodic variables, and the state space is then bounded. Thus, system (3.1) can be rewritten as a 4-dimensional autonomous system in state space $\mathbb{R}^2 \times \mathbb{T}^2$, i.e. the product of the real plane and the two-torus, by

3. Attractors and multistability for a quasiperiodically driven oscillator

adding two new variables θ_1 and θ_2

$$
\begin{aligned}
\dot{x} &= \epsilon \left(r_p - \sqrt{x^2 + y^2} \right) x - \omega_0 y, \\
\dot{y} &= \epsilon \left(r_p - \sqrt{x^2 + y^2} \right) y + \omega_0 x + \gamma[\sin \theta_1 + \sin \theta_2], \\
\dot{\theta}_1 &= \omega_1, \\
\dot{\theta}_2 &= \omega_2.
\end{aligned}
\tag{3.4}
$$

Here, two additional variables were necessary to account for the two frequencies of the quasiperiodic driving. For a periodic driving, only one suffices.

When $\gamma = 0$, the now sub-systems (x, y) an (θ_1, θ_2) are uncoupled, so that system (3.4) has two uncoupled sub-systems. The first sub-system, (x, y), is attracted to a limit-cycle oscillator in $\mathbb{R}^2$, whereas the second, (θ_1, θ_2), covers the whole two-torus $\mathbb{T}^2$ ergodically.

We now describe the different types of dynamics present in the system, as summarised in Tab. 3.1. A fixed point in the sub-system in $\mathbb{R}^2$ is equivalent to a two-torus in the extended state space $\mathbb{R}^2 \times \mathbb{T}^2$ [56]. That is the simplest attractor possible, and it corresponds to a quasiperiodic solution with 2 frequencies in the 4-dimensional space. In the case of higher-order mode-locking, as described in chapter 1, multiple point attractors can coexist [33]. This corresponds to having multiple 2-tori coexisting in the 4-dimensional space, or multiple moving point attractors in the 2-dimensional state space. Another type of dynamics can occur when no mode-locking occurs. The trajectory is then described by 3 phases and lives on a 3-torus in the extended space. In the 2-dimensional state space, what is observed is a moving limit-cycle (MLC), which can never be observed in an autonomous 2-dimensional system.

Additionally, quasiperiodically forced systems are known to exhibit strange nonchaotic attractors [47, 129, 130] and chaotic attractors [35]. For a long time, since the advent of chaos theory, it was thought that a strange attractor was always chaotic. SNAs showed that strangeness and chaoticity were actually independent concepts. One way of defining a strange attractor is for it to have a fractal dimension [34]. And, in the case of SNAs, a fractal dimension does not imply chaotic dynamics. In fact, the dynamics on an SNAs is notoriously *intermittent*, and yet, asymptotically stable in the sense of a negative ALE, contrary to a strange chaotic attractor that has a positive maximum

ALE. The intermittent dynamics on an SNA means a trajectory will intermittently alternate between epochs of smooth dynamics and epoch of erratic dynamics, and yet, overall, the dynamics is stable. One way to characterise SNAs is by the distribution of the (long enough) FTLEs. Indeed, over very short time windows, the ILE is highly fluctuating [141]. However, since their ALE is negative, if one takes a time-window of length T long enough (but smaller than the total time of the trajectory), all FTLEs should be negative. Nonetheless, the intermittent behaviour of SNAs means that even for long time windows, they still exhibit some positive FTLEs. This is often analysed by looking only at the distribution of LEs which characteristically has positive values even for long time windows [67, 131]. Another type of stable attractor will have the whole distribution of FTLEs covering only negative values already for relatively short time windows, and hence they can be differentiated. Other ways to characterise SNAs can be applied, such as phase sensitivity [124]. For more details about SNAs see [39] and references therein.

In terms of ALEs, the two phases θ_1 and θ_2 have a zero ALE. The driven oscillator (x, y) however, can have different values of ALE depending on the values of the strength of the driving γ and the natural frequency of the oscillator ω_0, as we shall see.

Attractor (4-d)	Lyap. spectrum	Strange	Behaviour (in 2-d)	Abbrev.
2-torus	$(0, 0, -, -)$	No	Moving point	1MPA
Double 2-torus	$(0, 0, -, -)$	No	2-point attractor	2MPA
3-torus	$(0, 0, 0, -)$	No	Moving limit-cycle	MLC
Strange nonchaotic	$(0, 0, -, -)$	Yes	1-d and folding	SNA
Strange chaotic	$(+, 0, 0, -)$	Yes	1-d and folding	SC

Table 3.1.: Characterisation of attractors. Modified from [56].

3.4.2. Major tongues: approximation

In this subsection, we give an analytical approximation of the border for the 1MPA solution, corresponding to $1:1$ synchronisation. As seen in chapter 1, in the case of periodic forcing of a phase oscillator, the border of the synchronisation – or Arnold tongue – can be derived analytically by requiring that the phase difference has a stable fixed point. In the present case, two independent frequencies, ω_1 and ω_2, are driving the

oscillator so that we can expect a double tongue structure: each tongue centred at the corresponding frequency, and corresponding to a solution that is synchronised to that frequency.

Another difference is that in the present case, the oscillator is nonlinear. We first make the rough assumption that radial dynamics in (3.3) is negligible in the 1MPA solution, $r(t) \simeq r_p = 1$, and that only the phase dynamics needs to be taken into account

$$\dot{\theta} = \omega_0 + \gamma[\sin(\omega_1 t) + \sin(\omega_2 t)]\cos\theta. \tag{3.5}$$

Using a trigonometric identity, Eq. (3.5) can be expanded as

$$\dot{\theta} = \omega_0 + \frac{\gamma}{2}[\sin(\theta + \omega_1 t) - \sin(\theta - \omega_1 t) + \sin(\theta + \omega_2 t) - \sin(\theta - \omega_2 t)]. \tag{3.6}$$

Now, we assume that the natural frequency of the oscillator is very close to the first frequency of the forcing, $\omega_0 - \omega_1 \ll 1$, and derive the border of the corresponding tongue similarly to chapter 2. In the reference frame rotating with angular velocity ω_1, $\psi = \theta - \omega_1 t$, the system reads

$$\dot{\psi} = (\omega_0 - \omega_1) + \frac{\gamma}{2}[\sin(\psi + 2\omega_1 t) - \sin(\psi) + \sin(\psi + (\omega_1 + \omega_2)t) - \sin(\psi + (\omega_1 - \omega_2)t)]. \tag{3.7}$$

Assuming γ is small, the second term on the right-hand side of the equation is $O(\gamma)$, and hence ψ is varying *slowly*. However, $2\omega_1 t$, $(\omega_1 + \omega_2)t$, and $(\omega_1 - \omega_2)t$ correspond to fast oscillations. Thus, we can approximate those terms by assuming that ψ is almost constant over one period of the fast oscillations, and average them over that time. This yields, for the first term, the average

$$\frac{1}{T_1}\int_0^{T_1} dt' \sin(\psi + 2\omega_1 t') = 0, \tag{3.8}$$

where $T_1 = \frac{2\pi}{2\omega_1}$. Similarly, integrated over their own period, the two other fast oscillating terms average to zero, so that (3.7) becomes

$$\dot{\psi} = (\omega_0 - \omega_1) - \frac{\gamma}{2}\sin(\psi). \tag{3.9}$$

This is the Adler equation (2.17) discussed in chapter 2, with a rescaled coupling strength.

As discussed previously, this equation exhibits synchronisation, which corresponds in this case to a phase-locked solution of the system, with main frequency ω_1. The fixed point is given by $\psi^* = \arcsin \frac{2\Delta\omega}{\gamma}$ which only exists for

$$\gamma \geq 2|\Delta\omega|. \tag{3.10}$$

The latter inequality is an approximation of a region of the phase diagram, for small γ, and natural frequency close to ω_1, where the system has a single point attractor. Another such regions, this time for a solution with main frequency ω_2 is derived similarly by assuming, $\omega \simeq \omega_2$. The derived borders, of slopes ± 2, are shown in parameter space in Fig. 3.2.
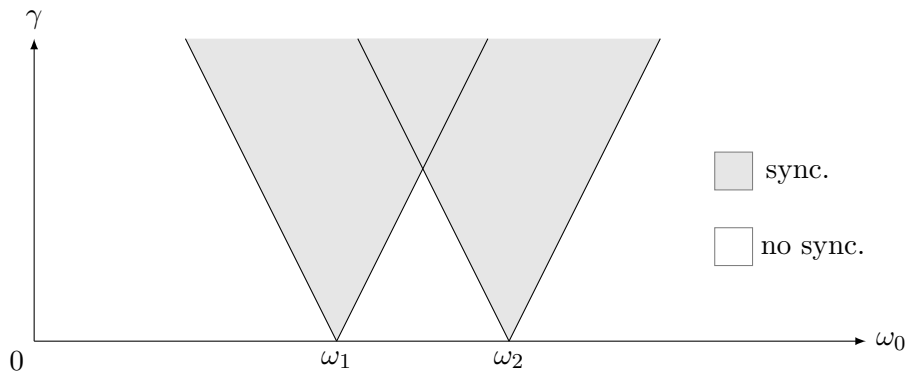
Figure 3.2.: Double Arnold tongue structure in parameter space, analytically approximated, and given by Eq. (3.10).

3.5. Numerical characterisation

In this section, we characterise the different dynamical regimes and determine the tongue structure of parameter space.

3.5.1. Lyapunov exponents

First, the maximal LE is computed numerically, over parameter space, as shown in Fig. 3.3. This is done by applying Benettin's algorithm [17, 18]. In order to do so, (x, y) of system (3.1) was integrated together with vectors $(\delta x, \delta y)$ in tangent space obeying
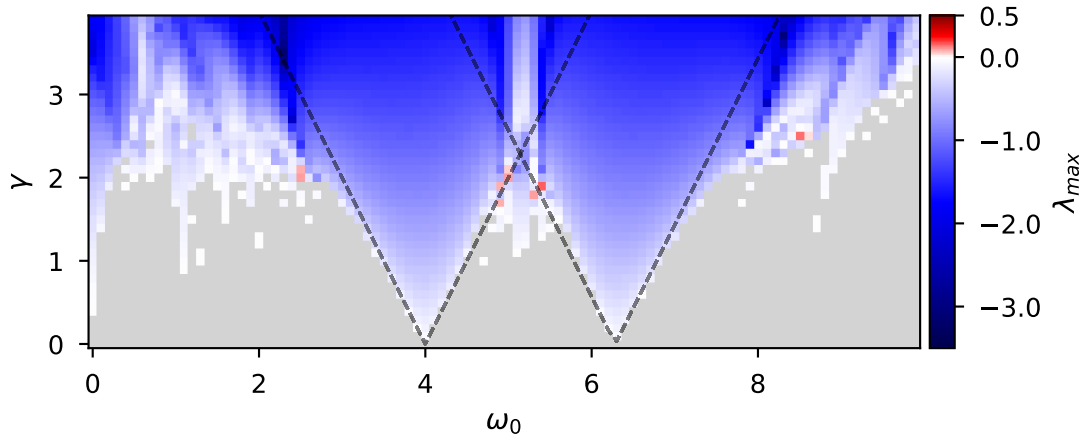
Figure 3.3.: Maximum Lyapunov exponent across parameter space: double Arnold tongue structure. Other subtongues are also present, as well as some small chaotic regions close to tongue borders. Dashed black lines represent the approximate border of the region 1MPA region, given by Eq. (3.10). Grey represents values that are numerically zero (in this case, when $|\lambda_{max}| < 10^{-2}$, due to numerical precision).

the linearised system (3.1).

$$
\begin{aligned}
\dot{\delta x} &= \left(\epsilon \left(r_p - \sqrt{x^2 + y^2} \right) - \frac{\epsilon x^2}{\sqrt{x^2 + y^2}} \right) \delta x - \left(\frac{\epsilon xy}{\sqrt{x^2 + y^2}} + \omega_0 \right) \delta y, \\
\dot{\delta y} &= \left(\epsilon \left(r_p - \sqrt{x^2 + y^2} \right) - \frac{\epsilon y^2}{\sqrt{x^2 + y^2}} \right) \delta y - \left(\frac{\epsilon xy}{\sqrt{x^2 + y^2}} - \omega_0 \right) \delta x.
\end{aligned}
\tag{3.11}
$$

The RK4 time step used was 0.01 s for a total time of 1000 s and the orthonormalisation was performed every 0.1 s using the Gram-Schmidt procedure. The LE was computed for a random initial condition, drawn for (x, y) in $[-1, 1] \times [-1, 1]$ and the 2 tangent vectors were drawn randomly, and then made orthonormal.

The maximum LE λ_{max} in Fig. 3.3 clearly shows two main tongues where $\lambda_{max} < 0$, corresponding to a synchronisation regime. Strictly speaking, a negative LE can correspond to synchronisation or to an SNA, as discussed previously and summarised in Tab. 3.1. However, further analysis such as the cluster analysis provided below confirms that in this case, a negative LE corresponds almost always to synchronisation and not to an SNA. The borders of those two Arnold tongues is well approximated by formula (3.10) (see dashed black lines). Finer details of the parameter space structure reveal sub-tongues of negative LE values, which correspond to $n{:}m$ synchronisation, as will be investigated below in further details. The rest of parameter space is, as expected, mainly a large region of the moving limit-cycle behaviour, defined unequivocally by a zero LE. Finally,

small regions of $\lambda_{max} > 0$ indicate chaotic dynamics. It is known that chaotic dynamics can occur in quasiperiodically forced oscillators, and that these are confined in regions in parameter space that tend to be small [35, 39]. Moreover, they tend to occur near (small) regions of SNAs. Different routes to chaos have been described in the literature, see [35] and references therein.

In the next section, we differentiate between single and multiple point attractors by means of a clustering analysis.

3.5.2. Multistability

In this section, we further analyse the synchronisation tongues, and differentiate between the different $n{:}m$ sub-tongues, which cannot be differentiated solely based on λ_{max}.

As described in chapter 2, $n{:}m$ synchronisation corresponds to the driving completing n of its periods while the driven oscillator completes exactly m. Here, we focus on the $n{:}1$ cases, where the driving oscillates n times faster than the oscillator it drives. As mentioned in [127] and explained in [33], in the case of periodic driving, for $n{:}1$ synchronisation, random initial conditions will converge to n different solutions. In other words, there are n coexisting attracting solutions, and different initial conditions will end up on the any of those: the system is multistable. Moreover, in the periodic forcing case, those coexisting solutions are periodic and time-shifted versions of each other. If the forcing is quasiperiodic as in the present case, however, there can still be multiple attracting solutions, but they are neither periodic, nor time-shifted versions of each other. The number of coexisting solutions depends on the parameters of the driving and of the driven system. Finally, the *basin of attraction* of a solution is defined as the region in state space in which initial conditions will converge to that solution. Basins of attraction give additional information about the structure of the state space and the stability of its attracting solutions.

In order to differentiate between the various synchronisation tongues, we follow the approach used in [33] and use a numerical clustering technique to assess multistability. The procedure is as follows. First, evolve a (large) number of random initial conditions covering the state space. Then take the positions of all trajectories at a fixed time, after transients: this is a so-called *ensemble snapshot* of the system at that time. Such a
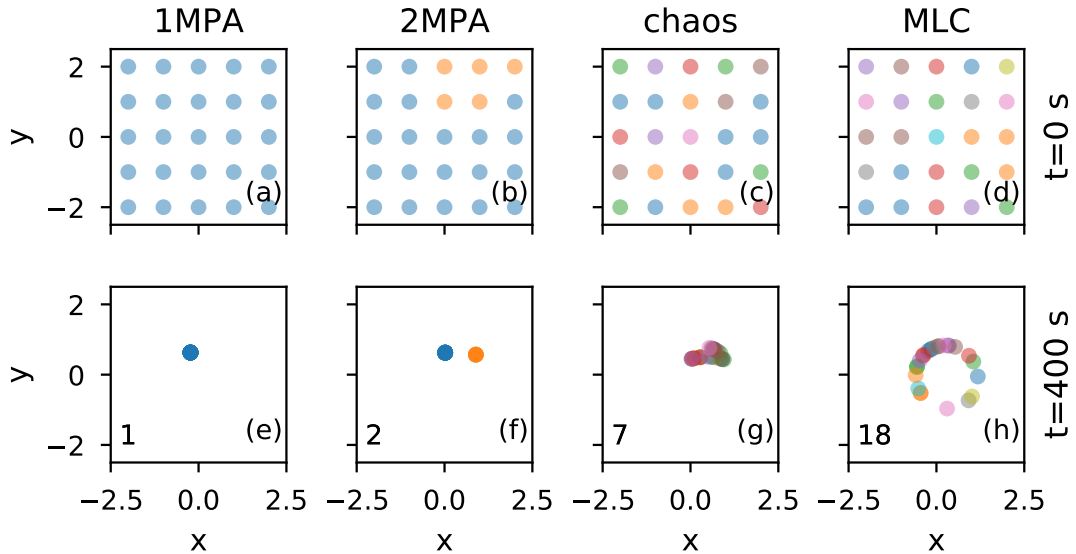
Figure 3.4.: Multistability from clustering. (a)-(d) Set of initial conditions covering state space for 4 different regimes and (e)-(h) their state after 400 s. In (e)-(h), the number in the bottom left corner indicates the number of clusters detected. Different colours represent different clusters, obtained form (e)-(h). Hence, in (a)-(d), all points of a given colour represent the basin of attraction of the cluster corresponding to that colour (meaningful here only for point attractors).

snapshot will resemble one of the cases of Fig. 3.1. Finally, using an appropriate clustering technique, count the number of clusters of trajectories present in the snapshot. For each set of parameters, 100 random initial conditions were evolved. A *mean shift* clustering [27] technique was used, namely the Python function `sklearn.cluster.MeanShift` with parameters `bandwidth=0.1` to optimise success of the clustering for the considered system, and `bin_seeding=True` to speed up the process.

The results obtained by such procedure are illustrated in Fig. 3.4 for 4 different regimes: 1MPA, 2MPA, chaos, and MLC. The clustering reaches the following conclusions: when the trajectories are clearly clustered in a few ($\lesssim 4$) clusters, the algorithm successfully detects the exact number of clusters. In the case of the moving limit-cycle regime, or the chaotic one-dimensional attractor however, the clustering technique detects multiple clusters. In both those cases, exactly how many clusters are detected is dependent on the clustering algorithm and the parameters used. However, the exact number is not important in this case, since there is no true number, and a high number is already indicative of not being a multiple point attractor. A clustering technique alone is not able to differentiate between the MLC and the chaotic attractor, but this can be achieved based on their LE which is zero and positive, respectively.
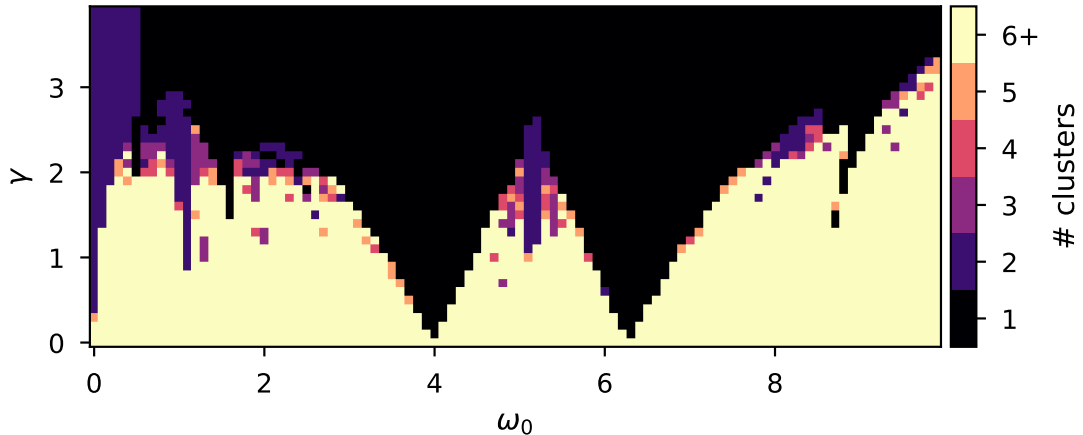
Figure 3.5.: Multistability: number of clusters across parameter space. A value of 1 corresponds to a single MPA. A value of 2 and 3 corresponds to a 2MPA and 3MPA, respectively. High values, i.e. higher than 6, are surely a one-dimensional attractor: either a MLC, or a chaotic attractor or SNA. Values in between 3 and 6, as computed here, do not differentiate unequivocally between point attractors and one-dimensional attractors. The number of clusters is computed as follow: evolve a grid of initial conditions, and after transients, use a mean shift clustering algorithm.[1] More details in main text.

The results of the described clustering analysis are shown in Fig. 3.5 over parameter space. First, the structure of state space obtained here agrees with that obtained from the LEs and shown in Fig. 3.3. Second, it allows to clearly associate different tongues to different regimes of multistability. Indeed one can clearly observe two main tongues of 1:1 synchronisation, as well as smaller tongues of 2:1 and 3:1 synchronisation.

The described clustering process is not perfect, as intermediate numbers of clusters such as 5 are not conclusive without a closer examination. The process can be fine tuned, but the present setting is good enough for our purpose, and reveals the tongue structure.

3.5.3. No rotation

In this section, the case with no rotation, $\omega_0 = 0$, is investigated, as it is makes a more analytical understanding of state space possible. For the ease of the reader, we write the system considered, i.e. system (3.1) with no rotation

$$
\begin{aligned}
\dot{x} &= \epsilon \left(r_p - \sqrt{x^2 + y^2} \right) x, \\
\dot{y} &= \epsilon \left(r_p - \sqrt{x^2 + y^2} \right) y + \gamma f(t),
\end{aligned}
\tag{3.12}
$$

First, note that the system is now invariant under the transformation $x \mapsto -x$. In other

words, the system on the right side of the y-axis is a mirror image of that on its left side. This symmetry is broken in the general rotating case.

We now derive the *nullclines* of the system. The x-nullcline is defined as the set of points for which $\dot{x} = 0$. Identically, the condition $\dot{y} = 0$ defines the y-nullcline. Fixed points are found at the intersection between the x and y-nullcline.

First, we simplify the system even more by assuming $\gamma = 0$. Then, nullclines are as follows

$$x\text{-nullcline:} \qquad x = 0 \text{ and } x^2 + y^2 = r_p, \tag{3.13}$$

$$y\text{-nullcline:} \qquad y = 0 \text{ and } x^2 + y^2 = r_p. \tag{3.14}$$

The circle of radius r_p is stable radially and neutrally stable in the angular direction. All trajectories are attracted to that circle, but do not rotate on it. The origin is an unstable fixed point.

Now, in general $\gamma \neq 0$. Then, the x-nullclines are not changed, but the y-nullclines are. Moreover, they are changing quasiperiodically in time. This is illustrated in Fig. 3.6, where the nullclines are computed numerically and shown for three fixed values of $f(t)$ showing different topology, namely 0, 0.5, and 1.3. Note the graph for $-f(t)$ is the same as that for $f(t)$ (opposite value), but upside-down ($y \mapsto -y$).

(a) $f(t) = 0$ **(b)** $f(t) = 0.5$ **(c)** $f(t) = 1.3$
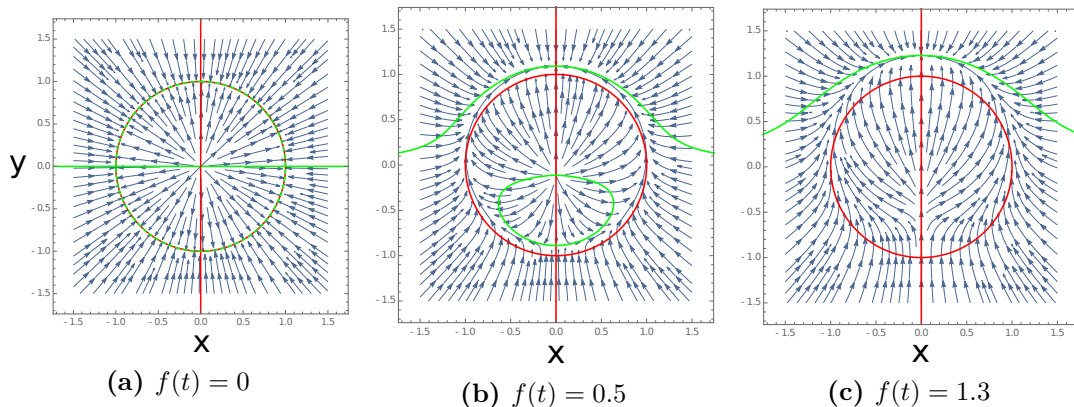
Figure 3.6.: Vector field in state space at different times, for $\epsilon = 5$, $r_p = 1$, and $\gamma = 1$. x and y nullclines are in red and green, respectively. The $f(t)$ interval for the existence of 3 fixed points (but only one stable) is $[-1.25, 1.25]$ (*cf* figure 3.7). The graph for $-f(t)$ is the same as that for $f(t)$ (opposite value), but upside-down ($y \mapsto -y$).

Here, investigating the structure of state space and its attractors for fixed values of time can provide at best qualitative insight about the dynamics. Indeed, since $f(t)$ changes at

a similar timescale to the driven oscillator, the latter does not have time to converge and reach the new attractors. Rather, the attractors change in time and trajectories keep converging to them without ever reaching them. Trajectories would reach the attractors only if $f(t)$ was very slow compared to the oscillator dynamics (this approach is used in chapters 4, 5, and 6).

Despite the above considerations, understanding the time-dependent structure of state space and the existence of attractors can be useful. From Fig. 3.6, one can see that all fixed points are on the y-axis at those fixed times. Other effective fixed points can also exist in the rest of the state space, as we shall see below, but first the fixed point on the vertical axis are investigated analytically.

Dynamics on the y-axis

First, notice that the y-axis is an invariant subspace. Indeed, $\dot{x} = 0$ if $x = 0$ so that all points on the y-axis remain on it. One can solve exactly the intersection of the y-nullcline with the y-axis, $x = 0$

$$\epsilon \left(r_p - |y| \right) y + \gamma f(t) = 0. \tag{3.15}$$

which has solutions

$$y_{\pm}^{+} = \frac{r_p}{2} \pm \frac{1}{2} \sqrt{r_p^2 + \frac{4\gamma f}{\epsilon}}, \tag{3.16}$$

if $y > 0$, and solutions

$$y_{\pm}^{-} = -\frac{r_p}{2} \pm \frac{1}{2} \sqrt{r_p^2 - \frac{4\gamma f}{\epsilon}}, \tag{3.17}$$

if $y < 0$.

These functions are illustrated in a bifurcation diagram in Fig. 3.7. The linear stability is assessed and displayed in the figure. For any given value of time t, $f(t)$ takes values in $[-2, 2]$. Outside of the interval $[\frac{-\epsilon}{4\gamma}, \frac{\epsilon}{4\gamma}]$, the system has one stable fixed point. Inside the interval, however, three fixed points are present: one stable, one unstable, and one saddle node. The saddle node is however stable along the y-axis so that the y-dynamics has two stable and one unstable fixed points. As time evolves, and $f(t)$ takes all possible values in the interval $[-2, 2]$, trajectories go through a hysteresis cycle. Indeed, when the driving $f(t)$ is maximum, all trajectories converge to the unique stable fixed point and

3. Attractors and multistability for a quasiperiodically driven oscillator
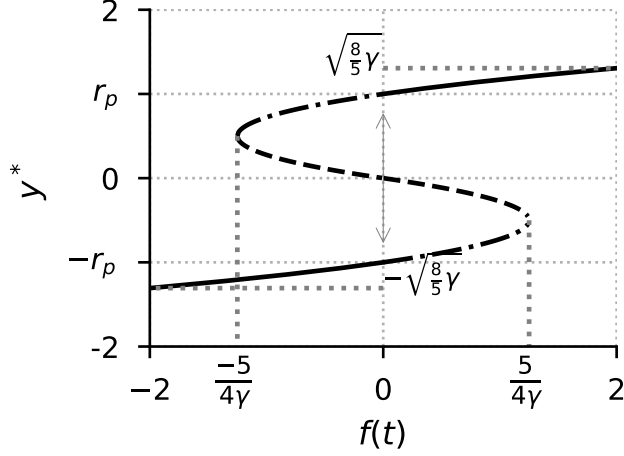
Figure 3.7.: Fixed points on the y-axis, as a function of the forcing $f(t)$, given by Eqs. (3.16) and (3.17). Solid, dashed, and dotted-dashed black curves represent stable, unstable, and saddle points, respectively. The saddle points are stable along the y-axis, so that the system exhibits hysteresis on the y-axis. Parameter $\epsilon = 5$.
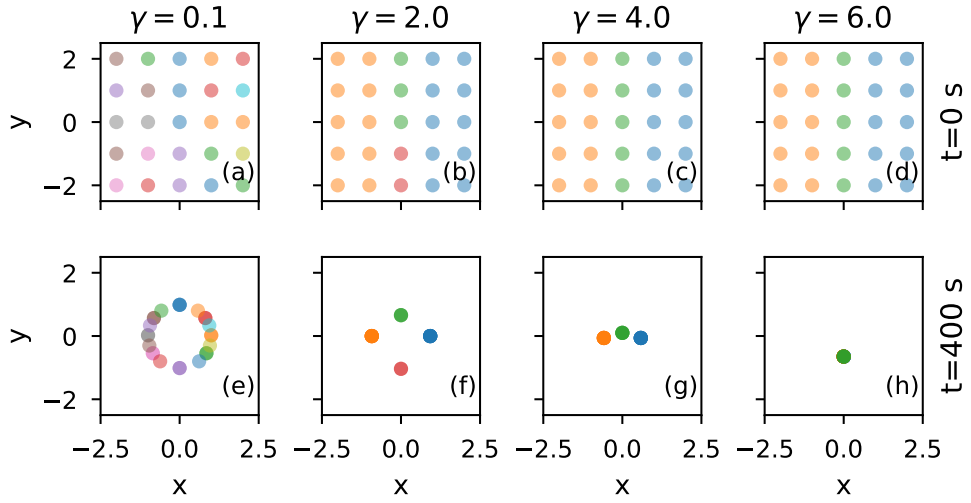
Figure 3.8.: Effective bifurcation for ω_0, no rotation, obtained by numerical integration and clustering. As γ is increased from 0, the system exhibits a first transition at $\gamma \simeq 0.5$ from MLC to 2+2 moving point attractors (2 on the y-axis and 2 elsewhere). At $\gamma \simeq 2.5$ the transition goes from 2+2 moving point attractors to 1+2 moving point attractors. Finally, above $\gamma \simeq 6$, all point attractors merge into a single 1MPA. This confirms the qualitative behaviour expected from Fig. 3.7: as γ is increased, on the y-axis, the two point attractors merge into one. Each cluster in (e)-(h) is represented by a different colour, and the same colour is used for the initial conditions in the corresponding basin of attraction in (a)-(d).

stay on the stable branch (black solid line in Fig. 3.7) as $f(t)$ takes lower values, and until it takes values smaller than $\frac{-\epsilon}{4\gamma}$ and jumps to the other unique stable fixed point.

The range of $f(t)$ values – and hence the amount of time – for which there exists two stable fixed points depends on the driving strength γ. Indeed, as γ is increased, the interval $\left[\frac{-\epsilon}{4\gamma}, \frac{\epsilon}{4\gamma}\right]$ tends to the singleton $\{0\}$, and the system has one stable fixed point at any moment in time. On the other hand, if $\gamma < \gamma^* = \epsilon/8$, the y-axis dynamics has two stable fixed points at any given time and does not go through hysteresis. The actual

bifurcation is illustrated in Fig. 3.8.

3.6. Summary

In this chapter, we have considered a quasiperiodically forced oscillator. Quasiperiodic driving was chosen as a starting point for the study of aperiodic driving, and other types of aperiodicity will be investigated in the subsequent chapters. The different types of dynamics exhibited by the system were described and investigated. In particular, the synchronisation and moving limit-cycle regimes were analysed in greater detail due to their relevance for the remainder of the thesis. Analytical and numerical results were provided. The structure of parameter space was assessed mainly using LEs and a clustering technique. The strange regimes – chaotic and nonchaotic – have been described and the chaotic regime has been identified in parameter space using Lyapunov exponents. The interested reader will find diverse techniques in the literature to characterise those regimes in greater detail, see for example [39] and references therein.

In the next chapter, aperiodicity in the driving consists of single main frequency, but modulated over time. Similar analysis in terms of Lyapunov exponents will be performed.

Part I.

Time-varying frequency of external driving

4. Stabilisation by nonautonomous driving

4.1. Introduction

Complex oscillatory dynamics abounds in nature. Despite many real-life examples exhibiting stable oscillations with a time-varying frequency (e.g., [22, 61, 85]), little is known theoretically about the properties of this type of behaviour. This kind of oscillation requires aperiodic external driving, making the system nonautonomous by nature [72], such that most of the traditional analytical methods are unusable or insufficient. The case of periodic forcing with a constant frequency, which has been extensively investigated to date, is often too simplistic to account for reality. In the previous chapter, quasiperiodic driving was considered, which is the simplest autonomous aperiodic driving.

In this chapter, we consider another much less studied type of aperiodic driving: driving with time-varying frequency. We consider oscillators subject to driving with slowly varying frequency, and investigate both short-term and long-term stability properties. This work aims at filling the gap between the existing theory of deterministically driven systems where constant frequency is typically assumed and the statistical theory of systems driven by noise.

We present three major contributions to the field of interacting nonautonomous systems: Firstly, we present notions of stability, synchronisation and instantaneous frequency entrainment in the nonautonomous setting, and the relationships between these concepts; and we investigate these concepts for the simplest example of a phase oscillator subject to driving with slowly time-varying frequency. In so doing, we enable the notion of chronotaxicity [149–151] to be broadened beyond its current description, and we compare the stability properties in this setting with the traditional settings of fixed-frequency driving on the one side and driving by stationary noise on the other. Secondly, we

introduce an approach to analysing time-dependent dynamical stability from a time-series consisting of time-localised LEs, that is, finite-time LEs taken over a time-window with a moving centre. By contrast, typically, dynamical stability is assessed only in terms of time-averaged stability, for example by the asymptotic LE [125]. Thirdly, numerically and analytically, we show enlargement of the stability region in parameter space for the phase oscillator subject to driving with slowly varying frequency, and we show that this growth is specifically due to the growth of a subregion characterised by intermittent synchronisation where the time-localised dynamical stability is varying. This mathematical phenomenon of stabilisation has two major practical implications: (i) deterministically varying the frequency of external driving could be implemented as a means of inducing stability in complex systems, and (ii) dynamical systems where stability is induced by deterministic frequency variation are an excellent candidate for modelling living systems, which are highly complex and yet usually operate stably within a time-varying environment.

The chapter is organised as follows. In Sec. 4.2, we introduce a simple one-dimensional phase oscillator model. We then provide an explanation of notions of synchronisation and stability for nonautonomous systems, followed by a theoretical analysis of the one-dimensional model, showing the enlargement of the stability region, as well as the birth of an intermediate region of intermittent synchronisation. We illustrate these phenomena with numerical results for both long-time and short-time behaviour. In particular, in Sec. 4.2.5, we discuss the relationship between the deterministic system considered here and the analogous case with noisy driving as considered in previous works. In Sec. 4.3, we illustrate the stabilisation phenomenon numerically in higher-dimensional systems, and argue that it is of general importance. Finally, in Sec. 4.4 we discuss the results, and in Sec. 4.5 we provide a brief summary.

4.2. One-dimensional case

4.2.1. Model

The system we consider is a driven phase oscillator of the form

$$\dot{\theta}_1 = \omega_1 + \gamma \sin[\theta_1 - \theta_0(t)], \tag{4.1}$$

4. Stabilisation by nonautonomous driving

where the driving has strength γ, phase $\theta_0(t)$, and a time-varying frequency

$$\dot{\theta}_0 = \omega_0[1 + kf(\omega_m t)], \tag{4.2}$$

where ω_0 is the non-modulated driving frequency, f is a bounded function, and ω_m and k are the modulation frequency and relative amplitude, respectively. The phase oscillator θ_1 may represent, for example, the phase on the stable limit cycle of an oscillator satisfying

$$\begin{cases} \dot{r} &= \epsilon(r_p - r)r \\ \dot{\theta}_1 &= \omega_1 + \gamma \sin[\theta_1 - \theta_0(t)] \end{cases} \tag{4.3}$$

where r_p is the amplitude of the limit cycle and ϵ is the restoring constant.

Note that if $f(\omega_m t)$ is itself the solution of a dynamical system, system (4.1)-(4.2) can be seen as an autonomous system in an extended state space by adding the variables corresponding to that system to the state space, as discussed in chapter 2. However, $f(\omega_m t)$ need not in general be the solution of a dynamical system. Moreover, even if it is, the dimension of that system can make the extended state space impractical to work with when too many variables need adding.

The unforced system (4.1) with $\gamma = 0$ is a typical autonomous phase oscillator [146], and hence its phase is neutrally stable (zero LE).

In the forced system, i.e. $\gamma \neq 0$, the traditional constant-frequency forcing case, presented in Eq. (2.15), is recovered for $k = 0$. As described in chapter 2, in this case, depending on the parameters, the system lies in one of two regimes: either 1:1 synchronisation (negative LE), or neutral stability (zero LE). The condition for synchronisation, $\gamma > |\Delta\omega|$, with the frequency mismatch $\Delta\omega = \omega_1 - \omega_0$, is derived analytically [127] by requiring that the equation for the phase difference

$$\dot{\psi} = \Delta\omega + \gamma \sin\psi \tag{4.4}$$

has a stable fixed point. This condition for synchronisation corresponds to a so-called Arnold tongue [6] in (γ, ω_1)-parameter space. This Arnold tongue can be seen in Fig. 4.2(a) as the region appearing in shades of blue, corresponding to negative values of

the numerically computed LE. Since (4.4) is an autonomous differential equation, the numerical LE computed over a long time will approximate well the asymptotic LE, except possibly when the parameters lie extremely close to the border of the Arnold tongue. Note that Eq. (4.4) is the in fact the Adler equation (2.17) presented in chapter 2, and will now be referred to as Eq. (4.4).

For $k \neq 0$, the equation for the phase difference is now the *nonautonomous* equation

$$\dot{\psi} = \Delta\omega(t) + \gamma \sin \psi, \tag{4.5}$$

with frequency mismatch $\Delta\omega(t) = \omega_1 - \omega_0[1 + kf(\omega_m t)]$. Throughout this paper, we assume that the modulation is much slower than the dynamics of the system, i.e. ω_m is very small.

4.2.2. Synchronisation in autonomous and nonautonomous systems

Suppose an oscillatory system θ_1 with no internal time-dependence is subject to driving from another oscillator θ_0 with fixed frequency different from the natural frequency of θ_1. We say that θ_1 *is synchronised to* θ_0 if over time, the trajectory of θ_1 loses memory of its precise initial phase and instead follows a periodic behaviour whose period is a rational multiple $\frac{n}{m}$ of the period of θ_0. In this case, we say that θ_0 *entrains* the frequency of θ_1, and we describe the synchronisation as $n:m$ synchronisation. This implies in particular that the difference in unwrapped phase between an n-fold cycle of θ_0 and an m-fold cycle of θ_1 stays bounded over all time – a phenomenon referred to as *phase-locking* between θ_1 and θ_0.

The particular phenomenon that $\theta_1(t)$ loses memory of its initial phase is called *phase stability*. If θ_1 is a phase oscillator (as in our model), then phase stability can be assessed in terms of the sign of Lyapunov exponent associated to the trajectory $\theta_1(t)$: a negative LE indicates stability. Stability inherently implies resilience against the effects of other possible perturbations not accounted for in the model. When the phase of a driven oscillator is stabilised by a fixed-frequency driving oscillator, typically this implies $n : m$ synchronisation for some integers n and m; we emphasise that this statement is specific to fixed-frequency driving. For $n : m$ synchronisation where (in lowest terms)

$n \geq 2$, it is not possible for $\theta_1(t)$ to lose *all* memory of its initial phase: for any $1 \leq i \leq n-1$, delaying the initial phase by a suitable amount will delay the phase of the eventual periodic motion by $\frac{i}{n}$. However, in the case of $1\!:\!m$ synchronisation, it is possible for θ_1 eventually to lose all memory of its initial phase; in this case, we say that the phase is *globally stable.*

Synchronisation has also been investigated in the context of systems driven by noise, such as zero-mean Gaussian white noise or a pulse train with independent and identically distributed consecutive waiting times [123, 127, 158]. For an oscillator θ_1 driven by such noise, one does not have a notion of $n\!:\!m$ synchronisation between this driven oscillator and the noise ξ driving the oscillator. This is because, even if the noise is stationary noise, any one realisation of the noise does not have a deterministic periodic behaviour. As described in [127, Section 15.2], instead of defining synchronisation in terms of "phase locking", one can think of synchronisation here as meaning that over time, θ_1 loses memory of its precise initial state and instead follows *some path* that is determined by the realisation of the noise – but since the noise itself has no deterministic regular behaviour, this phenomenon can only be physically manifested as *synchronisation by common noise* between copies of θ_1.

Synchronisation by common noise is a particular case of the phenomenon of synchronisation by common external driving (which may be noisy or deterministic): Suppose we have an array $\theta^1, \ldots, \theta^n$ of self-sustained oscillators whose internal dynamics are described by exactly the same system $\dot{\theta}^i = f(\theta^i)$, where f does not depend on i; and no *direct* coupling is introduced between these oscillators, but instead all these oscillators are *simultaneously subject* to driving from the same external driver $p(t)$ (which could be noisy or deterministic). Thus the n driven oscillators are now *indirectly* coupled, and it may happen that as a result of this indirect coupling, over time the trajectories of θ^i lose memory of their initial states and instead follow the same path as each other. This may be viewed as a kind of perfectly instantaneous $1\!:\!1$ synchronisation between the driven oscillators.

The relationship between the above concepts is as follows. For a self-sustained phase oscillator θ_1 subject to driving by an external driver $p(t)$, the following statements are equivalent:

4. Stabilisation by nonautonomous driving

The physical interpretation of the implication (ii)$\Rightarrow$(i) is that the driving $p(t)$ causes θ_1 to become resilient in its course of following the path laid out by $p(t)$, although as we shall see, this resilience may only be intermittent. Such driving-induced resilience may play an important role in many real-world systems that exhibit remarkable stability in the face of continuous environmental perturbations.

In our model, if $k \neq 0$ then the driving is a deterministic oscillator θ_0 with non-fixed frequency. Hence, it will be useful for us to discuss notions of synchronisation for oscillators subject to deterministic oscillatory driving with time-varying frequency. Such driving shares in common with fixed-frequency driving that it is deterministic and oscillatory, and it shares in common with noisy driving that it does not possess a phase which proceeds in cycles of a fixed period. Therefore, on the one hand, as with noisy driving, it is not clear that one can correctly define a notion of $n\!:\!m$ frequency entrainment, though the slightly weaker phenomenon of $n\!:\!m$ phase-locking can still occur; nonetheless, as in [65], one can still consider the question of whether identical copies of the driven oscillator are caused to synchronise by simultaneous driving from the driving oscillator.

Having stated that $n\!:\!m$ frequency entrainment is difficult to define in our setting, let us now highlight our slow variation assumption. Under this assumption, one can define a notion of *instantaneous frequency entrainment.* In general, if a pair of phase oscillators θ_1, θ_0 is governed by a *nonautonomous* differential equation

$$\begin{cases} \dot{\theta}_0 & = & f_1(t, \theta_0) \\ \dot{\theta}_1 & = & f_2(t, \theta_0, \theta_1) \end{cases} \tag{4.6}$$

and it is assumed that $f_1(t, \cdot), f_2(t, \cdot, \cdot)$ vary slowly with t, then we can say that there is frequency entrainment at time t if the solution of the associated autonomous differential equation

$$\begin{cases} \frac{\mathrm{d}}{\mathrm{d}s}\theta_0(s) & = & f_1(t, \theta_0(s)) \\ \frac{\mathrm{d}}{\mathrm{d}s}\theta_1(s) & = & f_2(t, \theta_0(s), \theta_1(s)) \end{cases} \tag{4.7}$$

exhibits frequency entrainment. In the case of our model, at any time t, there is instantaneous $1\!:\!1$ frequency entrainment between θ_1 and θ_0 if and only if the differential equation $\frac{\mathrm{d}}{\mathrm{d}s}\psi(s) = \Delta\omega(t) + \gamma\sin\psi(s)$ has a stable fixed point [compare with Eq. (4.4)].

Just as negative Lyapunov exponents are connected with the presence of frequency entrainment for fixed-frequency driving, so likewise instantaneous frequency entrainment will typically be connected with negative *finite-time* Lyapunov exponents defined over a suitable time-window. Finite-time Lyapunov exponents are a measure of stability over finite timescales. We will use the term *time-localised Lyapunov exponent* to refer to FTLE taken over a sliding time-window $[t, t + \tau]$ which slides along with time t. By contrast, we will use the term *long-term Lyapunov exponent* to refer to a Lyapunov exponent taken over a long time-interval $[0, T]$; when clear from the context, we will sometimes drop the word "long-term". Technically, a long-term LE is still a finite-time Lyapunov exponent, but it plays a similar role to asymptotic LE for autonomous systems. Asymptotic LE need not exist for nonautonomous systems – indeed, nonautonomous systems need not even be well-defined over infinite-time. But moreover, even if they can be defined, asymptotic LE may not necessarily be physically relevant for the limited timescales on which a system is considered in practice.

4.2.3. Theoretical analysis

In contrast to the autonomous case, the existence of an attracting equilibrium point for the vector field on the right-hand side of Eq. (4.5) (regarded as a function of ψ) can change with time t; as shown in Fig. 4.1(a), for a sinusoidal modulation $f(\cdot) = \sin(\cdot)$, if k is large enough then within each modulation period the vector field undergoes two saddle-node bifurcations. Since we assume that the modulation is much slower than the dynamics of the system, the system adiabatically follows the moving attracting point $\psi_{\text{slow}}(t) = \pi - \arcsin[-\Delta\omega(t)/\gamma]$ for Eq. (4.5), when it exists. (A more technically precise description of how ω_m needs to compare with the values of other parameters in order to qualify as "small" for the purposes of this adiabatic approach can be found in [65].) On faster timescales, one could view $\Delta\omega(t)$ as approximately constant and consider the stable point in the quasi-stationary limit.

Following the idea that solutions follow the moving attracting point ψ_{slow} when it exists, we derive three regions, with qualitative features corresponding to the following conditions on Eq. (4.5): (I) no existence of the attracting point at any time t, (II) existence of the attracting point for all t, and (III) alternation over time between the existence and
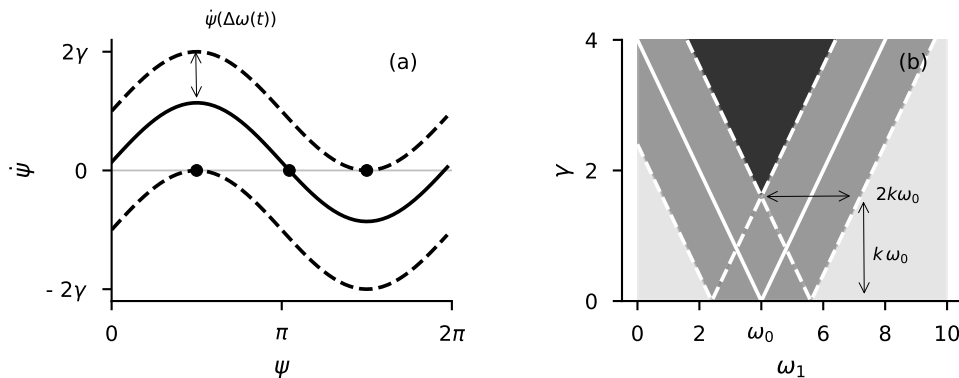
Figure 4.1.: (a) Time-varying existence of the attracting point of Eq. (4.5). The $(\Delta\omega(t))$-dependent curve of $\dot{\psi}$ against ψ moves up and down over time, as indicated by the two solid lines representing where the curve could be at two different instants in time. When this curve lies between the dashed lines, the system has an attracting point, and otherwise, not. (b) Phase diagram showing three regimes. Light (region I in the text), medium (region III), and dark grey (region II) show where the system is never synchronising, intermittently synchronising, and always synchronising, respectively. Solid white curves show the border between synchronisation and non-synchronisation for if $f(\cdot)$ is set to 0; and white dashed curves show the border between synchronisation and non-synchronisation for if $f(\cdot)$ is set to ± 1. When k is increased, regions I and II decrease while region III increases; hence in particular, the Arnold tongue consisting of the union of regions II and III increases.

non-existence of the attracting point. If we assume that $f(\cdot)$ varies throughout the interval $[-1, 1]$, then these conditions on the parameters are precisely

$$\text{(I):} \quad \gamma \leq |\omega_1 - \omega_0| - \omega_0 k, \tag{4.8}$$

$$\text{(II):} \quad \gamma \geq |\omega_1 - \omega_0| + \omega_0 k, \tag{4.9}$$

$$\text{(III):} \quad |\omega_1 - \omega_0| - \omega_0 k \leq \gamma \leq |\omega_1 - \omega_0| + \omega_0 k, \tag{4.10}$$

as illustrated in Fig. 4.1(b). In region I, the slow variation assumption implies that solutions behave similarly to the neutrally stable regime of the fixed-frequency-driving system; solutions of (4.1) or (4.5) will exhibit neutral stability, with a long-term Lyapunov exponent that is essentially zero. In region II, the attracting point exists at all times, and attracts solutions starting from throughout the circle to itself; thus, the driven oscillator θ_1 is globally stable, losing memory of its initial state and following the motion of $\theta_0(t) + \psi_{\text{slow}}(t)$. In particular, long-term LEs will be negative. There is instantaneous 1:1 frequency entrainment at all times; moreover, the attracting point moves within a bounded arc of the circle, and thus we have 1:1 phase-locking between θ_1 and θ_0.

In region III, the attracting point exists at some times but not other times. We refer to the

epochs during which the attracting point exists as stable epochs; the remaining epochs are epochs of neutrally stable dynamics. During the stable epochs, solutions from throughout the circle are attracted to the attracting point. While following the attracting point, these solutions pick up a negative contribution to the Lyapunov exponent, due to the gradient of the instantaneous vector field being itself negative at the attracting point; and then during each of the epochs of neutral stability, the solutions receive zero net contribution to the Lyapunov exponent, meaning that overall, as in [65], long-term LE are negative and the solutions remain synchronised with each other over all time. There is instantaneous $1:1$ frequency entrainment during the stable epochs but no instantaneous frequency entrainment during the epochs of neutral stability; we will refer to this phenomenon as *intermittent synchronisation*. Overall, we do not have phase-locking between θ_1 and θ_0. However, unlike in the case of fixed-frequency driving, synchrony of an array of identical copies of θ_1 [represented as different simultaneous solutions of Eq. (4.1)] is achieved and endures (even through the epochs of neutral stability) in the absence of a phase-locking mechanism. In other words, there does not need to be a phase-locking mechanism in place in order for the driving $\theta_0(t)$ to cause θ_1 to lose all memory of its initial condition and follow a path determined by the evolution of $\theta_0(t)$.

Let us mention that there will be some very small subregions of region III where in theory, if one waits long enough, θ_1 will come close to the instantaneous repeller around the start of a stable epoch [48] and thus receive a positive contribution to the LE, such that the reasoning here and in [65] can eventually break down and the asymptotic LE (if $f(\,\cdot\,)$ is defined *ad infinitum*) could even be zero.

So then, in analogy to the case of fixed-frequency driving, we define the *Arnold tongue* as being the union of region II and region III, that is, the total region where the long-term LE will be negative.

From Eq. (4.10), the role of the modulation amplitude k here is clear: as k increases from 0, regions I and II decrease in size (although still extending infinitely), being symmetrically pushed back by the appearance and growth of region III, such that overall, the Arnold tongue is enlarged. In other words, increasing modulation amplitude induces stability.

4.2.4. Numerical results

For our numerics in this section, we take $\theta_0(t) = \omega_0(t - \frac{k}{\omega_m}\cos(\omega_m t))$; so the frequency modulation $f(\omega_m t)$ is a sine wave $f(\omega_m t) = \sin(\omega_m t)$. Nonetheless, the results presented are just as valid for more general aperiodic slow modulation, and are demonstrated numerically to be true for aperiodic modulations in Sec. 4.2.6. We set $\omega_0 = 4$ and $\omega_m = 0.05$, except where stated otherwise, and we investigate the effect of the remaining free parameters γ, ω_1, and k. We integrate the two-dimensional system (4.3) with $r_p = 1$ and $\epsilon = 5$, except that for Fig. 4.3 (showing synchronisation between solutions of (4.1) with different initial conditions) and Fig. 4.6 (showing long-term LE together with average frequency entrainment), we simply integrate (4.1). All Lyapunov exponents, both long-term and time-localised, are computed following Benettin's canonical algorithm [17, 18]; for the time-localised LE, we use a moving average of the expansion coefficient. In (4.3), the radial LE at the limit cycle is equal to -5; therefore, since the maximum LE is greater than -5 in all our numerical experiments, it follows that this maximum LE corresponds to the phase dynamics defined by (4.1). The same is also true of time-localised LE, at least after the first few moments needed for the trajectory to approach the limit cycle.

First, we investigate the long-term stability of the system, by means of the numerically computed maximum LE defined over a long time-window. Stability is indicated by a negative value for the LE. In Fig. 4.2, we see that there is an Arnold tongue (shades of blue) similar to that shown in Fig. 4.1(b). As illustrated in Fig. 4.3, solutions of Eq. (4.1) synchronise with each other when the parameters lie in the Arnold tongue, but not when the parameters do not lie in the Arnold tongue. As shown in Fig. 4.2, the Arnold tongue is enlarged as the amplitude k of the frequency modulation is increased.

In other words, stability is induced by varying the frequency of the forcing over time. Quantitatively, we observe that the width of the Arnold tongue grows linearly with k.

While Fig. 4.2 shows the long-time stability, region III can only be distinguished and understood from the point of view of time-localised stability. The dynamics of Eq. (4.1) is illustrated over time for the three regions in Figs. 4.4(a)–4.4(f), by time-frequency representation and by time-localised LE – namely, maximum LE defined over the time-window $[t, t + \tau]$ where τ is a fixed number. Here, we take $\tau = 0.1$ s.
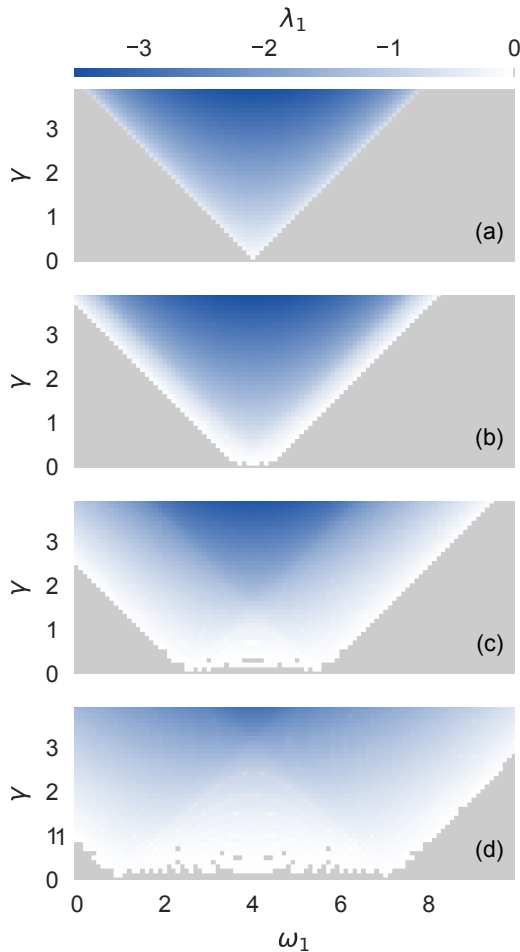
Figure 4.2.: Numerically obtained long-term maximum Lyapunov exponent λ_1 over parameter space for (4.3), with different k. The LE are computed over 5 cycles of the frequency modulation (about 630 s). In each case, 20 random initial conditions were taken from the square $[-1, 1] \times [-1, 1]$, and the average maximum LE over these trajectories is plotted. (a) $k = 0$, (b) $k = 0.1$, (c) $k = 0.4$, (d) $k = 0.8$. The Arnold tongue (shades of blue) is enlarged as k increases. Grey represents zero values.

Region III is a region of intermittent synchronisation where trajectories alternate between epochs of time-localised stability and epochs of time-localised neutral stability; indeed, as the time t evolves, the time-localised LE alternates between epochs where it is negative, and epochs where it oscillates with high frequency around an average value of zero, as is seen in Fig. 4.4(e). Averaging over the total time yields a negative LE, meaning overall stability on average, even though the short-term stability is time-varying. Region I is thus the only region with a long-term LE of zero, and this region decreases in size, which means that the region of stability increases.

The distinction between the three regions can be seen by looking at the time-frequency representation of a trajectory in each of these regions, as shown in Figs. 4.4(a)–4.4(c). In all three cases, the changing frequency of the driver is reflected in the frequency content of the driven oscillator. In Fig. 4.4(a), representing region II, the driving frequency is the only frequency present, as the frequency of the driven oscillator is entrained by that of the driving at all times. In Fig. 4.4(c), representing region I, we also see the natural

Figure 4.3.: Trajectories of five solutions $\theta^1(t), \ldots, \theta^5(t)$ of Eq. (4.1), with initial conditions $\theta^i(0) = \frac{i-1}{5}.2\pi$, subject to the same driving $\theta_0(t)$. Here, $\gamma = 2.5$ and $k = 0.4$. In (a), $\omega_1 = 4$, and so the system is in region II according to Eq. (4.9); in (b), $\omega_1 = 6$, and so the system is in region III according to Eq. (4.10); in (c), $\omega_1 = 9$, and so the system i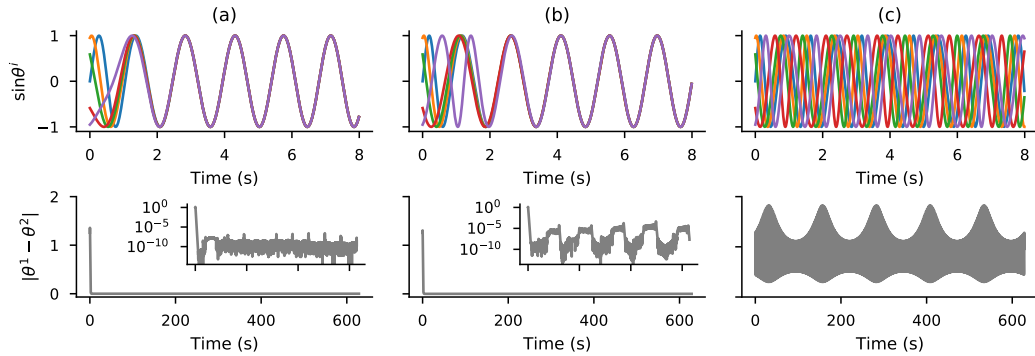s in region I according to Eq. (4.8). In each case, the upper plot shows the first 8 seconds of the sine of the five trajectories, while the lower plot shows the distance between $\theta^1(t)$ and $\theta^2(t)$ over about the first 630 seconds (more precisely, 5 cycles of the frequency modulation); in (a) and (b), the inner graph shows the same information on a logarithmic scale. In (a) and (b), the system lies within the Arnold tongue as described in Sec. 4.2.3, and the five trajectories are observed to synchronise and to remain in synchrony; by contrast, in (c), the system does not lie within the Arnold tongue, and no synchronisation is observed.

frequency of the driven oscillator (cream, representing the highest amplitude), though slightly modulated by the driving. The fact that these two frequency modes are distinct shows that the driven oscillator's frequency is not entrained by the driving at any time. In Fig. 4.4(b), representing region III, we see the maximum-amplitude frequency mode overlapping the driving frequency at some times, but not at other times. The times of overlap are when the frequency of the driven oscillator is entrained by that of the driving, and the other times are when there is no frequency entrainment. Thus, in this region, we have intermittent frequency entrainment. Comparing (a), (b), and (c) with (d), (e), and (f) in Fig. 4.4, we can see that in all three regions, absence of frequency entrainment coincides with time-localised LE that oscillate about 0, while the occurrence of frequency entrainment coincides with time-localised LE that stay negative over a longer time-interval.

Now when investigating numerically the time-evolution of the time-localised LE, as in Fig. 4.4(e) one can clearly distinguish between those time-intervals where the time-localised LE oscillates with high frequency around zero, and those time-intervals of length much greater than the periods of these aforementioned high-frequency oscillations during which the time-localised LE remains negative; and hence, one can numerically distinguish between the three regions. The proportion P_t of time taken up by time-intervals where the
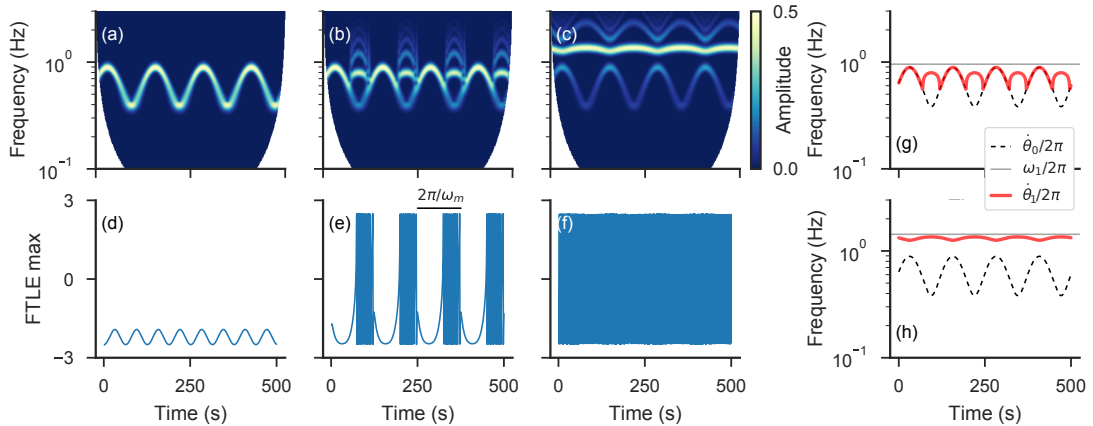
Figure 4.4.: Analysis of the time-variable dynamical properties of a trajectory of (4.3), in the three regions [see Fig. 4.1]; in (a)–(f), a random initial condition is taken from the square $[-1,1] \times [-1,1]$. (a)–(c) Time-frequency representation (showing amplitude) of $\theta_1(t)$ obtained as the (unwrapped) polar angle of the trajectory of (4.3), extracted using a continuous Morlet wavelet transform ($p = 1$) with central frequency 3; and (d)–(f) maximum FTLE for the trajectory of (4.3) over a time-window of width $\tau = 0.1$ s for regions II, III, and I, from left to right. Parameters are set to $k = 0.4$ and $\gamma = 2.5$; in (a) and (d) $\omega_1 = 4$, in (b), (e), and (g) $\omega_1 = 6$, and in (c), (f), and (h) $\omega_1 = 9$. (a), (d) Region II exhibits frequency entrainment and a stable phase at all times. (b), (e) Region III shows intermittent, but regular, epochs of frequency entrainment; the phase is stable on average over a long time. (c), (f) Region I, no frequency entrainment, and a FTLE rapidly oscillating around zero. (g), (h) Prediction (red) of the main observed frequency of the system over time, based on Eq. (4.12) with values of $\Omega_\psi(t)$ taken from the Ω_ψ curve with $k = 0$ in Fig. 4.6(b), for (g) region III, and (h) region I. Interestingly, in region I, the main observed frequency oscillates in anti-phase with those of the driving frequency (dashed). Note that we here only predict the main frequency, and not the higher harmonics observed in (b) and (c).

time-localised LE remains negative is plotted in Figs. 4.5(a) and 4.5(c), across different parameter values. As in Figs. 4.4(d)–4.4(f), we expect $P_t = 1$ in region II, $0 < P_t < 1$ in region III, and $P_t = 0$ in region I. We also plot in Figs. 4.5(b) and 4.5(d) the analytically obtained proportion P_t of time for which the instantaneous vector field has a stable equilibrium. This is given by

$$
P_t = \begin{cases}
0, & \text{(A) if } \gamma < |\Delta\omega(t)| \, \forall t, \\[2mm]
1, & \text{(B) if } \gamma > |\Delta\omega(t)| \, \forall t, \\[2mm]
\frac{1}{\pi}\left[\arcsin\left(\frac{\gamma-(\omega_1-\omega_0)}{\omega_0 k}\right) - \arcsin\left(\frac{-\gamma-(\omega_1-\omega_0)}{\omega_0 k}\right)\right], & \text{(C) if } -\gamma \geq \Delta\omega_- \text{ and } \gamma \leq \Delta\omega_+, \\[2mm]
\frac{1}{\pi}\arcsin\left(\frac{\gamma-|\omega_1-\omega_0|}{\omega_0 k}\right) + \frac{1}{2}, & \text{(D) else,}
\end{cases}
\tag{4.11}
$$

where $\Delta\omega_\pm = \omega_1 - \omega_0(1 \mp k)$. The close resemblance between (a), (c) and (b), (d) helps confirm the validity of the numerical approach to distinguishing between the three

regions. Figure 4.5(b) provides a quantitative picture for the qualitative skeleton shown in Fig. 4.1(b).
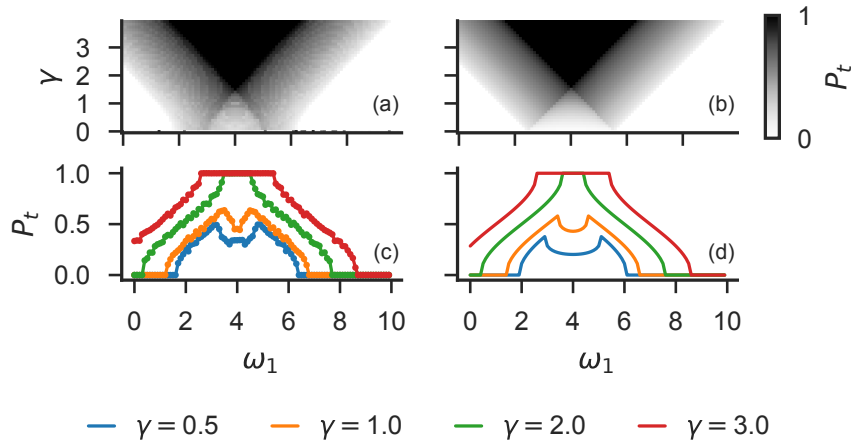
Figure 4.5.: Analytical and numerical characterisation of the three regions based on the proportion of time spent in the stable regime, over (γ, ω_1)-parameter space with $k = 0.4$. In (a) and (c), P_t is calculated numerically based on time-localised maximum LE (with window $\tau = 0.1$ s) for 20 trajectories of (4.3) with random initial conditions in the square $[-1, 1] \times [-1, 1]$, over four cycles of the frequency modulation (about 500 s), and the result is averaged over the 20 trajectories. In (b) and (d), the analytical result according to Eq. (4.11) is shown. Plots (c) and (d) show P_t from (a) and (b) for selected γ values. Three distinct regions appear clearly, respectively with P_t values of zero (region I), one (region II), and in between zero and one (region III). Analytical and numerical characterisations show good agreement.

The average frequency difference $\Omega_\psi = \langle \dot{\psi} \rangle = \langle \dot{\theta}_1 \rangle - \omega_0$ is a measure of the "average frequency entrainment" of the system [127]. In the traditional autonomous case $k = 0$ where the driving frequency is constant, nullity of Ω_ψ is equivalent to actual frequency entrainment, as discussed in chapter 1. The quantity Ω_ψ is shown in Fig. 4.6(b) for $\gamma = 2.5$ across different values of k. In Fig. 4.6(a), the corresponding curves for the long-term Lyapunov exponent are displayed. Curves for Ω_ψ for $k > 0$ are extremely similar to the case of driving with bounded noise $\xi(t)$, $\dot{\psi} = \Delta\omega + \gamma \sin(\psi) + \xi(t)$ (see [127]). This will be explored in further detail in Sec. 4.2.5. The similarity is due to the fact that only averages are considered, and time is forgotten. However, investigation of finite-time dynamics reveals that in region III, the frequency difference alternates between epochs where it is zero and epochs where it is non-zero [as in Fig. 4.4(g)]. To obtain this, we calculate the main observed frequency $\dot{\theta}_{1,\text{main}}/2\pi$ of trajectories using the slow modulation assumption, by taking

$$\dot{\theta}_{1,\text{main}}(t) = \dot{\theta}_1(t) + \Omega_\psi(t) \tag{4.12}$$

where $\Omega_\psi(t)$ is the Ω_ψ-value associated with the autonomous differential equation $\frac{d}{ds}\psi(s) = \Delta\omega(t) + \gamma\sin\psi(s)$; results are plotted in Figs. 4.4(g) and 4.4(h).
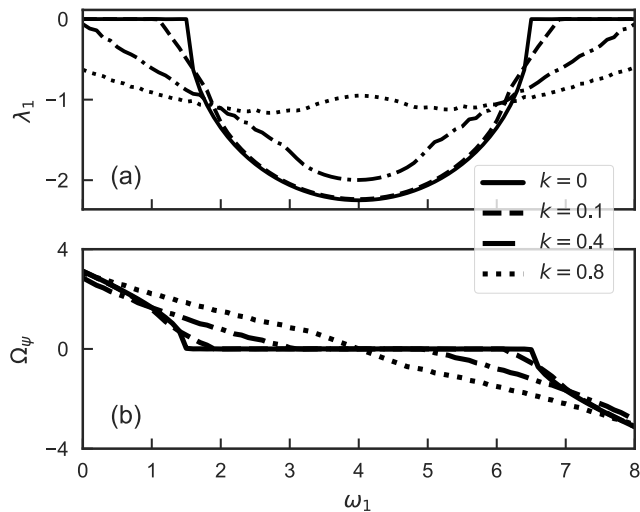
Figure 4.6.: Numerically obtained time-averaged stability properties for a trajectory of Eq. (4.1) starting at $\theta_1(0) = 0$, computed over 10 cycles of the frequency modulation (about 1260 s). (a) Lyapunov exponent λ_1, and (b) average frequency difference Ω_ψ, for $\gamma = 2.5$ and different values of the frequency modulation amplitude k. For $k = 0$, the region of phase stability (as given by $\lambda_1 < 0$) and the region of permanent frequency entrainment (as given by $\Omega_\psi = 0$) coincide; but for $k > 0$, the regions do not coincide: as k is increased, the region with $\lambda_1 < 0$ is increased while the region with $\Omega_\psi = 0$ is decreased. The graphs look very similar to those in the case of harmonic driving with bounded noise [127]; therefore, investigation of time-variable dynamics for nonautonomously driven oscillators is necessary for an accurate understanding of the dynamical nature of the system.

4.2.5. Comparison between nonautonomous and noisy systems

Experimental science essentially seeks to understand the underlying mechanics of a system that gives rise to the observed behaviour. Since the study of time-homogeneous dynamics (deterministic or noisy) is very well developed in comparison to the study of nonautonomous dynamics, there is a tendency to assume that for modelling purposes, the dynamics of a real-world system may be treated as statistically time-homogeneous. In this section we will illustrate, using our above-identified phenomenon of intermittent time-localised stability, how such a tendency may lead to the complete misidentification of some key aspect of the internal mechanics of a system.

There are various methods for analysing experimentally obtained time-series that are based on time-averaged properties of the time-series, such as power spectra. The theory of both deterministic autonomous dynamical systems and autonomous systems perturbed

by stationary noise is well developed, and in particular it is well-known that adding noise to a system can create stability which was not present in the absence of noise, e.g. [97, 106, 123, 127, 158]. Indeed, a one-dimensional phase oscillator model will almost invariably exhibit asymptotic stability of solutions when driven by stationary white noise [95]. Therefore, when seeking to understand the mechanism by which a real-world system behaves robustly against unpredictable external perturbations, if one observes in a time-series of measurements from the system a power spectrum similar to that of some noisy model, and if moreover this noisy model is known to exhibit stability with negative Lyapunov exponents as a consequence of the noise, then naturally one may come to the conclusion that the real-world system under investigation is subject to a significant level of noise and that this noise plays the key role in causing stability.

However, our results for the deterministic system (4.1)–(4.2) demonstrate that such a conclusion may be profoundly erroneous. The frequency modulation in (4.2) may be an entirely deterministic process that is not subject to any significant levels of noise. This gives rise to the deterministic nonautonomous equation (4.5), and we will illustrate that the time-averaged properties of (4.5) [with $f(\cdot) = \sin(\cdot)$] are very similar to those of a noisy counterpart

$$\dot{\psi} = (\omega_1 - \omega_0) + \gamma \sin \psi + \xi(t) \tag{4.13}$$

where $\xi(t)$ is bounded noise. Physically, Eq. (4.13) represents the phase difference under a model in which the driving frequency modulation is assumed to be noisy. The similarity that we shall illustrate between the time-averaged properties of (4.5) and (4.13) proves an important point: Since real-world systems are open and therefore subject to time-variability, one must examine temporally evolving dynamical properties of a system rather than just time-averaged properties, in order to account for the possibility that the mechanisms behind features of the observed behaviour are due to nonautonomicity. In the case of the system (4.1)–(4.2), in region III, the mechanism behind stability is not stationary noise but deterministic intermittent frequency entrainment between driving and driven oscillators, arising from the slow variation of the driving frequency.

For simulations, dichotomous Markov noise $\xi(t)$, which switches between $\pm D$ at rate μ (with $\xi(0) = +D$), was used [70]. Nonetheless, it is expected that any bounded noise will show similar behaviour to that presented here [127]; moreover, although the asymptotic
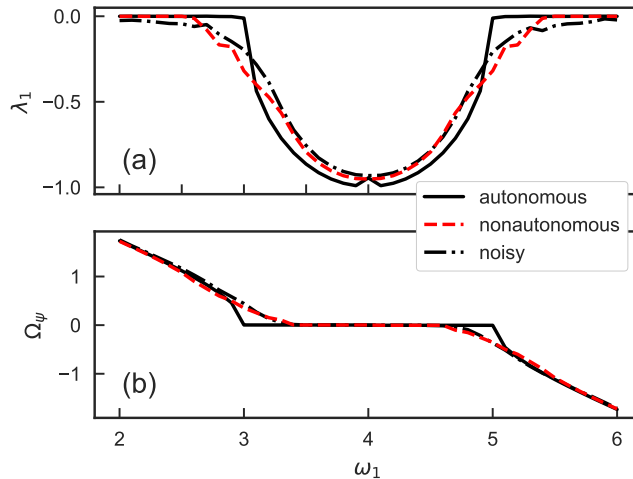
Figure 4.7.: Numerically obtained time-averaged stability properties for autonomous (plain black), nonautonomous (dashed red), and bounded noise (dotted-dashed black) driving, computed over about 1260 s (10 cycles of the periodic frequency modulation used for the nonautonomous case). For the autonomous and nonautonomous cases, Eqs. (4.4) and (4.5) respectively were integrated, with $\psi(0) = 0$; for the noisy case, one sample path of $\xi(t)$ was generated, and Eq. (4.13) was integrated with $\psi(0) = 0$, using the same sample path $\xi(t)$ for all ω_1 values. Parameters are set to $\omega_0 = 4$ and $\gamma = 1$; for the nonautonomous case, $f = \sin(\cdot)$, $k = 0.1$ and $\omega_m = 0.05$, and for the noisy case $D = 1.6$ and $\mu = 10$. (a) Lyapunov exponent λ_1, and (b) average frequency difference Ω_ψ. The nonautonomous and noisy cases, observed on average, present the same enlarging of the negative Lyapunov exponent region, and their Ω_ψ is almost exactly identical, including the plateau.

properties of unbounded noise models exhibit a slightly different behaviour [127], any noise will effectively serve as bounded noise over typical physically relevant finite timescales.

On average, the noisy and the nonautonomous systems will have properties as illustrated in Fig. 4.7 that look essentially the same. Indeed, both can be made to have an increased region for negative LE [see Fig. 4.7(a)] and a smaller plateau for average frequency entrainment [see Fig. 4.7(b)], as compared to the autonomous case given by $k = 0$ or $D = 0$.

The noisy and the nonautonomous systems can, however, be distinguished based on their dynamics over time. This is illustrated in Fig. 4.8 by trajectories and their time-frequency representation. In the nonautonomous case, one can see the regularly intermittent frequency entrainment between driving and driven phases in Fig. 4.8(c), where frequency entrainment corresponds to those times where the instantaneous power-frequency spectrum has only a single peak, and in Fig. 4.8(b), where frequency entrainment corresponds to the regular plateaus in the phase difference. By contrast, in the noisy case, the instantaneous power-frequency spectrum shown in Fig. 4.8(e) is significantly
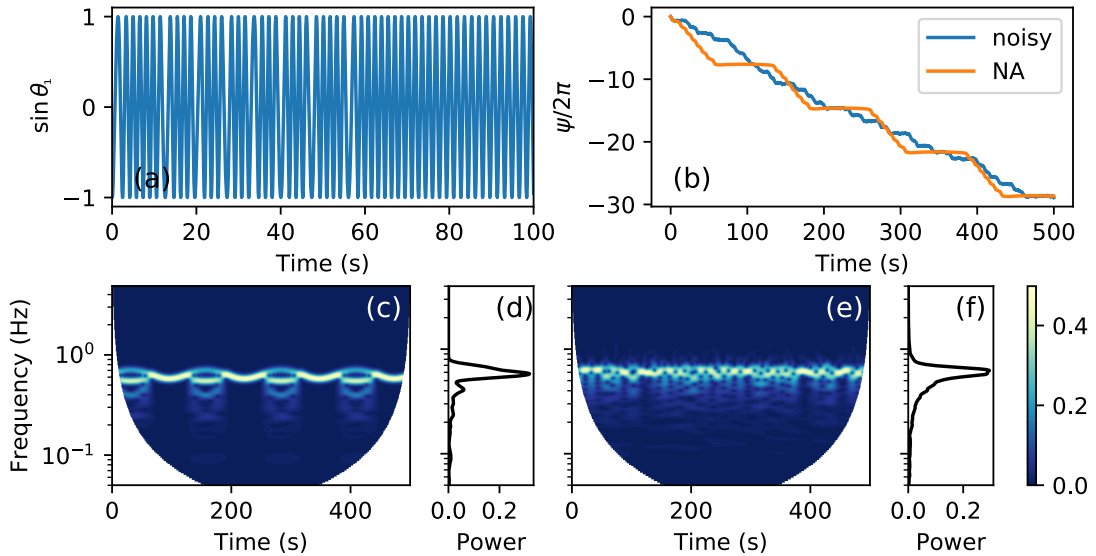
Figure 4.8.: Dynamics of driven oscillator θ_1 with (a)–(d) nonautonomous and (b), (e), and (f) bounded noise driving; here θ_1 evolves according to Eq. (4.1) with $\theta_0(t) = \omega_0[t - \frac{k}{\omega_m}\cos(\omega_m t)]$ in the nonautonomous case, and $\theta_0(t) = \omega_0 t - \int_0^t \xi(s)\,ds$ in the noisy case, and $\theta_1(0) = \theta_0(0)$ in both cases. Parameters are set to $\omega_0 = 4$, $\gamma = 1$, $\omega_1 = 3$; for the nonautonomous case $k = 0.1$ and $\omega_m = 0.05$, and for the noisy case $D = 1$, $\mu = 4$. First $\psi(t)$ is numerically obtained by integrating Eq. (4.5) or (4.13) as appropriate, with $\psi(0) = 0$, and then $\theta_1(t)$ is obtained by $\theta_1(t) = \psi(t) + \theta_0(t)$. (a) Sine of the driven phase θ_1, in the nonautonomous setting. (b) Phase difference ψ between the driving and driven oscillators, over time. The nonautonomous case presents epochs of phase-locking as seen by the regular plateaus, whereas the noisy phases' difference drifts without ever phase-locking to the driving, with an average velocity that is close to that of the nonautonomous curve. (c), (e) Time-frequency representation (showing power, i.e. square of the amplitude) for θ_1 extracted using continuous Morlet wavelet transform (with $p = 1$) with central frequency 3, and (d, e) the associated time-averaged power. The main difference is the presence of intermittent frequency entrainment in the nonautonomous case. The average-power spectra are very similar, and do not clearly distinguish the two cases. Long-term LEs were also found to be negative in both cases: for the nonautonomous Eq. (4.5) with $\psi(0) = 0$, the LE over 500 s was about -0.32, and for the noisy Eq. (4.13) with $\psi(0) = 0$, the LE over 500 s was about -0.24.

more bumpy around a peak that stays roughly fixed over time, and the phase difference in Fig. 4.8(b) looks like it is essentially drifting at all times. Despite these starkly visible differences in time-variable properties, the average power spectra as shown in Figs. 4.8(d) and 4.8(f) are reasonably similar to each other.

4.2.6. Aperiodic modulation

We now consider numerically a quasi-periodic frequency modulation function $f(\cdot)$ given by

$$f(t) = 0.5[\cos(\omega_m t) + \cos(\omega_m \pi t/4)]. \tag{4.14}$$
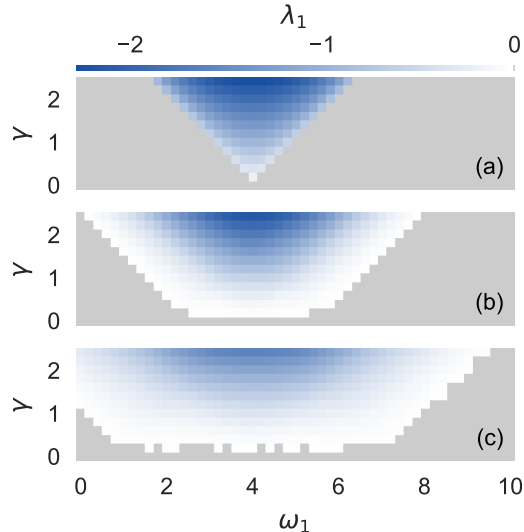
Figure 4.9.: Numerically obtained long-term maximum Lyapunov exponent λ_1 over parameter space for (4.3) with $\theta_0(t) = \omega_0\{t + \frac{0.5k}{\omega_m}[\sin(\omega_m t) + \frac{4}{\pi}\sin(\omega_m \pi t/4)]\}$. Here, as in Sec. 4.2.4, $\omega_0 = 4$, $\omega_m = 0.05$, $r_p = 1$ and $\epsilon = 5$. The LE are computed over 5 cycles of the frequency modulation (about 630 s). In each case, 20 random initial conditions were taken from the square $[-1, 1] \times [-1, 1]$, and the average maximum LE over these trajectories is plotted. (a) $k = 0$, (b) $k = 0.4$, (c) $k = 0.8$. The Arnold tongue (shades of blue) is enlarged as k increases. Grey represents zero values.

As expected, and shown in Fig. 4.9, the enlargement of the Arnold tongue holds. Moreover, more quantitatively, the results shown in Figs. 4.9(b) and 4.9(c) are almost identical to those shown in Figs. 4.2(c) and 4.2(d), respectively. This is because $f(\cdot)$ oscillates throughout the interval $[-1, 1]$ in both cases, and therefore Eqs. (4.8)–(4.10) for the three different regions still hold.

4.3. Higher-dimensional cases

In the above section, we showed analytically, and confirmed numerically, that enlargement of the stability region will always occur in the simple one-dimensional case. Nonetheless, the phenomenon of stabilisation by slow variation of the driving frequency, and the phenomenon of intermittent synchronisation under such variation of the driving frequency, may be found in a broader class of systems. To illustrate the more general scope of the stabilisation phenomenon, we illustrate it numerically in nonlinear driven oscillators. We consider three cases: first, a typically forced van der Pol (vdP) oscillator; second, a vdP oscillator with the phase driven via diffusive coupling; and finally, a typically forced Duffing oscillator. All three cases are investigated with nonautonomous driving
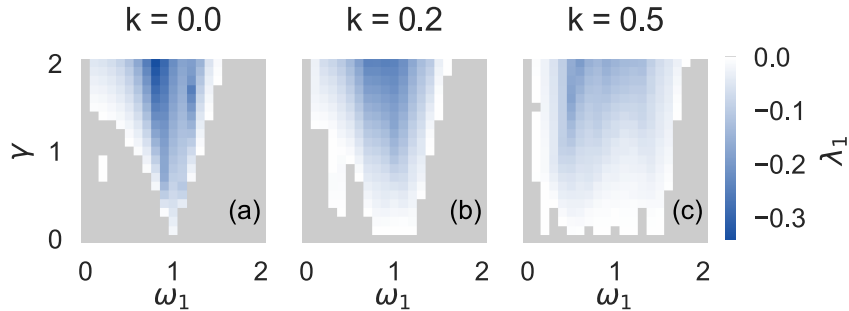
Figure 4.10.: Numerically obtained long-term maximum Lyapunov exponent λ_1 over parameter space for the forced weakly nonlinear vdP oscillator [see Eq. (4.15)], with $\epsilon = 0.1$, $\omega_0 = 1$, and $\omega_m = 0.02$, for different amplitude of frequency modulation k. In each case, 20 random initial conditions $(x(0), \dot{x}(0))$ were taken from the square $[-1, 1] \times [-1, 1]$, and the average maximum LE over these trajectories is plotted. The negative LE region (blue shades) increases as k is increased. Grey represents zero values.

$\theta_0(t) = \omega_0(t - \frac{k}{\omega_m}\cos(\omega_m t))$, with $\omega_m = 0.02$. Long-term LE are computed over 10 cycles of the frequency modulation (about 3140 s).

4.3.1. Typically forced van der Pol

We consider a vdP oscillator that is *directly* forced by the external phase oscillator $\theta_0(t)$, so that the vdP oscillator satisfies the differential equation

$$\ddot{x} = \epsilon(1 - x^2)\dot{x} - \omega_1{}^2 x + \gamma \sin[\theta_0(t)]. \tag{4.15}$$

For investigation of LE, we treat this as a first-order equation in (x, y)-space with $\dot{x} = y$ (and numerically integrate it as such). The long-term maximum LE is shown over parameter space in Fig. 4.10. The region with negative LE increases with the amplitude k of the frequency modulation, showing that the enlargement of the negative LE region still holds in this nonlinear case.

Moreover, consideration of time-localised LE, as shown in Fig. 4.11(b), suggests that for some parameter values we have intermittency between epochs of stable dynamics and epochs of neutrally stable dynamics. Unlike in Fig. 4.4(e), the stable epochs are not characterised by negativity of LE defined over a very short sliding window, but rather over a suitably longer sliding window. This is because, if one were to freeze the driving frequency $\dot{\theta}_1$ at any moment in time during such an epoch of stable dynamics, the solution of the resulting periodic differential equation (4.15) would not converge to

a fixed point but most likely to a stable periodic orbit, for parts of which the vector field is locally contractive and other parts not, with contraction on average over each period. Hence, the intermittency is demonstrated most clearly by taking time-localised LE over a wider moving time-window, whose width is likely to incorporate several periods of the aforementioned stable periodic orbit. In Fig. 4.11(b), we see quite clearly (in red) the alternation between plateaus of zero time-localised LE and epochs where the time-localised LE dips to become negative. In the time-frequency representation shown in Fig. 4.11(a), during the epochs of zero time-localised LE, the power is shared mostly between two distinct peaks in the instantaneous spectrum, but during the epochs of negative time-localised LE, virtually all the power is concentrated around a single peak. As in Fig. 4.4(e), this suggests that instantaneous $1:1$ frequency entrainment is taking place during the epochs of negative time-localised LE, but not the epochs of zero time-localised LE, and so overall the system exhibits intermittent synchronisation.
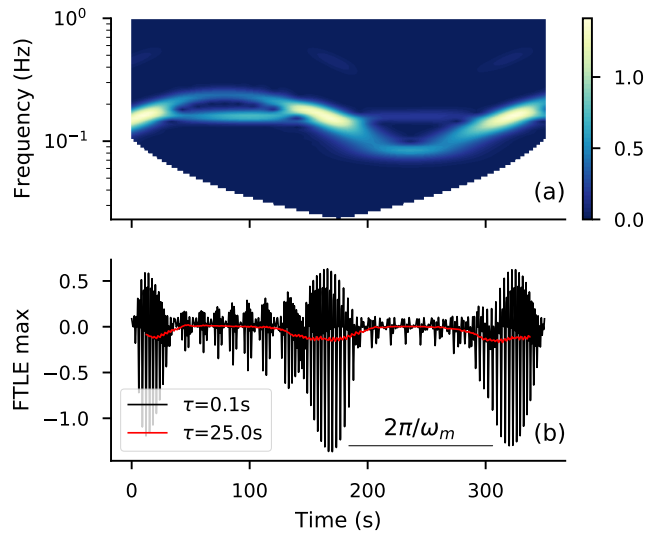
Figure 4.11.: Intermittency in the typically forced vdP system (4.15). Parameters are set to $k = 0.5$, $\gamma = 1$, $\omega_1 = 1$, $\epsilon = 0.1$, $\omega_m = 0.02$, $\omega_0 = 1$; results are for a random initial condition $(x(0), \dot{x}(0))$ taken from the square $[-1, 1] \times [-1, 1]$. (a) Time-frequency representation (showing amplitude) of $x(t)$, extracted using a continuous Morlet wavelet transform $(p = 1)$ with central frequency 2. (b) Shorter-time-window FTLE max, with window length 0.1 s, is shown in black, and longer-time-window FTLE max, with window length 25 s, is shown in red. The longer-time-window FTLE alternates between epochs where it is negative, and epochs where it is zero. These epochs of negative values coincide with those epochs where, in (a), there appears to be a single main peak in the instantaneous power-frequency spectrum.

4.3.2. Diffusively forced van der Pol

We take the polar coordinate representation of the unforced vdP oscillator (Eq. (4.15)) without $\gamma \sin[\theta_0(t)]$) as a first-order equation in $(x, \dot{x})$-space, and we now drive the angular component with a diffusive coupling:

$$
\begin{aligned}
\dot{r} =& (1 - \omega_1{}^2) r \cos\theta_1 \sin\theta_1 + \epsilon(1 - r^2 \cos^2\theta_1) r \sin^2\theta_1, \\
\dot{\theta}_1 =& \epsilon(1 - r^2 \cos^2\theta_1)\sin\theta_1 \cos\theta_1 - \omega_1{}^2 \cos^2\theta_1 - \sin^2\theta_1 + \gamma \sin[\theta_1 - \theta_0(t)].
\end{aligned}
\tag{4.16}
$$

The long-term maximum LE is shown over parameter space in Fig. 4.12. Increasing k reduces both the region of neutral stability and the very small region of chaos, while the region of stability grows.
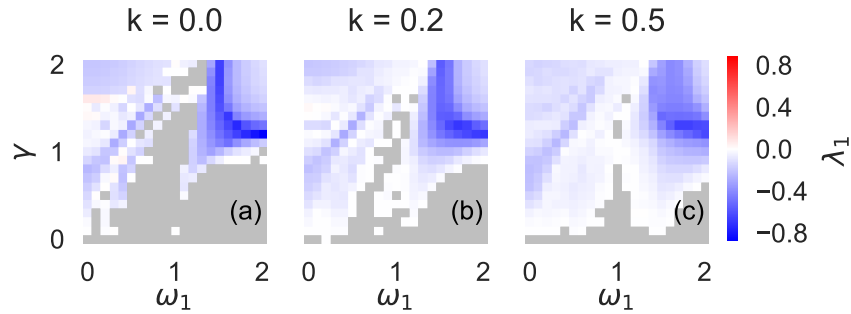
Figure 4.12.: Numerically obtained long-term maximum Lyapunov exponent λ_1 over parameter space for the diffusively phase forced van der Pol oscillator [see Eq. (4.16)], with $\epsilon = 0.1$, $\omega_0 = 1$, and $\omega_m = 0.02$, for different amplitude of frequency modulation k. In each case, 20 random initial conditions $(x(0), \dot{x}(0))$ were taken from the square $[-1, 1] \times [-1, 1]$, and the average maximum LE over these trajectories is plotted. The stability region (shades of blue) is enlarged as k increases, and chaotic (red) points in (a) are turned stable (shades of blue) in (c). Grey represents zero values.

4.3.3. Forced and coupled Duffing oscillator

Here, we consider two Duffing oscillators, x and x_1, unidirectionally diffusively coupled with strength g_d so that x_1 drives x. Additionally, the driven Duffing oscillator is directly forced with external nonautonomous driving:

$$
\begin{aligned}
\ddot{x} =& -\delta\dot{x} - \omega_1{}^2 x - \beta x^3 + g_d(x - x_1) + \gamma \cos(\theta_0(t)), \\
\ddot{x}_1 =& -\delta\dot{x}_1 - \omega_1{}^2 x_1 - \beta x_1^3,
\end{aligned}
\tag{4.17}
$$

We fix parameters $\delta = 0.3$, $\beta = 0.1$, $\omega_0 = 1.2$, $\omega_m = 0.02$, and coupling strength $g_d = 0.5$. For investigation of LE, we treat the system as a first-order equation in (x, y, x_1, y_1)-space with $\dot{x} = y$, $\dot{x}_1 = y_1$ (and numerically integrate it as such). The long-term maximum LE is shown over parameter space in Fig. 4.13. As k is increased, the chaotic region essentially decreases, giving way to either stability or neutral stability. The stability region does not strictly increase, as parts of the stability region become neutrally stable as k is increased; nonetheless, the phenomenon is still observed that for various fixed values of all the parameters other than k, increasing k has the effect of turning chaos into stability. From a control point of view, if the region of interest in parameter space is the chaotic region, one can stabilise the dynamics by adding time-variation to the forcing frequency.
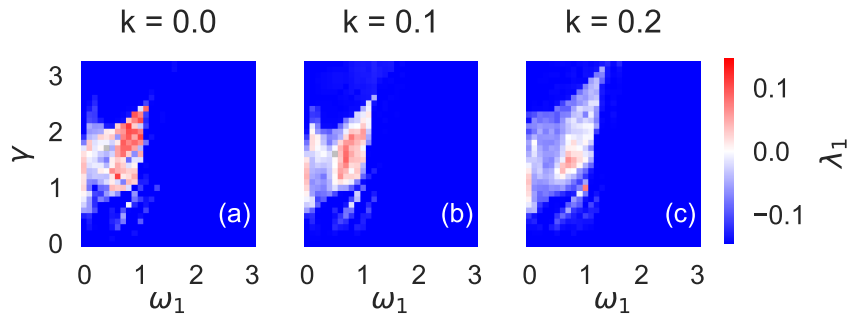
Figure 4.13.: Numerically obtained long-term maximum Lyapunov exponent λ_1 over parameter space for the coupled and forced Duffing oscillator (4.17), for different amplitude of frequency modulation k. In each case, 20 random initial conditions $(x(0), \dot{x}(0), x_1(0), \dot{x}_1(0))$ were taken from $[-1, 1]^4$, and the average maximum LE over these trajectories is plotted. The region of chaotic behaviour (red) is reduced as many points are turned stable (shades of blue) as k is increased. Grey represents zero values.

4.4. Discussion

The work was motivated by real systems that exhibit dynamics with time-varying frequencies and are stable against external perturbation [22, 33, 61, 85, 98, 149, 153, 161]. Surprisingly, not much analytical work has been carried out on such systems, and most of the work that has been carried out has used noisy driving [97, 106, 145] as the foundation of the model, or noise consisting of impulses at random times [123, 127]. In these studies, it was shown that noise can create and increase stability. Outside of a stochastic approach, the only other way to incorporate time-variability is to model the system as a deterministic nonautonomous dynamical system. However, not much analytic

theory of nonautonomous systems has been developed yet. The problem is additionally complicated by the fact that an asymptotic approach does not give the full picture as the evolving dynamics over shorter timescales is missed. As illustrated in this work, changes in dynamical behaviour over shorter timescales are of crucial importance in the types of systems considered. For if they had not been considered in this work, the phenomenon of intermittent synchronisation would have been missed. The work in this paper has provided a key insight into systems subject to time-varying influences, by identifying the phenomenon of intermittent synchronisation and the region in parameter space where it occurs, and thereby showing the enlargement of the Arnold tongue. This insight also has potential for being the foundation of future methods to induce stability in complex or other systems; the fact that nonautonomous driving allows for average stability to be achieved without the need to maintain frequency entrainment at all times may be of significant advantage.

The basic adiabatic reasoning underlying our analytical approach is the same as that employed and investigated in [65]. It is this reasoning that has led us to our new discovery that increasing time-variability inherently induces stability in phase oscillators. We have also employed numerical tools to visualise time-localised dynamics as derived by this adiabatic reasoning, namely time-localised LEs as in Figs. 4.4(d)–4.4(f) and time-frequency representation as in Figs. 4.4(a)–4.4(c). We hypothesise that for a time-frequency representation applied to experimental data, a result resembling Fig. 4.4(b) could be a signature of intermittent synchronisation. We also investigated the slow variation assumption in higher-dimensional systems, and numerically illustrated the creation of stability as the amplitude of variation is increased, as well as the occurrence of intermittent synchronisation. In this way, we showed that the phenomena of stabilisation and intermittent synchronisation under slow variation of the driving frequency occur more broadly than just in the case of phase oscillators.

Chronotaxic systems have been introduced to model the distinctive feature of real-life oscillatory systems, that they are able to keep their time-varying dynamics resistant to external perturbations [149–151]. Chronotaxic systems were defined in previous works by the necessary condition that a time-dependent attractor exists, and that trajectories in its close vicinity always move closer to it [149], or alternatively just by the existence of a

positively invariant time-varying region in which the dynamics is always contracting [151]. However, it seems reasonable to expect that in real life, there exist stable oscillatory systems for which no trajectory is always instantaneously locally attractive. Instead, in contrast to currently existing definitions of chronotaxicity, an intermittent synchronisation phenomenon such as identified in this work would give rise to stability on average. Thus, we have broadened the definition of chronotaxic systems, increasing its potential for effectively modelling and understanding real-life systems, which are nonisolated and therefore continuously subjected to time-varying external influences.

4.5. Summary

In this chapter, we have shown that driving a phase oscillator with an arbitrary slowly varying frequency always induces stability in the following sense: the larger the amplitude of the frequency modulation, the larger the stability region. Note, however, that for a given point in parameter space, the strength of the stability, i.e. the magnitude of the LE, can either decrease or increase as the amplitude of the frequency modulation is increased. We have furthermore shown numerically that this phenomenon occurs in more complex cases where the driven oscillator is higher-dimensional and nonlinear, hinting at the wider scope and importance of the effect at hand. We have even shown numerically that chaotic regions in parameter space can be made stable by the same mechanism. If only the quantities λ_1 and Ω_ψ, which describe time-averaged properties of the system, are considered, the system looks the same as in the case of driving with noise. However, in reality, our fully deterministic example exhibits some time-localised frequency entrainment, whereas none is exhibited in the case of driving with bounded noise. It is therefore clear that the nonautonomous deterministic system could be misinterpreted as a noisy one if only time-averaged quantities are considered.

The enlarged stability region makes time-variable driving very suitable for real-world modelling and for engineering, where a controlled adjustment of the frequencies is often of key importance. We believe that this type of model will find applications in many fields, including physics, biology, medicine, and climate dynamics.

In the next chapter, the study is extended to a system with a more general modulation. Results are extended and expressed in a more formal mathematical language. The system considered is used as an example to highlight the possible mismatches between a long but finite-time analysis and an asymptotic one.

5. A bounded-time approach to dynamics analysis

5.1. Introduction

Dynamics, as introduced by Newton to describe celestial motion, and later extended by Lyapunov [94] and Poincaré [128] to include stability analysis, has been fruitfully applied to various fields in the sciences. Still, all of this has mostly, to date, been based on two main assumptions, that the dynamics of the systems is time-homogeneous, and that the physical behaviour exhibited can be described by coordinate-invariant time-asymptotic dynamics. However, many real-world systems are *open* [22, 31, 33, 40, 49, 85, 99, 118, 139] and thus too prone to time-variable influences to be reasonably modelled by a time-independent evolution law [72, 73], as argued in chapter 1. Even the external driving may follow no time-homogeneous deterministic or probabilistic model, making most existing nonautonomous dynamics theory [72, 73] unsuitable. When dealing with the finiteness of experimental data, infinite-time models can and their asymptotic analysis have proven successful in various cases, but can also be unsuitable because of their very own nature.

Accordingly, *finite-time dynamical systems* theory has recently been gaining attention [19, 44, 53, 68, 69, 89, 135]. Such theory and associated data-analysis methods have been applied most notably to studying *coherent structures* in diverse fluids [54, 55, 64, 88, 100, 134, 140, 154, 156, 163]. Time-localised dynamical stability for a multispecies population was investigated from data in [160].

In this chapter, we demonstrate the limitations of the above-mentioned two assumptions by uncovering a dynamical phenomenon that cannot be described by the standard

approach based on these assumption. Specifically, we show that for very general slowly varying one-dimensional phase-oscillator systems – a generalisation of the system of chapter 4 – sufficiently broad variation inherently induces stability in the system.

This chapter is composed of three main sections. In Sec. 5.2, a dynamical system defined over finite-time is defined ,and the analytical bases for finite-time stability are established. In Sec. 5.3, results form the section before are generalised. Finally, in Sec. 5.4, an infinite-time system is considered, and it is shown how a finite-time analysis gives results different from a traditional asymptotic approach.

5.2. Finite-time model and stability

First let us consider, over the time-interval $[0, T]$ with $T = 2\pi \times 10^5$ s, the differential equation

$$\dot{\psi}(t) = -\gamma \sin(\psi(t)) + \Delta\omega + Kg(t) \tag{5.1}$$

with $\gamma = \frac{1}{3}$ rad/s and $\Delta\omega = 1$ rad/s, and with $g \colon [0, T] \to \mathbb{R}$ being a continuous function whose graph is as shown in Fig. 5.1. The study of Eq. (5.1) is motivated by Eq. (4.5) from chapter 4. For consistency, the notation is kept the same, even though Eq. (5.1) is now studied independently of Eq. (4.5). The parameter $K > 0$ rad/s represents the breadth of time-variability, just like $\Delta\omega$ in Eq. (4.5) (strictly speaking $K = k\omega_1$, since the frequency modulation is relative in Eq. (4.5), and absolute in Eq. (5.1)).
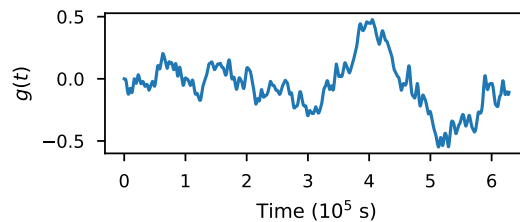
Figure 5.1.: Graph of $g(t)$ in Eq. (5.1).

The function $g(t)$ in Fig. 5.1 was effectively constructed by taking a sample realisation of a Brownian $[0, T]$-bridge and passing it through a lowpass filter with very low cut-off frequency (namely $\frac{1}{2\pi \times 10^3}$ Hz), so that, as seen in Fig. 5.1, the rate of change of g over time is slow compared to the values of $\Delta\omega$ and γ. Since $g(t)$ originates from a Brownian bridge process, there is no physically meaningful way to extend the model (5.1)

beyond the time-range $[0, T]$ of the bridge itself, while both its extremities at 0. Thus, *asymptotic-dynamics concepts and methods are inapplicable.*

A Brownian bridge effectively describes the result of conditioning a finite-time zero-drift Brownian motion on the event that the start and end values are the same. For the construction of $g(t)$, we start by simulating a realisation of Brownian motion $(W_t)_{0 \leq t \leq T}$, $T = 2\pi \times 10^5$ s, with $W_t \sim \mathcal{N}(0, \frac{t}{T})$. We then construct the Brownian bridge realisation $(B_t)_{0 \leq t \leq T}$ by $B_t := W_t - \frac{t}{T}W_T$. We pass the signal $(B_t)_{0 \leq t \leq T}$ through a 5th order Butterworth lowpass filter with cut-off frequency $1/(2\pi \times 10^3)$ Hz. The output is $g(t)$.

Numerically, we used a time step of 0.01 s to construct the Brownian bridge, and the Butterworth filter was performed via cascaded second-order sections (in Python, with the function "scipy.signal.sosfilt"). Finally, we linearly interpolated the output of the filter to get $g(t)$ as shown in Fig. 5.1.

All numerical integration in this chapter was performed using the RK4 scheme with a time step of 0.01 s, unless stated otherwise.

5.2.1. Stabilisation phenomenon

A bifurcation diagram for the system (5.1) with respect to the parameter K, obtained by simulating the trajectories of 50 initial conditions up to time $T = 2\pi \times 10^5$ s, is shown in Fig. 5.2(b).

The results shown in Figs. 5.2(a) and 5.2(b) were obtained by numerically integrating Eq. (5.1). The long-term FTLE shown in (a) were calculated according to Eq. (5.4). The results in Fig. 5.2(c) were obtained by evolving the 50 points $\frac{2\pi i}{50}$ under the time-reversed version of (5.1), namely the differential equation

$$\dot{\psi}(t) = \gamma \sin(\psi) - \Delta\omega - Kg(T - t). \tag{5.2}$$

Despite the non-existence of infinite-time dynamics for this inherently timebound model, we clearly see in Fig. 5.2(b) a transition from neutrally stable dynamics, where trajectories
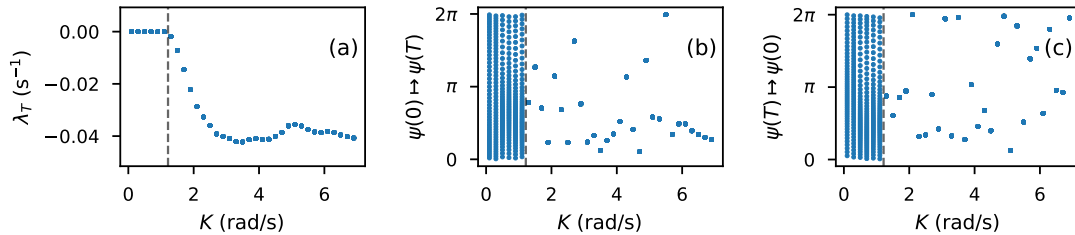
Figure 5.2.: Dynamics of (5.1) with varying K. The system becomes stables for $K > K^*$. In (a) and (b), for each K-value, results for the evolution $\psi(t)$ of 50 equally spaced initial conditions $\psi(0) = \frac{2\pi i}{50}$, $i = 0, \ldots, 49$, are shown: (a) shows the FTLE λ_T, as defined by (5.4), for these trajectories; (b) shows the positions $\psi(T)$ of these trajectories at time T. In (c), for each K-value, the positions of $\psi(0)$ for the 50 trajectories ending at the points $\psi(T) = \frac{2\pi i}{50}$, $i = 0, \ldots, 49$, are shown. In all three plots, the value K^* as defined in (5.3) is marked in dashed black, and $T = 2\pi \times 10^5$ s.

fill the circle, to stable dynamics, where trajectories cluster around a point. So, as in chapter 4, sufficient breadth of time-variability induces stability.

The dashed line in Fig. 5.2(b) marks the value

$$K^* \ := \ \frac{\gamma - \Delta\omega}{\min_{0 \le t \le T} g(t)}, \tag{5.3}$$

that is, the upper end of the range of K-values for which every solution $\psi(t)$ of (5.1) has $\dot{\psi}(t) > 0$ for all time $t \in [0, T]$. We see in Fig. 5.2(b) that the transition from neutral stability to stability takes place precisely at $K = K^*$. This stabilisation can be further assessed via the long-term FTLE λ_T associated to each trajectory $(\psi(t))_{0 \le t \le T}$ of (5.1), computed by

$$\lambda_T \ = \ \frac{1}{T} \int_0^T -\gamma \cos(\psi(t)) \ \mathrm{d}t. \tag{5.4}$$

The values of λ_T for the trajectories of 50 initial conditions are shown in Fig. 5.2(a), and again K^* is marked. For each K-value, we see that the 50 trajectories share indistinguishably the same FTLE value, being indistinguishable from 0 for $K < K^*$ and clearly negative for $K > K^*$. This confirms the stabilisation shown in Fig. 5.2(b). A reverse-time bifurcation diagram is shown in Fig. 5.2(c); from plots (b) and (c) we see that if $K > K^*$, then trajectories are repelled away from a very small repulsive area and are mutually attracted into a very small area. Thus, the stabilisation phenomenon that we see strongly resembles a *saddle-node bifurcation* of autonomous dynamical systems. And yet, the bifurcation observed in Fig. 5.2 cannot in any way be related to autonomous, or even time-asymptotic nonautonomous, dynamics.

The stabilisation as K rises above K^* is explained by the following adiabatic reasoning. Locally around each time t, if the instantaneous vector field $-\gamma \sin(\,\cdot\,) + \Delta\omega + Kg(t)$ has no equilibrium then trajectories move approximately periodically round the circle with no significant clustering or dispersion of trajectories, but if the instantaneous vector field $-\gamma \sin(\,\cdot\,) + \Delta\omega + Kg(t)$ has an equilibrium y then trajectories cluster together increasingly tightly near y.

We now show the same stabilisation phenomenon is still occurring when we consider (5.1) not on the whole time-interval $[0, T]$ but just on a subinterval $[0, T']$, where $T' = \pi \times 10^4$ s. We use the same function $g(t)$, only going up to time T'. This function still attains negative values on the subinterval $[0, T']$, and so the critical K-value is now given by

$$K^* = \frac{\gamma - \Delta\omega}{\min_{0 \leq t \leq T'} g(t)}. \tag{5.5}$$

Results are shown in Fig. 5.3, with γ and $\Delta\omega$ as in Fig. 5.2. Plots (a) and (b) are
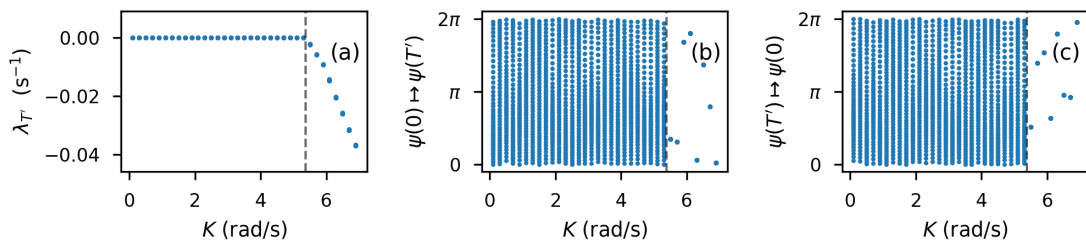
Figure 5.3.: Stabilisation of (5.1) on time $[0, T']$ with $T' = \pi \times 10^4$ s. Other parameters are $\gamma = \frac{1}{3}$ rad/s and $\Delta\omega = 1$ rad/s. In (a) and (b), for each K-value, results for the evolution $\psi(t)$ of 50 equally spaced initial conditions $\psi(0) = \frac{2\pi i}{50}$, $i = 0, \ldots, 49$, are shown: (a) shows the FTLE $\lambda_{T'}$, as defined by Eq. (5.4), for these trajectories; (b) shows the positions $\psi(T')$ of these trajectories at time T'. In (c), for each K-value, the positions of $\psi(0)$ for the 50 trajectories of (5.1) with $\psi(T') = \frac{2\pi i}{50}$, $i = 0, \ldots, 49$, are shown. The value K^* as defined in (5.5) is marked by the black dashed line.

obtained exactly as for Fig. 5.2, and likewise plot (c) by evolving the 50 points under the differential equation

5.3. Generalisation

In this section and the next, mathematical propositions are presented, not as original work from the candidate of this thesis, but rather to highlight a relevant development in a preprint co-authored by the aforementioned candidate. A future publication will

comprehensively present the full details of the propositions and of the proofs. The propositions themselves were the result of discussion with the candidate and inspired by the work presented in the previous chapter. All numerical analysis was carried out by the candidate.

To generalise, consider on the phase space $\mathbb{S}^1 = \mathbb{R}/(2\pi\mathbb{Z})$ a differential equation

$$\dot{\psi}(t) \;=\; F(\psi(t), \tfrac{t}{T}) \tag{5.6}$$

defined on the time-interval $[0, T]$, where $F \colon \mathbb{S}^1 \times [0, 1] \to \mathbb{R}$ is a function that we will assume to be smooth. In this time-varying differential equation, F *specifies the overall shape* of variation, while T *specifies the slowness* at which this shape of variation is realised. Eq. (5.6) could describe various physical situations, due to existence of phase reduction methods for slowly varying systems [83, 84, 115]. At any time $t \in [0, T]$, an *instantaneous stable equilibrium of* (5.6) means a point $y_{\frac{t}{T}} \in \mathbb{S}^1$ such that $F(y_{\frac{t}{T}}, \frac{t}{T}) = 0$ and $\frac{\partial F}{\partial \psi}(y_{\frac{t}{T}}, \frac{t}{T}) < 0$.

We consider two cases:

- Case I: either $F(\psi, \tau) > 0$ for all ψ and τ, or $F(\psi, \tau) < 0$ for all ψ and τ.

- Case II: there exist times $t \in [0, T]$ at which (5.6) has a unique instantaneous stable equilibrium.

For generic F, if the function $F(\,\cdot\,, 0)$ or $F(\,\cdot\,, 1)$ has no zeros then the system is either in Case I or Case II. Generalising results of [65] and chapter 4, adiabatic consideration as exemplified above for (5.1) yields the following. *Assuming slow variation of F: in Case I,* (5.6) *exhibits neutrally stable dynamics; in Case II, typically,* (5.6) *exhibits global-scale stable dynamics.* The neutral stability in Case I means that there is no significant attractivity or repulsivity of the solutions. The global-scale stability in Case II means that all solutions starting outside some very small "repulsive" arc will cluster together over time into a very small arc.

We can make this finite-time-dynamics analysis more rigorous. An *arc $J \subset \mathbb{S}^1$* will mean a closed connected proper subset of $\mathbb{S}^1$ with non-empty interior. Given an arc $J_0 \subset \mathbb{S}^1$ of initial conditions $\psi(0)$, we write J_t for the arc of subsequent positions $\psi(t)$ at time t. The neutral stability in Case I is described by the following.

Proposition 1. *Fix any F within Case I. There exists a constant $c_F \geq 1$ independent of T, such that for every arc J_0, for all $t \in [0, T]$,*

$$\frac{1}{c_F} \leq \frac{\text{length}(J_t)}{\text{length}(J_0)} \leq c_F.$$

Proposition 1 can be obtained without a formula for c_F as an immediate consequence of [48, Theorem 2]. However, a constructive proof with a formula for c_F (obtained using Grönwall's inequality [36]) is given in the Supplementary Material of [107]. Proposition 1 implies in particular that the FTLE associated to all trajectories over $[0, T]$ are bounded in absolute value by $\frac{1}{T} \log c_F$, and thus these FTLE tend to 0 as $T \to \infty$.

In Case II, if there is only one time-interval during which an instantaneous stable equilibrium exists, the stability can be mathematically formalised and quantified [1] as follows.

Proposition 2. *Fix F such that there exist $0 \leq \tau_1 < \tau_2 \leq 1$ satisfying:*

- *for all $\tau \in [0, \tau_1) \cup (\tau_2, 1]$ and $\psi \in \mathbb{S}^1$, we have $F(\psi, \tau) \neq 0$;*

- *there is a continuous map $\tau \mapsto y_\tau$ from $[\tau_1, \tau_2]$ to $\mathbb{S}^1$ such that for each $\tau \in (\tau_1, \tau_2)$, we have $F(y_\tau, \tau) = 0$ and $\frac{\partial F}{\partial \psi}(y_\tau, \tau) < 0$;*

- *there exists $0 < \delta \leq \tau_2 - \tau_1$ and a continuous map $\tau \mapsto z_\tau$ from $[\tau_1, \tau_1 + \delta]$ to $\mathbb{S}^1$ such that for each $\tau \in (\tau_1, \tau_1 + \delta]$, we have $F(z_\tau, \tau) = 0$, $\frac{\partial F}{\partial \psi}(z_\tau, \tau) > 0$ and $F(\psi, \tau) \neq 0$ for all $\psi \in \mathbb{S}^1 \setminus \{y_\tau, z_\tau\}$.*

Let

$$\Lambda := \int_{\tau_1}^{\tau_2} \partial_1 F(y_\tau, \tau) \, d\tau < 0. \tag{5.7}$$

Fix any $\varepsilon > 0$. Then, provided T is sufficiently large, there exists an arc P with length$(P) < \varepsilon$ such that for every arc J_0 not intersecting P,

$$\left| \frac{1}{T} \log \left(\frac{\text{length}(J_T)}{\text{length}(J_0)} \right) - \Lambda \right| < \varepsilon.$$

---

[1]The proof is very similar to the proof of [48, Proposition], following adiabatic reasoning as described for Eq. (5.1), such that in principle one could construct an explicit formula defining "sufficiently large" T. The full proof, while not requiring any deep insight, is nonetheless technically involved, and will be published in a future work.

The quantity Λ defined in (5.7) is an approximation of the FTLE over $[0, T]$ associated to all trajectories except those starting in a small arc P.

If there is more than one time-interval during which an instantaneous stable equilibrium exists, then generally this will just further reinforce the mutual synchrony of trajectories. However, it is also theoretically possible that the cluster of trajectories formed over one or more of these time-intervals will happen to land in the small repulsive arc associated to the next of these time-intervals, causing the cluster to be re-dispersed. Generally (apart from some degenerate classes of examples), this behaviour will be very rare and will require extremely fine tuning of parameters.

5.4. Infinite-time model

We now consider a second example, namely the differential equation

$$\dot{\psi}(t) \;=\; -\gamma \sin(\psi(t)) + \Delta\omega + K\cos(\omega_m t) \tag{5.8}$$

with $\gamma, \omega_m > 0$ and $\Delta\omega, K \geq 0$. This is essentially the same as used for the numerics in chapter 4. It has also been studied in [23, 41, 48, 63] and references therein.

Slow variation here means that $K\omega_m$ is small. If we fix $\Delta\omega > \gamma$, and consider Eq. (5.8) over a time-interval $[0, T]$ with $T > \frac{\pi}{\omega_m}$, then the critical K-value between Case I and Case II is $K^* = \Delta\omega - \gamma$: for $K < K^*$ we expect neutrally stable dyamics, and for $K > K^*$ we expect stable dynamics, just as in (5.1). Moreover, if the duration is a whole number of periods $T = \frac{2\pi n}{\omega_m}$, then one can derive as in [65] and Eq. (5.7) above an approximation $\tilde{\Lambda}$ for the FTLE associated to the trajectories of (5.8) (apart from those starting in some very small arc), by adiabatically following the instantaneous stable equilibrium when it exists; that is, we define

$$\tilde{\Lambda} = \frac{1}{\pi} \int_{\{0 \leq s \leq \pi \,:\, |\Delta\omega + K\cos(s)| < \gamma\}} -\gamma \cos(y_\tau) \, \mathrm{d}\tau \tag{5.9}$$

where y_τ is the instantaneous stable equilibrium at time $t = \frac{\tau}{\omega_m}$, given by $y_\tau = \arcsin\left(\frac{\Delta\omega + K\cos(\tau)}{\gamma}\right)$. For $K < K^*$, we have $\tilde{\Lambda} = 0$, and for $K > K^*$, we have $\tilde{\Lambda} < 0$.

5.4.1. Stabilisation phenomenon

Fig. 5.4 shows bifurcation diagrams in terms of forward-time, reverse-time and FTLE simulations over 100 periods of the nonautonomous driving, for varying K and for varying $\Delta\omega$. These all very clearly show neutral stability for $K < \Delta\omega - \gamma$ and stability for $K > \Delta\omega - \gamma$, as predicted, with FTLE being approximated very well by $\tilde{\Lambda}$ (as also in Fig. 5.6 for small ω_m).

In Figs. 5.4 and 5.6, computation of initial positions $\psi(0)$ given final positions $\psi(T)$ (where T is a multiple of $\frac{2\pi}{\omega_m}$) is achieved by evolving the given values of $\psi(T)$ under the time-reversed system

$$\dot{\psi}(t) = \gamma \sin(\psi) - \Delta\omega - K\cos(\omega_m t). \tag{5.10}$$

Finite-time LE are computed according to Eq. (5.4). The value of $\tilde{\Lambda}$ in (5.9) is computed
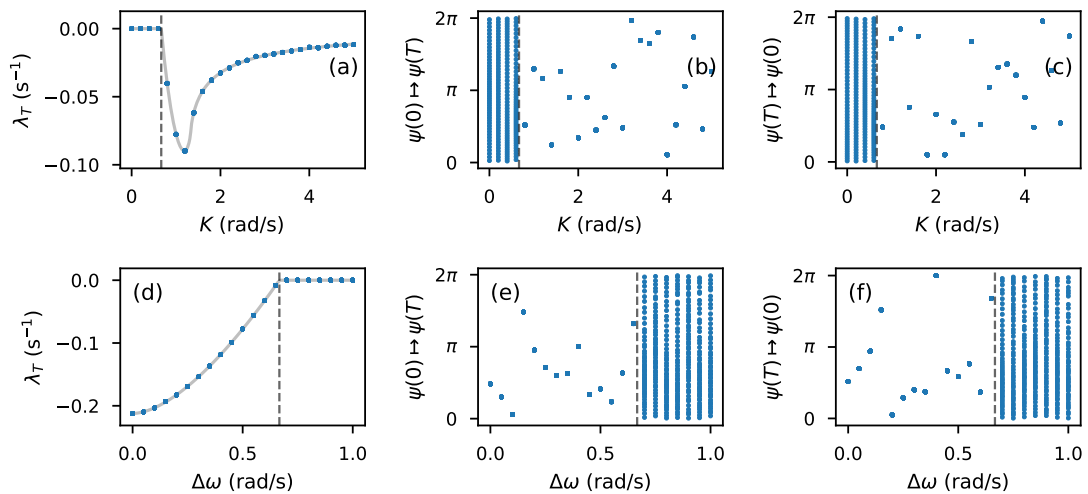
Figure 5.4.: Dynamics of (5.8), with varying K in (a)–(c) and varying $\Delta\omega$ in (d)–(f). In all plots, $\omega_m = 10^{-3}$ rad/s, $T = 2\pi \times 10^5$ s, and $\gamma = \frac{1}{3}$ rad/s. In (a)–(c), $\Delta\omega = 1$ rad/s and the value $\Delta\omega - \gamma = \frac{2}{3}$ rad/s is marked by the black dashed line. In (d)–(f), $K = \frac{1}{3}$ rad/s and the value $K + \gamma = \frac{2}{3}$ rad/s is marked by the black dashed line. In (a), (b), (d), and (e), results for the evolution $\psi(t)$ of 50 equally spaced initial conditions $\psi(0) = \frac{2\pi i}{50}$, $i = 0, \ldots, 49$, are shown: (a) and (d) show the FTLE λ_T, as defined by (5.4), for these trajectories, and also shows $\tilde{\Lambda}$ (defined in (5.9)) in grey; (b) and (e) shows the positions $\psi(T)$ of these trajectories at time T. In (c) and (f), the positions of $\psi(0)$ for the 50 trajectories of (5.8) with $\psi(T) = \frac{2\pi i}{50}$, $i = 0, \ldots, 49$, are shown.

by the explicit formula

$$
\tilde{\Lambda} = \begin{cases}
0 & \Delta\omega > \gamma \text{ and } K \leq \Delta\omega - \gamma \\[2mm]
-\frac{1}{\pi} \int_0^\pi \sqrt{\gamma^2 - (\Delta\omega + K\cos(t))^2} \, dt & \Delta\omega < \gamma \text{ and } K < \Delta\omega - \gamma \\[2mm]
-\frac{1}{\pi} \int_{\arccos\left(\frac{\gamma-\Delta\omega}{K}\right)}^\pi \sqrt{\gamma^2 - (\Delta\omega + K\cos(t))^2} \, dt & \textit{either } \Delta\omega \geq \gamma \text{ and } \Delta\omega - \gamma < K < \Delta\omega + \gamma, \\[2mm]
& \textit{or } \Delta\omega < \gamma \text{ and } \gamma - \Delta\omega \leq K < \gamma + \Delta\omega \\[2mm]
-\frac{1}{\pi} \int_{\arccos\left(\frac{\gamma-\Delta\omega}{K}\right)}^{\arccos\left(-\frac{\Delta\omega+\gamma}{K}\right)} \sqrt{\gamma^2 - (\Delta\omega + K\cos(t))^2} \, dt & K \geq \Delta\omega + \gamma
\end{cases}
$$

where γ, $\Delta\omega$ and K are all assumed to be nonnegative.

Now, let us illustrate the synchronising dynamics developing over time, for $\Delta\omega = K = 1$ rad/s and $\gamma = \frac{1}{3}$ rad/s, again with $\omega_m = 10^{-3}$ rad/s. Fig. 5.5 shows behaviour over the first 5 periods of $\cos(\omega_m t)$: above each t-value are shown the values of $\log f'_{0,t}(\psi_0)$ for 50 equally spaced points $\psi_0 = \frac{2\pi i}{50}$, $i = 0, \ldots, 49$, where $f_{0,t} \colon \mathbb{S}^1 \to \mathbb{S}^1$ is the map sending an initial condition to its position at time t. These values are computed by

$$
\log f'_{0,t}(\psi_0) = t\lambda_t
$$

where, for each t, λ_t is the FTLE as in Eq. (5.4) with $\psi(0) = \psi_0$. In agreement with the description give earlier, all the trajectories exhibit neutrally stable evolution until some time when they start to synchronise, corresponding to when the instantaneous vector field has a fixed point; the achieved synchrony is maintained during the next time-interval corresponding to when there is no fixed point for the instantaneous vector field; this synchrony is then strengthened further during the next time-interval corresponding to when there is a fixed point again; and so on. Again, we see $\tilde{\Lambda}$ being a good prediction for the FTLE over integer time-periods.

5.4.2. Mismatch between infinite-time and finite-time analysis

But unlike in (5.1), the nonautonomous term $K\cos(\omega_m t)$ in Eq. (5.8) happens to be periodic. Accordingly, analysing (5.8) within the framework of coordinate-invariant asymptotic dynamics, one obtains the following basic fact.[2]

Proposition 3. *Fix $\Delta\omega > \gamma > 0$. For any $K > 0$, there are intervals of ω_m-values arbitrarily close to 0 for which the system* (5.8) *is neutrally stable, with all trajectories having an asymptotic Lyapunov exponent of exactly zero.*

---

[2]This follows from [63, Theorems 1 and 4].
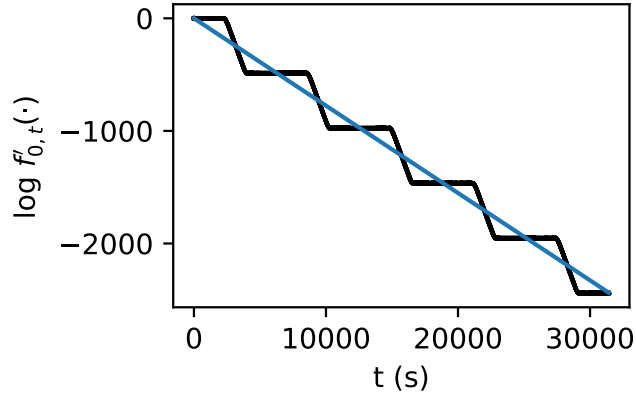
Figure 5.5.: Evolution of synchrony of solutions of (5.8), over the time-interval $[0, \frac{10\pi}{\omega_m}]$, i.e. 5 time-periods. Parameters are $\omega_m = 10^{-3}$ rad/s, $\Delta\omega = K = 1$ rad/s and $\gamma = \frac{1}{3}$ rad/s. For each t-value, the values of $\log f'_{0,t}(\psi_0)$ for 50 equally spaced points $\psi_0 = \frac{2\pi i}{50}$, $i = 0, \ldots, 49$, are shown in black, where $f_{0,t} : \mathbb{S}^1 \to \mathbb{S}^1$ is the map sending an initial condition to its position at time t. Also, for each t-value, the value of $t\tilde{\Lambda}$ is shown in blue.

This stands in contrast to what the numerics in Fig. 5.4 would suggest – namely that as expected from our finite-time adiabatic reasoning, provided $K\omega_m$ is small, $K > \Delta\omega - \gamma$ implies stable dynamics. The discrepancy between this and Proposition 3 is illustrated in Fig. 5.6. This discrepancy is due precisely to the re-dispersion effect described further above; it requires extreme fine-tuning (as evidenced further in Fig. 5.7 below) and thus is not observed in any of our simulations. But the mathematical tools necessary to obtain Proposition 3 do not reveal any such information. Thus, an asymptotic-time approach risks positively obscuring the very significant stabilisation phenomenon observed in Fig. 5.4, which would generally be of far greater physical relevance than the tiny intervals of exceptional ω_m-values.

Three cases

Before explaining in more details the reasons for the discrepancy, we detail the three types of dynamics that Eq. (5.8) exhibits. As a slight generalisation of Eq. (5.8), we can consider

$$\dot{\psi}(t) = -\gamma \sin(\psi(t)) + \Delta\omega + Kp(\omega_m t) \tag{5.11}$$

where $p(\,\cdot\,)$ is any smooth 2π-periodic function satisfying $\int_0^{2\pi} p(s)\, ds = 0$.

Once again, an *arc* is a closed connected proper subset of $\mathbb{S}^1$ with non-empty interior. Given an arc $J_0 \subset \mathbb{S}^1$ of initial conditions, we write J_t for the arc of positions of the subsequent trajectories of (5.11) at time t. By [63, Theorems 1 and 4], from the point of view of coordinate-invariant asymptotic dynamics, Eq. (5.11) may exhibit neutrally stable dynamics or global-scale stable
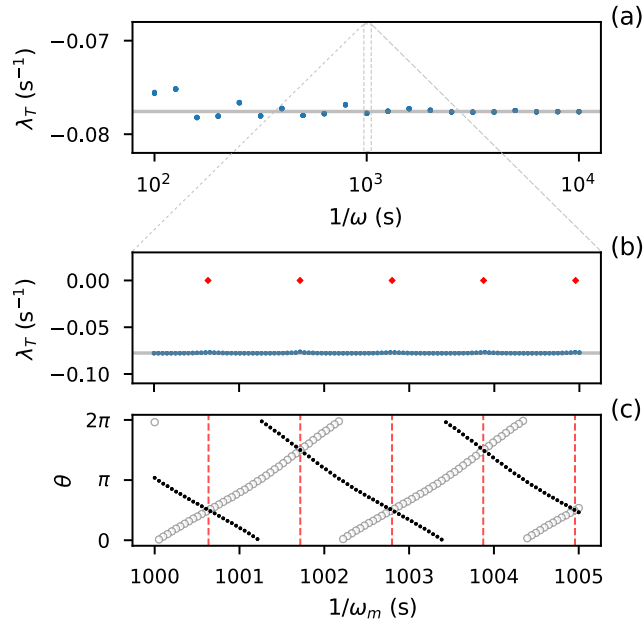
Figure 5.6.: Discrepancy between finite-time approach and asymptotic analysis, in system (5.8) with varying ω_m. Other parameters are $\gamma = \frac{1}{3}$ rad/s and $K = \Delta\omega = 1$ rad/s. (a) For each ω_m-value, the FTLE λ_T as defined by (5.4) are shown for the trajectories of 50 equally spaced initial conditions $\psi(0) = \frac{2\pi i}{50}$, $i = 0, \dots, 49$, with $T = \frac{200\pi}{\omega_m}$ (i.e. 100 periods). The value $\tilde{\Lambda}$ defined in (5.9) is marked in grey. The FTLE are indeed approximately equal to $\tilde{\Lambda}$ over the whole ω_m-range, especially for smaller ω_m. (b) Zoomed-in version of (a); the red points indicate the location of the small intervals of ω_m-values for which all initial conditions have zero asymptotic Lyapunov exponent. (c) Forward (hollow circle) and backward (solid circle) evolution of 50 equally spaced points $\frac{2\pi i}{50}$, $i = 0, \dots, 49$, over the time-interval $[0, \frac{2\pi}{\omega_m}]$. In both forward and backward time, the 50 trajectories cluster around one point; the values of ω_m where the two curves of clustered points cross correspond to where the red points are marked in (b).

dynamics, otherwise it must exhibit dynamics lying at the "boundary" between these two. More precisely, the three possible scenarios are as follows:

- *Neutrally Stable Scenario*: There exists $c \geq 1$ such that for every arc J_0, for all $t \in [0, \infty)$,

$$\frac{1}{c} \leq \frac{\text{length}(J_t)}{\text{length}(J_0)} \leq c.$$

  In this case, the ALE associated to all trajectories is 0.

- *Stable Scenario*: There exists $\lambda^{(\infty)} < 0$ and $p \in \mathbb{S}^1$ such that for every arc J_0 with $p \notin J_0$,

$$\frac{1}{t} \log\left(\frac{\text{length}(J_t)}{\text{length}(J_0)}\right) \to \lambda^{(\infty)} \quad \text{as} \quad t \to \infty.$$

  In this case, the ALE associated to every trajectory except the trajectory starting at p is $\lambda^{(\infty)}$. The trajectory starting at p is an unstable $\frac{2\pi}{\omega_m}$-periodic trajectory, and all other trajectories are attracted to a stable $\frac{2\pi}{\omega_m}$-periodic trajectory.

- *Boundary Scenario*: There is a $\frac{2\pi}{\omega_m}$-periodic solution which asymptotically attracts all trajectories from one direction but is unstable due to being locally repulsive in the other direction. In this case, the ALE associated to every trajectory is 0.

The first two scenarios are infinite-time analogues of the dynamics described in Propositions 1 and 2 respectively. Proposition 3 asserts that if $\Delta\omega > \gamma$ then for any $K > 0$ there are intervals of ω_m-values arbitrarily close to 0 for which the dynamics is described by the neutrally stable scenario. The reason for this is as follows:

If there does not exist a $\frac{2\pi}{\omega_m}$-periodic solution, the system must be in the neutrally stable scenario. By classical Poincaré-Denjoy theory, the existence or non-existence of $\frac{2\pi}{\omega_m}$-periodic solutions can be determined by the *asymptotic rotation number*

$$\Omega \;:=\; \lim_{t\to\infty} \frac{\hat{\psi}(t)}{t} \tag{5.12}$$

where $\hat{\psi}\colon \mathbb{R} \to \mathbb{R}$ is any lift of any solution of (5.11); the value of $\hat{\psi}(0)$ does not affect the value of Ω. There exists a $\frac{2\pi}{\omega_m}$-periodic trajectory if and only if Ω is an integer multiple of ω_m. Now it is well-known that Ω depends continuously on parameters – in this case, if we fix $\Delta\omega$ and γ, then Ω depends continuously on K and ω_m. But also, observe that $\Omega \in [\Delta\omega - \gamma, \Delta\omega + \gamma]$. Therefore, if $\Delta\omega > \gamma$, then $\frac{\Omega}{\omega_m}$ must tend continuously towards ∞ as $\omega_m \to 0$ regardless of the value of K (even if K is not actually a fixed value but varies as a continuous function of ω_m). Hence in particular, there must be intervals of ω_m-values arbitrarily close to 0 for which $\frac{\Omega}{\omega_m}$ is not an integer and so (5.11) is in the neutrally stable scenario.

Discrepancy

We now turn back to explaining the discrepancy shown in Fig. 5.6. The value of $\tilde{\Lambda}$ marked in grey in Figs. 5.6(a) and 5.6(b), as defined by Eq. (5.9), is given by

$$\tilde{\Lambda} = -\frac{1}{\pi} \int_{\arccos(-\frac{2}{3})}^{\pi} \sqrt{\frac{1}{9} - (1 + \cos(t))^2}\, dt.$$

In Fig. 5.6(b), the ω_m-values at which the red points are marked were numerically obtained as follows: For the unwrapped phase $x(t)$ as governed by the differential equation

$$\dot{x}(t) \;=\; -\gamma \sin(x(t)) + \Delta\omega + K \cos(\omega_m t)$$

on the real line, setting $x(0) = 0$, it was observed that $x(\frac{2\pi}{\omega_m})$ increased approximately linearly with $1/\omega_m$, with increments across consecutive values in the $(1/\omega_m)$-discretisation being strictly positive and very small compared to 2π. Hence it is possible to carry out linear interpolation of

the wrapped phase $\psi(\frac{2\pi}{\omega_m})$ as a function of $1/\omega_m$ (with $\psi(0) = 0$). Where this linearly interpolated function of $1/\omega_m$ crosses $\frac{\pi}{2}$ and $\frac{3\pi}{2}$ is where the red points are marked; as in Fig. 5.6(c), the locations of $\psi(\frac{2\pi}{\omega_m})$ are the same for the other 49 initial conditions $\psi(0) = \frac{2\pi i}{50}$ as for $\psi(0) = 0$.

Let us now explain the reasoning behind why these points indicate the location of Neutrally Stable Scenario intervals:

Let $f_{0,\frac{2\pi}{\omega_m}} : \mathbb{S}^1 \to \mathbb{S}^1$ be the map sending an initial condition $\psi(0)$ to its position $\psi(\frac{2\pi}{\omega_m})$ at time $\frac{2\pi}{\omega_m}$. It is not hard to show that the reflection $\psi \mapsto \pi - \psi$, i.e. the reflection preserving the points $\frac{\pi}{2}$ and $\frac{3\pi}{2}$, is a conjugacy between $f_{0,\frac{2\pi}{\omega_m}}$ and its inverse $f_{\frac{2\pi}{\omega_m},0}$.

By [63, Theorems 1 and 4], $f_{0,\frac{2\pi}{\omega_m}}$ either has: (i) no fixed points, corresponding to the Neutrally Stable Scenario; (ii) two fixed points s_{ω_m} and $p_{\omega_m} = \pi - s_{\omega_m}$, with s_{ω_m} attracting and p_{ω_m} repelling, corresponding to the Stable Scenario; or (iii) exactly one fixed point $p_{\omega_m} \in \{\frac{\pi}{2}, \frac{3\pi}{2}\}$, corresponding to the Boundary Scenario. Since K lies in the interval $(\Delta\omega - \gamma, \Delta\omega + \gamma)$, Eq. (5.8) defined on the time-interval $[0, \frac{2\pi}{\omega_m}]$ fulfils all the assumptions of Proposition 2 (with $F(\psi, \tau) := -\gamma\sin(\psi) + \Delta\omega + K\cos(\pi\tau)$). Hence, for small enough ω_m, it is guaranteed that the map $f_{0,\frac{2\pi}{\omega_m}}$ has nearly zero gradient throughout the circle minus a tiny arc P_{ω_m}, and maps $\mathbb{S}^1 \setminus P_{\omega_m}$ onto some tiny arc S_{ω_m}. Note that the reflection $\pi - S_{\omega_m}$ of S_{ω_m} is contained in P_{ω_m}, and that if the arcs S_{ω_m} and P_{ω_m} do not overlap then (5.8) is in the Stable Scenario with $s_{\omega_m} \in S_{\omega_m}$ and $p_{\omega_m} \in P_{\omega_m}$. Conversely, whenever (5.8) is in the Stable Scenario, we have that $p_{\omega_m} \in P_{\omega_m}$, and therefore $s_{\omega_m} \in \pi - P_{\omega_m}$.
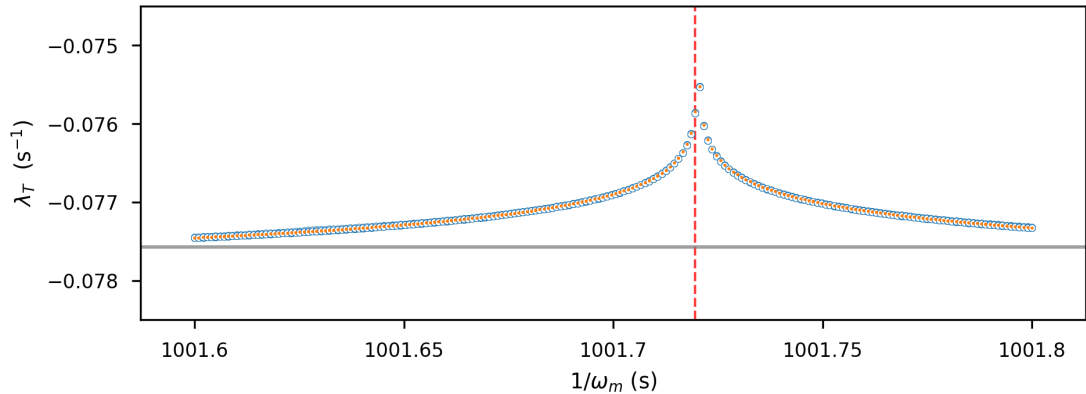
Figure 5.7.: FTLE for (5.8) near a red-marked point in Fig. 5.6(b). Parameters are $\Delta\omega = K = 1$ rad/s and $\gamma = \frac{1}{3}$ rad/s. For each ω_m-value, in blue are shown the FTLE λ_T associated to the trajectories of 10 initial conditions $\psi(0) = \frac{2\pi i}{10}$ with $T = \frac{200\pi}{\omega_m}$ (i.e. 100 periods), and in orange are shown the FTLE λ_T associated to the trajectories of 2 initial conditions $\psi(0) = 0, \pi$ with $T = \frac{2000\pi}{\omega_m}$ (i.e. 1000 periods). The red dashed line indicates the location of a small interval of ω_m-values for which the asymptotic Lyapunov exponent is 0. The value of $\tilde{\Lambda}$ is shown in grey.

The locations of S_{ω_m} and P_{ω_m} are represented in Fig. 5.6(c) by a hollow circle and a solid circle respectively. As $1/\omega_m$ increases, S_{ω_m} moves anticlockwise and P_{ω_m} moves clockwise. As these

small arcs cross past each other – which is the same as when they cross past $\frac{\pi}{2}$ or $\frac{3\pi}{2}$ – there must be a point at which the attracting and repelling fixed points of $f_{0,\frac{2\pi}{\omega_m}}$ collide. At the moment of collision, the system is in the Boundary Scenario. As $1/\omega_m$ is increased beyond this point, before the system can return to the Stable Scenario there must be some interval of $(1/\omega_m)$-values on which $f_{0,\frac{2\pi}{\omega_m}}$ has no fixed points, corresponding to the Neutrally Stable Scenario.

Zoom in

Now Fig. 5.6(b) showed FTLE as a function of ω_m. We now zoom in on Fig. 5.6(b), near one of the ω_m-values that was marked by a red point to indicate the presence of a small interval of ω_m-values for which the asymptotic dynamics is described by the Neutrally Stable Scenario. Results are shown in Fig. 5.7. The location of this small interval is indicated by the red dashed line; the location on this zoomed in plot was computed by the same method as described above for Fig. 5.6(b).

In Fig. 5.7, even with the much higher $(1/\omega_m)$-resolution than in Fig. 5.6(b), only stable dynamics is observed for both $T = \frac{200\pi}{\omega_m}$ (as in Fig. 5.6(b)) and $T = \frac{2000\pi}{\omega_m}$; moreover, the values of λ_T remain essentially the same as T is changed from $\frac{200\pi}{\omega_m}$ to $\frac{2000\pi}{\omega_m}$.

How slow is slow?

Finally, most of the numerics so far have assumed very slow variation – which, for (5.8), means that $K\omega_m$ is very small – and assumed very long times. We now illustrate that the stabilisation phenomenon described can be observed when the slowness of variation is not so extreme, and the time is not so long. Fig. 5.8 shows the dynamics of (5.8) for varying K, with $\omega_m = 0.03$ rad/s
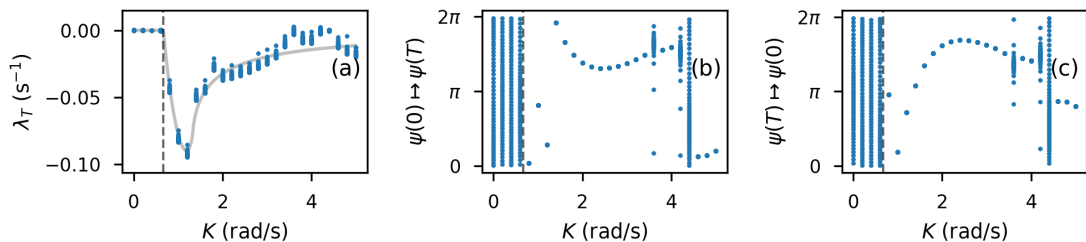
Figure 5.8.: Dynamics of (5.8) with varying K. Other parameters are $\omega_m = 0.03$ rad/s, $\gamma = \frac{1}{3}$ rad/s and $\Delta\omega = 1$ rad/s, and (5.8) is integrated over $[0, T]$ with $T = \frac{10\pi}{\omega_m}$. In (a) and (b), for each K-value, results for the evolution $\psi(t)$ of 50 equally spaced initial conditions $\psi(0) = \frac{2\pi i}{50}$, $i = 0, \ldots, 49$, are shown: (a) shows the FTLE λ_T, as defined by Eq. (5.4), for these trajectories, and also shows $\tilde{\Lambda}$ in grey; (b) shows the positions $\psi(T)$ of these trajectories at time T. In (c), for each K-value, the positions of $\psi(0)$ for the 50 trajectories of (5.8) with $\psi(T) = \frac{2\pi i}{50}$, $i = 0, \ldots, 49$, are shown. The value $\Delta\omega - \gamma = \frac{2}{3}$ rad/s is marked by the black dashed line.

and $T = \frac{10\pi}{\omega_m} \approx 10^3$ s (i.e. 5 time-periods), again with $\gamma = \frac{1}{3}$ rad/s and $\Delta\omega = 1$ rad/s. We clearly see neutral stability for $K < \Delta\omega - \gamma = \frac{2}{3}$ rad/s. At the point that K rises above $\Delta\omega - \gamma$, we clearly see stabilisation occurring; this stability persists for K-values up to about 3.4 rad/s.

5.5. Summary

Thus, in this chapter, we have seen that restricting the analysis of dynamics to the traditional framework has the potential to impede progress in diverse fields of scientific inquiry, such as all those mentioned further above. The time-variable and finite-time nature of open systems needs to be incorporated in the development and application of dynamical systems theory.

Specifically, we have analysed the finite- but long-time stability of a system defined only over finite-time, to which the asymptotic framework cannot be applied. In doing so, we have uncovered a stabilisation phenomenon, which is a generalisation of that in the previous chapter. For a system that can be defined over infinite time, we have shown that the asymptotic analysis misses the stabilisation phenomenon. More specifically, the ALE is zero for some small intervals at arbitrary large values of parameter K, whereas the FTLE is negative above a critical K. Note that existence of these intervals is proven, and that we estimated their locations. Determining the exact intervals, or at least their size remains however a challenge, and would improve our understanding of the system.

In conclusion, restricting the analysis of dynamics to the time-asymptotic framework has the potential to impede progress in diverse fields of scientific inquiry. The true temporal nature of open systems needs to be incorporated in the development and application of dynamical systems theory. The reality of unignorable time-variability also has implications for inverse problem methodologies; *time-localised* analysis and inference methods [29, 142] will not only reveal more information than their time-independent counterparts but also allow for much more reliable conclusions about systems that may be time-varying.

In the next chapter, we extend the ideas of this chapter and chapter 4 to study a driven network of oscillators.

6. Stability in network of identical oscillators

6.1. Introduction

Ensembles of coupled oscillators driven by a common external driving can represent natural and man-made systems. A typical example is the day-light cycles drive the suprachiasmatic nucleus neurons in our brain, which in turn control all circadian rhythms in our bodies, making sure the body's different clocks tick together [40]. In this chapter, we extend the study of chapter 4 by considering network of oscillators driven by a time-varying external oscillator. The network is composed of identical copies of the driven oscillator of chapter 4. Two cases are considered: attractive and repulsive couplings. Results of chapter 4 are extended in both cases, analytically and numerically. Results indicate when time-variability in the driving is beneficial for stability, and provides control strategies to stabilise the dynamics.

This chapter is composed of two main sections. In Sec. 6.3, we provide an analytical linear stability analysis of the synchronous solutions. These results are then discussed and confirmed numerically in Sec. 6.4, in the attractive and repulsive cases.

6.2. Model

We consider a driven network of N identical oscillators defined by phases θ_i and frequency ω,

$$\dot{\theta}_i = \omega + D \sum_{j=1}^{N} A_{ij} \sin(\theta_i - \theta_j) + \gamma \sin[\theta_i - \theta_0(t)], \tag{6.1}$$

for $i = 1, \ldots, N$, with coupling constant D, and where $\mathbf{A}$ stands for any (undirected) adjacency matrix with elements $A_{ij} \in \{0, 1\}$. Each oscillator is driven with strength $\gamma \geq 0$ by the same external oscillator with phase $\theta_0(t)$ and time-varying frequency

$$\dot{\theta}_0 = \omega_0[1 + kf(\omega_m t)], \tag{6.2}$$

where ω_0 is the non-modulated frequency, f is a bounded function, and k and ω_m are the amplitude and frequency of the imposed modulation, respectively. Note that $f(\omega_m t)$ is a generic function, and need not be periodic; without loss of generality, we bound its image in $[-1, 1]$. System (6.1)-(6.2) is a direct generalisation to networks of the single driven oscillator system presented in chapter 4.

The non-driven network, $\gamma = 0$, is an autonomous system. In this case, a (fully) *synchronous* solution always exists, i.e. a solution where all oscillators are in the same state at all times, $\theta_i = \theta_j$ for all $i \neq j$. This is as long as the network is connected, meaning that there is a path between any two nodes (oscillators). The synchronous solution is stable (unstable) if the coupling between oscillators is *attractive* (*repulsive*), i.e., $D < 0$ (> 0) [155]. In the repulsive case, the system is attracted to an incoherent state.

6.3. Theoretical analysis

In the driven system, $\gamma \neq 0$, synchronous solutions also exist. It is convenient to go to the rotating frame of the driving, $\psi_i = \theta_i - \theta_0(t)$, where system (6.1) is rewritten

$$\dot{\psi}_i = \Delta\omega(t) + D\sum_{j=1}^{N} A_{ij}\sin(\psi_i - \psi_j) + \gamma\sin\psi_i, \tag{6.3}$$

for $i = 1, \ldots, N$, where $\Delta\omega(t) = \omega - \omega_0[1 + kf(\omega_m t)]$ is the time-dependent frequency mismatch. We refer to the θ_i as the *phases*, and to the ψ_i as the *phase differences* between the phase of the driving and that of the i-th oscillator. System (6.3) is nonautonomous due to the time-dependent frequency mismatch, and is hence hard to treat in general. In the rest of the study, we assume ω_0 is modulated slowly, i.e., $\omega_m \ll \omega_0$, and use an adiabatic approach to study the existence and stability of synchronous solutions.

6.3.1. Autonomous case

To that end, we first consider the simpler case of a constant driving frequency, recovered for $k = 0$, for which $\Delta\omega(t) = \Delta\omega = \omega - \omega_0$ is constant and system (6.3) is autonomous. A *synchronous* solution, $\psi_i = \tilde{\psi}$ for all $i = 1, \ldots, N$, always exists, and obeys

$$\dot{\tilde{\psi}} = \Delta\omega + \gamma\sin\tilde{\psi}, \tag{6.4}$$

which is the so-called Adler equation describing a single driven oscillator [127]. From Eq. (6.4), two types of synchronous solutions can be identified: *synchronised* (to the driving), or not . First,

if $\gamma \geq |\Delta\omega|$ is satisfied, there exists a stable fixed point. This fixed point corresponds to the synchronous synchronised (SS) solution, $\psi_{\mathrm{SS}} = \pi - \arcsin(-\Delta\omega/\gamma)$, characterised by a constant phase difference, $\dot{\psi}_{\mathrm{SS}} = 0$. Second, if the synchronisation condition is not met, $\gamma < |\Delta\omega|$, there exists a synchronous not synchronised (SNS) type of solutions, denoted ψ_{SNS}, which grows (or decays) monotonically, $\dot{\psi}_{\mathrm{SNS}} > 0$ (or < 0).

We now investigate the linear stability against a small heterogeneous perturbation $\delta\psi_i$ around those solutions. This is determined by linearising Eq. (6.3) for each node around a solution $\tilde{\psi}(t)$, which stands for either the SS or SNS,

$$\delta\dot{\psi}_i = -D\sum_{j=1}^{N} L_{ij}\delta\psi_j + \gamma\delta\psi_i \cos\tilde{\psi}(t). \tag{6.5}$$

Here, $L_{ij} = A_{ij} - K_i\delta_{ij}$ denotes the Laplacian matrix of the network, defined in terms of the connectivity of each node $K_i = \sum_{j=1}^{N} A_{ij}$, and the Kronecker delta δ_{ij}. One can now decouple this N-dimensional problem by projecting it onto the eigenbasis of the Laplacian, defined as

$$\sum_{j=1}^{N} L_{ij}\phi_i^{(\alpha)} = \Lambda_\alpha\phi_i^{(\alpha)}, \tag{6.6}$$

where the $\boldsymbol{\phi}^{(\alpha)}$ are the eigenvectors associated to the eigenvalues Λ_α, for $\alpha = 1, \ldots, N$. The latter are non-positive and real, since the network is assumed to be undirected, and ordered $\Lambda_1 = 0 > \Lambda_2 \geq \ldots \geq \Lambda_N$. The perturbation can be decomposed in that basis, and we look for solutions of the form $\delta\psi_i(t) = \sum_{\alpha=1}^{N} c_\alpha e^{\int_0^t \lambda^\alpha(t')\,\mathrm{d}t'}\phi_i^{(\alpha)}$. Plugging into Eq. (6.5) and solving for each α yields the instantaneous Lyapunov exponent spectrum

$$\lambda^\alpha(t) = -D\Lambda_\alpha + \gamma\cos\tilde{\psi}(t), \tag{6.7}$$

which is completely general and also valid in the nonautonomous case, as will be seen later. Now in the autonomous case, $\tilde{\psi}(t)$ is periodic modulo 2π [127] and hence (long-term) Lyapunov exponent spectrum is well defined as the time-average of the instantaneous values

$$\lambda^\alpha = -D\Lambda_\alpha + \gamma\langle\cos\tilde{\psi}(t)\rangle. \tag{6.8}$$

For the sake of clarity, note that by A choice of notation, the λ^α (superscript) are, in general, not in descending order whereas the λ_α (subscript) are by definition the exponents in descending order, as introduced in Eq. (2.8) of chapter 2.

An explicit form of formula (6.8) is obtained by splitting it into two cases

$$\lambda^\alpha = \begin{cases} -D\Lambda_\alpha - \sqrt{\gamma^2 - \Delta\omega^2} & \text{if } \gamma > |\Delta\omega|, \\ -D\Lambda_\alpha & \text{else.} \end{cases} \qquad (6.9)$$

For the synchronised case, $\gamma > |\Delta\omega|$, the explicit solution $\psi_{\text{SS}} = \pi - \arcsin(-\Delta\omega/\gamma)$, which is constant, was plugged into formula (6.8). For the not synchronised case, the solution is ψ_{SNS}, for which the averaging term in formula (6.8) vanishes.

6.3.2. Nonautonomous case

In general, the driving frequency is time-dependent, $k \neq 0$, and synchronous solutions obey a nonautonomous version of Eq. (6.3)

$$\dot{\tilde{\psi}} = \Delta\omega(t) + \gamma \sin \tilde{\psi}, \qquad (6.10)$$

which was studied in [65] and chapter 4. As previously mentioned, here and throughout the paper, we assume slow modulation of the frequency, i.e. ω_m small. Equivalently, $\Delta\omega(t)$ varies much more slowly than the dynamics of the system. Hence, there is a separation of timescales: $\Delta\omega(t)$ is the slow variable, and $\tilde{\psi}(t)$ the fast one. Thus, over the fast timescale, the frequency mismatch is quasi-static, and the slowly moving point attractor $\psi_{\text{SS}}(t) = \pi - \arcsin(-\Delta\omega(t)/\gamma)$ is followed adiabatically, when it exists [65]. This state corresponds to the SS solution of the autonomous case, and differs with it in being only *quasi*-constant, i.e., $\dot{\tilde{\psi}}_{\text{SS}} = 0$ over the fast timescale, and existing only at times such that $\gamma > |\Delta\omega(t)|$.

Consequently, in contrast to the autonomous case, Eq. (6.10) shows three types of synchronous solutions: two of them correspond to the SS and SNS solutions as discussed in the autonomous case, whereas a third type exhibits *intermittent* synchronisation. Three regions in parameter space can thus be defined, each corresponding to the existence of one of those types solutions, as in chapter 4, as illustrated in Fig. 6.1. In region I, the condition $\gamma > |\Delta\omega(t)|$ is not met at any time. The solution grows (or decays) monotonically and we denote it $\psi_{\text{SNS}}(t)$. In region II, the condition $\gamma > |\Delta\omega(t)|$ is met at all times. The solution is denoted by $\psi_{\text{SS}}(t)$ and has an approximately null time derivative, as described above. In region III, $\gamma > |\Delta\omega(t)|$ is met only at certain times. The phase difference alternates between times of growth (or decay), and quasi-constant (bounded) epochs. We call it synchronous intermittently synchronised (SIS), and denote it $\psi_{\text{SIS}}(t)$. The three types of solutions are illustrated in Fig. 6.2(a) and will be discussed in the next section.

The three regions, depicted in Fig. 6.1, are equivalently defined by the following time-independent

Figure 6.1.: Regions of existence of synchronous solutions. Region I: no synchronisation (SNS). Region II: synchronisation (SS). Region III: intermittent synchronisation (SIS).
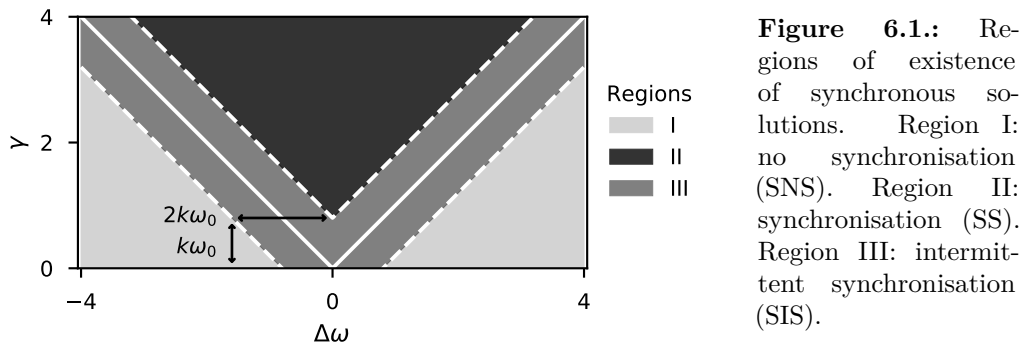
conditions: (I) $\gamma \geq |\Delta\omega| + \omega_0 k$, (II) $\gamma \leq |\Delta\omega| - \omega_0 k$, and (III) $|\Delta\omega| - \omega_0 k \leq \gamma \leq |\Delta\omega| + \omega_0 k$, where we denote $\Delta\omega \equiv \omega - \omega_0$ the central frequency mismatch, or alternatively, the frequency mismatch of the autonomous case (see chapter 4). Note that these regions are defined based on the condition of existence of the aforementioned types of solutions, and not based on their stability.

The adiabatic assumption allows us to obtain the following formula for the adiabatic LE spectrum, as a nonautonomous version of formula (6.9), by retracing the same reasoning

$$\lambda^\alpha(t) = \begin{cases} -D\Lambda_\alpha - \sqrt{\gamma^2 - \Delta\omega(t)^2} & \text{for } t : \gamma > |\Delta\omega(t)|, \\ -D\Lambda_\alpha & \text{else.} \end{cases} \tag{6.11}$$

Equation (6.11) enables us to draw conclusions about the stability of the aforementioned states. The stability of the SS solution can be assessed by the first condition in Eq. (6.11). The stability of the SNS is determined by the second condition in Eq. (6.11). Finally, the stability of the SIS is determined by the first condition of Eq. (6.11) at times such that $\gamma > |\Delta\omega(t)|$, and the second condition the rest of the time.

Note that this result holds true regardless of the network size, topology, or the shape of the frequency modulation function $f(\omega_m t)$.

6.4. On the stability of the synchronous solution

We now examine the stability of the synchronous solutions further via formula (6.11) in the attractive and repulsive cases.

6.4.1. Attractive case

In this case, $D < 0$, all oscillators tend to display the same phase, when not driven. For a given network, only the largest LE $\lambda_{max}(t)$ determines the stability. In this case, it is $\lambda_{max}(t) = \lambda^1(t)$ which corresponds to $\Lambda_1 = 0$ in formula (6.11), and reads

$$\lambda_{max}(t) = \begin{cases} -\sqrt{\gamma^2 - \Delta\omega(t)^2} & \text{for } t : \gamma > |\Delta\omega(t)|, \\ 0 & \text{else,} \end{cases} \tag{6.12}$$

a condition which is identical to that obtained for the single oscillator case considered in chapter 4, even though we have now an arbitrary network of oscillators.

For the sake of clarity, we set $f(\omega_m t) = \sin(\omega_m t)$ in numerical examples. Note, however, that the analysis is independent of the explicit form of $f(\omega_m t)$, which can in general be aperiodic, or even defined only over a finite timespan, as discussed in chapter 5.

Typical dynamics of the ψ_i is shown for the three regions in Fig. 6.2(a). The SS (solid) and SNS (dotted) are bounded and unbounded, respectively, as mentioned in the previous section. For the SS (SNS), $\gamma > |\Delta\omega(t)|$ ($\gamma < |\Delta\omega(t)|$) is always met, and hence the LE is negative (zero), i.e., stable (neutrally stable) at all times, as seen from Eq. (6.12). However, the SIS (dashed) stays bounded only intermittently. In this example, the timescale that controls the alternation of those epochs is the period of the imposed modulation, $T_m = 2\pi/\omega_m$, which could be arbitrarily long. Note that these epochs of growth are not the typical 2π *phase slips* of the fixed-frequency single oscillator case [127], observed close to the synchronisation border. Here, the "slip" is a drift caused by the temporary neutral stability, and its relative importance depends on the length of that neutrally stable epoch, as seen from Fig. 6.2(b).

Now, the SIS is analysed further as shown in Fig. 6.2(b)-(d). Figure 6.2 (b) shows the adiabatic LE (dashed black) (6.12). Epochs where it is negative (null) correspond to the ψ_i growing (staying bounded). Moreover, Fig. 6.2 (b) shows the agreement between the instantaneous LE (6.7) (grey) and the adiabatic LE (6.12). This confirms *a posteriori* the adequacy of the adiabatic approach. The intermittency can also be seen in the time-frequency representation of $\sin\theta_1(t)$ for a trajectory of system (6.1), as shown in Fig. 6.2(c). Here, stability epochs correspond to the frequency being entrained by the driver (one frequency mode), whereas neutral stability epochs correspond to the presence of two frequency modes plus harmonics. Finally, a negative maximum LE guarantees convergence of different initial conditions, as long as they are in the basin of attraction of the synchronous solution, even if the trajectory is only intermittently synchronised to the driving. This is illustrated in Fig. 6.2(d).
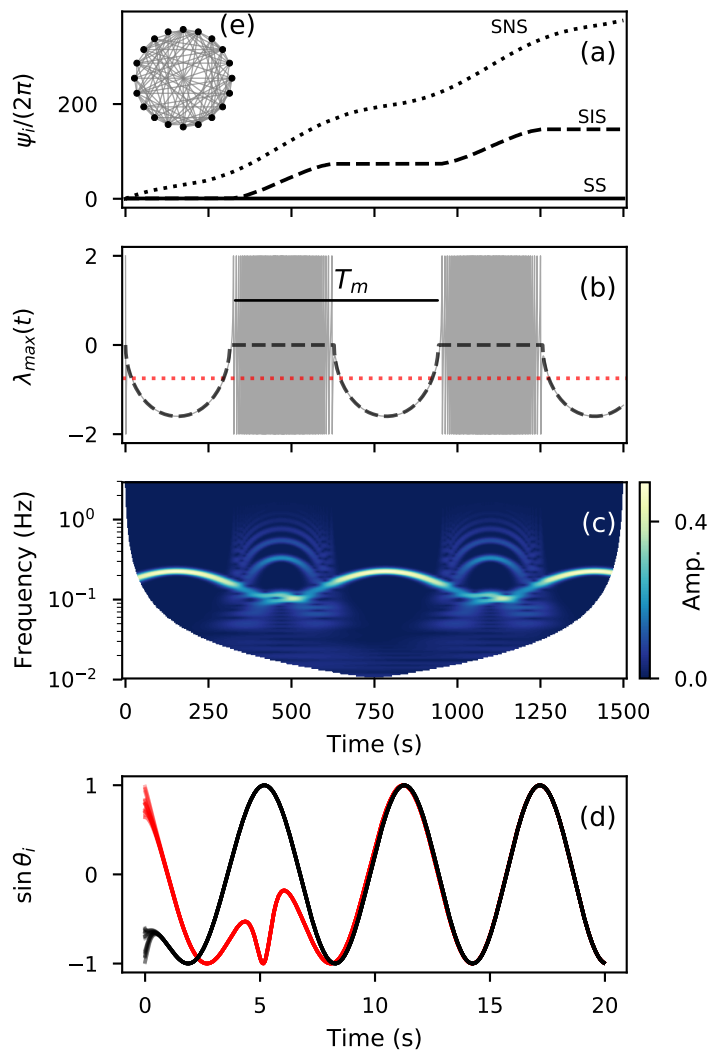
Figure 6.2.: Finite-time dynamics and stability, in the attractive case $D < 0$. (a) Typical dynamics of the phase difference ψ_i in the three regimes: synchronised (solid, $\gamma = 3$), intermittently synchronised (dashed, $\gamma = 2$), and not synchronised (dotted, $\gamma = 1$). Panels (b)-(d) only consider the intermittently synchronised trajectory. (b) Instantaneous stability, measured by the instantaneous LE (grey) given by Eq. (6.8) and the adiabatic approach (dashed black) of Eq. (6.12). The average LE, as defined in Eq. (6.13) is negative (dotted red). (c) Time-frequency representation computed applying continuous Morlet wavelet transform with central frequency 3 to the signal $y(t) = \sin\theta_1(t)$. Epochs of boundedness (drift) ψ_i correspond to negative (zero) $\lambda(t)$, and (no) frequency entrainment in (c) (respectively). (d) Convergence of two different initial conditions, in red and black, respectively, in the intermittent synchronisation regime. Each initial condition is a quasi-synchronous N-dimensional state. Each state first quickly becomes synchronous, and then converges to the synchronised solution. Other parameters are $N = 20$, $D = -0.5$, $k = 0.4$, $\Delta\omega = 2$, $\omega_0 = 1$. (e) Network used for the numerics: random with connection probability $p = 0.5$ and $\Lambda_N = -15.9$. Note that the results do not depend on the network considered.

Note that all other non-maximal LEs of the spectrum are negative at all time, $\lambda^i(t) < 0$, for $i = 2, \ldots, N$, since the corresponding Laplacian eigenvalues are negative. The exponent λ^1 measures the stability against a homogeneous perturbation, whereas the rest of the spectrum corresponds to any heterogeneous perturbation. In other words, any synchronous solution will

stay synchronous – all oscillators with the same phase – against any perturbation. During stable epochs, even the common phase of the synchronous state is stable. During neutrally stable epochs, however, the common phase of the synchronous solution can be pushed by a homogeneous perturbation, and change without the perturbation decaying or growing.
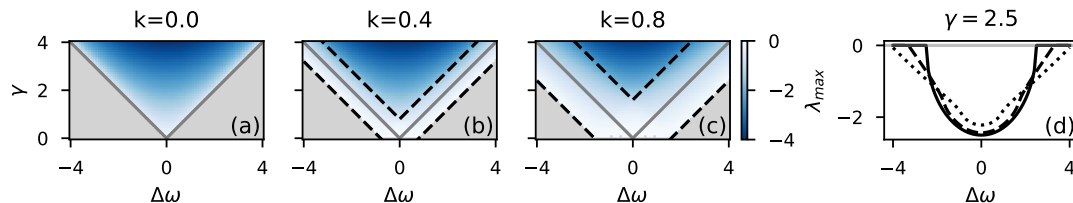
Figure 6.3.: Stability region increases with amplitude of nonautonomicity k, in the attractive case $D < 0$. (a)-(c) Quantitative stability measured by the LE of formula (6.13): the region of stability (shades of blue) increases with k. Gray values represent zero values of the LE. (d) Same LE values as in (a)-(c), shown only for $\gamma = 2.5$, for the different k values: 0.0 (solid), 0.4 (dashed), and 0.8 (dotted). The range of $\Delta\omega$ for which $\lambda_{max} < 0$ increases with k. Parameters are $D = -0.5$, $w_0 = 2$. This picture holds true for any network topology.

On average, over a time T, the maximum exponent is

$$\lambda_{max} = \tfrac{1}{T} \int_0^T \mathrm{d}t \; \lambda_{max}(t) \leq 0. \tag{6.13}$$

Note that the LE in Eq. (6.13) is strictly zero only in region I where the system does not synchronise to the driving at any time. Indeed, in region III, the adiabatic LE alternates between zero and negative values, and is negative on average. Moreover, region I decreases in size as k is increased, and so the remainder of parameter space, corresponding to stability $\lambda_{max} < 0$, grows. In other words, by increasing the amplitude of the nonautonomous modulation, one makes the region of stability larger in parameter space. In this region of stability, different initial conditions converge to one unique trajectory. In Fig. 6.3, panels (a)-(c) show the enlargement of the negative LE region in parameter space as k increases from 0.0 to 0.4, and 0.8. Panel (d) combines and shows those LE values for all three values of k, but for a single value of the forcing strength $\gamma = 2.5$. The region of stability is the union of regions II and III. Region II, where trajectories are always synchronised to the driving, decreases in size as k is increased, but region III grows enough so that their union grows. The phenomenon does not depend on the explicit form of $f(\omega_m t)$ and was also illustrated numerically, in the single driven oscillator case, for different aperiodic $f(\omega_m t)$ in chapter 4, and $f(\omega_m t)$ defined over a finite time in chapter 5.

6.4.2. Repulsive case

In this case, $D > 0$, all oscillators have a tendency towards pairwise asynchrony, when not driven. In the unforced network, the synchronous solution is always unstable, but if forced, the synchronous solution can be stable or unstable. The largest adiabatic LE, in this case $\lambda_{max}(t) = \lambda^N(t)$ corresponding to $\Lambda_N < 0$ in formula (6.11), is given by

$$\lambda_{max}(t) = \begin{cases} -D\Lambda_N - \sqrt{\gamma^2 - \Delta\omega(t)^2} & \text{for } t : \gamma > |\Delta\omega(t)|, \\ -D\Lambda_N > 0 & \text{else.} \end{cases} \quad (6.14)$$

Firstly, when the driving strength is not large enough, i.e., $\gamma < |\Delta\omega(t)|$, synchronous solutions are unstable – i.e., always for the SNS and during the non-synchronised epochs for the SIS. This is in contrast with the attractive case, which exhibited neutral stability under the same condition. Secondly, when $\gamma > |\Delta\omega(t)|$, two effects compete: the network couplings push oscillators away from each other (positive first term) whereas the external driving brings them back towards a synchronous state (negative second term). This is again in contrast with the attractive case, which only exhibits stability under the same condition. Those two effects exactly compensate each other if

$$\gamma = \sqrt{(D\Lambda_N)^2 + \Delta\omega^2(t)}, \quad (6.15)$$

which has a minimum when $\Delta\omega = 0$ at $\gamma = -D\Lambda_N$. This is shown for the autonomous case $k = 0$ in Fig. 6.4(a) (dashed white).
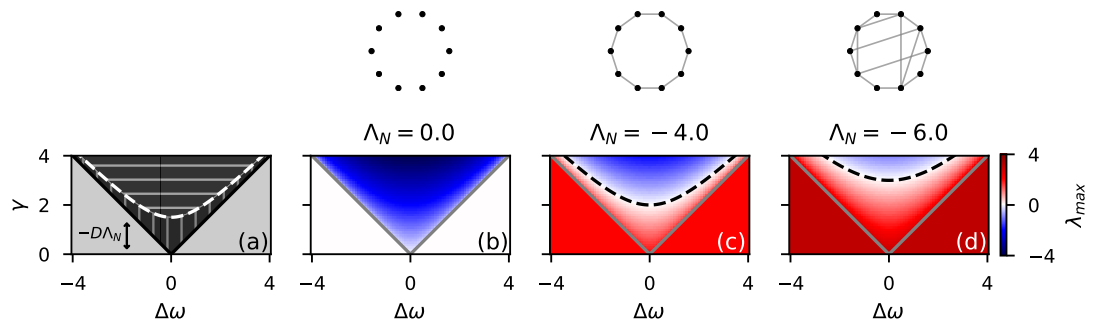
Figure 6.4.: Stability region decreases with Λ_N, i.e. with largest degree of connectivity, in the repulsive, $D > 0$, autonomous, $k = 0$, case. (a) Theoretical qualitative regions. Region I: no synchronisation (light grey). Region IIa: synchronisation unstable (dark grey vertically hatched). Region IIb: synchronisation stable (dark grey horizontally hatched). (b)-(d) Quantitative stability measured by the LE: the region of stability IIb (shades of blue) decreases with Λ_N, while the region of instability IIa (shades of red) increases. White values represent zero values of the LE. Above each panel, an example network that has the corresponding value of Λ_N is shown. Parameters are $D = 0.5$, $w_0 = 2$.

In the autonomous case, $k = 0$, the frequency mismatch is constant in time. Hence, condition (6.15) divides region II into two subregions based on stability: regions IIa (IIb) where the SS is unstable
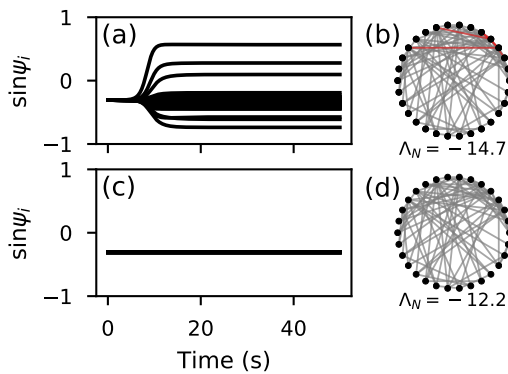
Figure 6.5.: Control of the stability by cutting a few chosen links, in the repulsive case $D > 0$. (a), (c) Trajectory of a synchronous synchronised initial condition of the phase difference ψ_i, in (b), (d) the corresponding network, respectively. In the initial network (b), the synchronous state is unstable (a). By cutting a few chosen links (red), in the new network (d), the synchronous state is made stable (c). The initial network is a Barabási-Albert with $N = 30$, and 5 links are cut. Other parameters are $D = 0.5$, $\gamma = 6.5$, $\Delta\omega = 2$, $\omega_0 = 1$, $k = 0$.

(stable) corresponding to γ values smaller (larger) than that of condition (6.15). The regions are shown in parameter space in Fig. 6.4(a), and are confirmed by the computation of the λ_{max}, as shown Fig. 6.4(b)-(d) for different values of Λ_N. As the largest-magnitude eigenvalue Λ_N of the Laplacian, or alternatively the network coupling strength D, is increased, the region of negative λ_{max} decreases in size.

This observation can be used as a viable control strategy. Indeed, note that the eigenvalues of the Laplacian, and in particular Λ_N, are determined by the topology of the network considered. Moreover, the inequality $|\Lambda_N| \leq 2K_{max}$ holds, where K_{max} is the number of connections of the most connected node [2]. In other words, the stability of the dynamics is directly determined by the topology, and in particular by the connectivity of the most connected node. Here, in the repulsive case, more connections between nodes, and in particular to the most connected one, means less stability. So then, one can optimally decrease the absolute value of Λ_N – or equivalently increase the region of stability – by cutting the edges of the most central node, which in turn amounts to reducing K_{max}. This is illustrated in Fig. 6.5 where the SS is stabilised by cutting only 5 chosen links (red) out of 81 ($\approx 6\%$). The original network is a Barabási-Albert one [see Fig. 6.5(b)] [1], for which this strategy is most effective, since only a few nodes have very high connectivity.

As a by-product of the analysis, in region IIa, we numerically observed partially-locked states [74], or chimera-like states [82, 114], where most of the oscillators are phase-locked to the driving in a quasi-synchronous cluster, while the rest of the oscillators drift independently. Such dynamics is illustrated in Fig. 6.6.

In general, in the nonautonomous case, $k \neq 0$, an additional type of intermittent synchronisation can be exhibited, which here alternates between stability and instability. That is, the adiabatic

---

[1]The network topology was created with the Python function `barabasi_albert_graph(N, m)` from the `NetworkX` package [51], with $N = 30$ the total number of nodes, and $m = 3$ the number of nodes added.
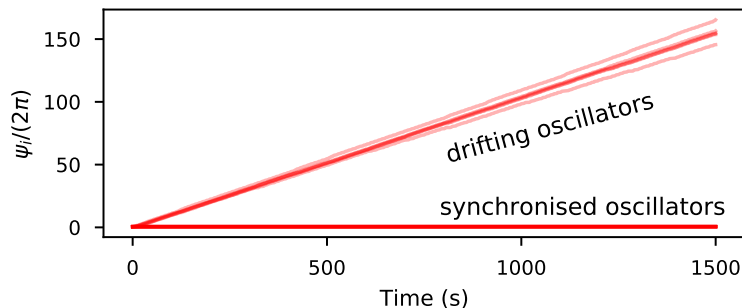
Figure 6.6.: Chimera-like behaviour: mix between synchronised and drifting oscillators. The network used is random with connexion probability $p = 0.5$. Other parameters are $D = 0.5$, $\gamma = 4.6$, $\Delta\omega = 2$, $\omega_0 = 2$, $k = 0$.

LE for the synchronous solutions alternates between negative and positive values. This happens in a new region IIc which, as k is made progressively larger than 0, appears at the border between regions IIa and IIb and subsequently grows, as illustrated in Fig. 6.7(a) in squared grey hatch. Region IIc can be defined as all pairs $(\gamma, \Delta\omega)$ such that γ is greater than the value of condition (6.15) at certain times and smaller at others. Equivalently, it is $\{(\gamma, \Delta\omega) : \exists t : \gamma = \sqrt{(D\Lambda_N)^2 + \Delta\omega^2(t)}\}$. The region is constant in time, and the explicit form of its boundaries is uninformative and is hence omitted here. In region IIc, the long-term LE can be either positive or negative. For small enough values of the coupling strength D, the region of negative LE increases with k, just as in the attractive case of Sec. 6.4.1. This effect can be achieved for relatively small values of the coupling strength D.
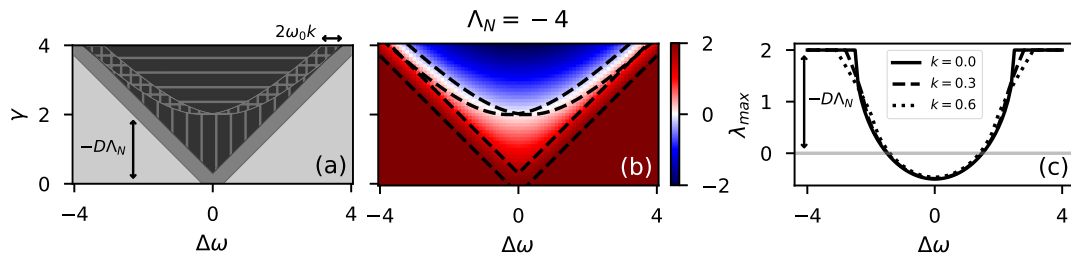
Figure 6.7.: Stability regions, in the repulsive, $D > 0$, nonautonomous, $k = 3$, case. (a) Theoretical qualitative regions. Birth of region IIc (square hatch), where the SS is alternates between stability and instability. Other regions are I (light grey) and III (medium grey) [see Fig. 6.3], and IIa (vertical hatch) and IIb (horizontal hatch) [see Fig. 6.4]. (b) Quantitative stability measured by the LE. White values represent zero values of the LE. (c) LE for a fixed $\gamma = 2.5$ and different values of k. Other parameters are $D = 0.5$, $w_0 = 1$.

However, while alternation between neutral stability and stability guaranteed overall stability and convergence in the previous section, alternation between stability and instability does not. Here, in region IIc, for a synchronous initial condition, a negative LE associated to its trajectory does not guarantee the state will stay synchronous and converge to the SS solution, as shown in Fig. 6.8(b). Indeed, during epochs of instability, any perturbation can push the state far
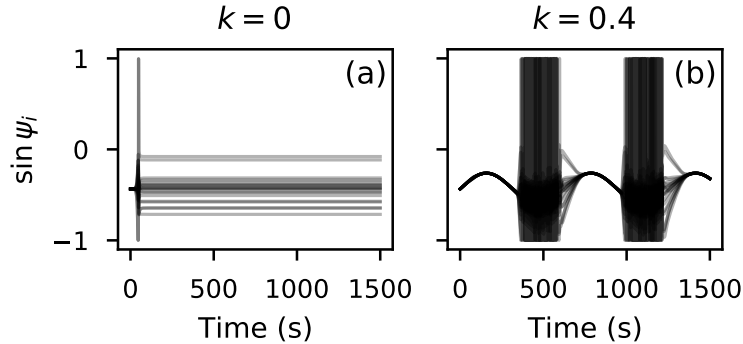
Figure 6.8.: Control strategy: fully synchronous state enforced intermittently by nonautonomous driving. Trajectory of a synchronous initial condition for $N = 20$ oscillators for (a) constant and (b) modulated driving frequency. (a) Synchronous solution is unstable and yields patterns. (b) Time-variability of the driving forces state to be synchronous intermittently. Other parameters are $D = 0.5$, $\gamma = 4.6$, $\Delta\omega = 2$, $\omega_0 = 2$. Network used is random with $p = 0.2$ and $\Lambda_N = -8.68$.

away from its original synchronous solution exponentially fast. However, if no other attractor exists during the epochs of stability, then the system will return to the synchronised synchronous state when the next epoch of stability occurs. Thus it alternates between the two regimes, as shown numerically in Fig. 6.8(b). This effect is purely due to the time-variability of the driving, controlled by k. Moreover, there is subregion in parameter space which is unstable (region IIa) when $k = 0$, but turns intermittently stable (region IIc) for $k > 0$. This can be used as a control strategy as illustrated in Fig. 6.8: one forces a completely incoherent state [panel (a)] to be synchronous and synchronised indefinitely often and long, by allowing time-variability in the driving frequency. Thus, time-variability can also be used to counter-balance the desynchronising effect which is produced by a highly connected network, as shown in Fig. 6.5. Finally, this strategy can be useful when the requirement for synchronicity are not so stringent and the system under inspection does not need to be synchronous at all times.

6.5. Summary

In this chapter, we studied the effect of driving an arbitrary network of identical phase oscillators with an external time-varying-frequency oscillator, extending the work of chapter 4. This is in contrast with previous studies of forced networks, which do not consider time-variability, a crucial ingredient in real-world systems. Stability – both short- and long-term – of the synchronous solutions was assessed by linear stability analysis, and results were confirmed via numerical simulations. The system studied is nonautonomous and hard to treat in general, hence we assumed slow time-variability. Two cases were treated: attractive and repulsive couplings, where oscillators tend to be in phase and out of phase, respectively.

In the attractive case, we showed that increasing the amplitude k of the frequency modulation enlarged the stability region in parameter space, as defined by a negative Lyapunov exponent. In other words, a more variable driving makes the stability of synchronous behaviour more robust against parameter changes. This is the direct generalisation to networks of the result that was obtained for a single driven oscillator in chapter 4. An additional region of intermittency between stability and neutral stability appears, as a result of the time-variability in the frequency.

In the repulsive case, we first demonstrated a control strategy, where the synchronous solution can be made stable by cutting a few chosen links in the network. Moreover, we established the phase diagram of the synchronous solutions. We then showed that one could counter-balance the desynchronising effect of connectivity by allowing time-variability in the driving frequency. Indeed, we showed that the time-variability of the frequency can drive the system back to a synchronous state intermittently, where it was asynchronous with a fixed-frequency driving. This observation can serve as an alternative control protocol. Finally, as a by-product of the analysis, we numerically observed chimera-like states.

Dynamics of the phase and frequency is illustrated in detail in the different cases. Such classification can potentially be of use to experimentalists who can only measure phase and frequency, and may have only limited or no knowledge of an external driving. Moreover, we illustrated diverse and simple control strategies to enhance synchronisability that could explain how living systems maintain stability in a changing environment, and could also be implemented directly.

Finally, many of the interesting and physically relevant features observed in this system were either happening over finite time, or explained by the finite-time analysis of dynamics. Consequently, a solely asymptotic analysis would have missed much of the dynamical intricacies at hand. From this, we conclude that nonautonomous networks of coupled oscillators, such as the present one, exhibit features reminiscent of those observed in living systems, and that a finite-time approach is crucial to their understanding.

In the next chapter, the nonautonomicity of the system comes from the evolving network topology, and we show how such plasticity can lead to desynchronisation and oscillation death.

Part II.

Time-varying network topology

7. Desynchronisation in network with fast-varying couplings

7.1. Introduction

As argued in chapter 1, natural and artificial systems are often composed of individual oscillatory units, coupled together so as to yield complex collective dynamics [46, 81, 109, 127, 146]. Weak coupling of nonlinear oscillators leads to synchronisation [127], a condition of utmost coordination which is eventually met when the parts of a system operate in unison. In the last decade, the emphasis being primarily placed on the pivotal role exerted by the – fixed – topology of the graph that shapes the underlying couplings [5, 15].

At the other extreme entirely, when the coupling strength is made to increase, oscillations may go extinct. Oscillation death is observed in particular when an initially synchronised state evolves towards an asymptotic inhomogeneous steady configuration [25, 60, 103, 169], in response to an externally injected perturbation [78]. The ability of disrupting synchronous oscillation may prove to be relevant for e.g. neuroscience applications. It could be in fact exploited as a dynamical regulator [13, 71, 79], to oppose pathological neuronal states that are found to consistently emerge in Alzheimer and Parkinson diseases

In this chapter, we investigate the role of time-variability on synchronisation from a different angle from previous chapters: that of an evolving network topology, as opposed to previous chapters which considered time-variability in the driving frequency. Moreover, here, the variation is chosen to be fast compared to the nonlinear dynamics on each node. In a recent Letter [119], the process of pattern formation for a multispecies model anchored on a time-varying network was analysed. It was in particular shown that a homogeneous stable fixed point can turn unstable, upon injection of a non-homogeneous perturbation, via a symmetry breaking instability which is reminiscent of the Turing mechanism [159], but solely instigated by the intrinsic network dynamics. Starting from these premises, the aim of this chapter is to extend the theory presented in [119] to the relevant setting where the unperturbed homogeneous solution typifies as a collection of synchronised

limit-cycles. In other words, we analyse how the synchrony of a large population of nonlinear, diffusively coupled oscillators may be disrupted by network plasticity. Surprisingly, oscillation death can be induced by a piecewise constant time-varying network, also when synchrony is guaranteed on each isolated network snapshot. Our analysis provides a solid theoretical backup to the work of [148], where the oscillation death phenomenon is numerically observed on fast time-varying networks.

7.2. Model

Consider two different species living on a network that evolves over time and denote by x_i and y_i their respective concentrations, as seen on node i. The structural properties of the (symmetric) network are stored in a time-varying $N \times N$ weighted adjacency matrix $A_{ij}(t)$. For the ease of calculation, we will hereafter assume N constant. As in the previous chapter, the Laplacian matrix is denoted by $\mathbf{L}$ and its elements read $L_{ij}(t) = A_{ij}(t) - K_i(t)\delta_{ij}$, where $K_i(t) = \sum_j A_{ij}(t)$ stands for the connectivity of node i, at time t. The coupled dynamics of x_i and y_i, for $i = 1, ..., N$, is assumed to be ruled by the following, rather general equations

$$
\begin{aligned}
\dot{x}_i &= f(x_i, y_i) + D_x \sum_{j=1}^{N} L_{ij}(t/\epsilon) x_j, \\
\dot{y}_i &= g(x_i, y_i) + D_y \sum_{j=1}^{N} L_{ij}(t/\epsilon) y_j,
\end{aligned}
\tag{7.1}
$$

where D_x and D_y are appropriate coupling parameters. Here, f and g are nonlinear reaction terms, chosen so that system (7.1) exhibits a homogeneous stable solution $(x_i, y_i) \equiv (\bar{x}(t), \bar{y}(t))$ $\forall i$ which is periodic of period T. To state it differently, when $D_x = D_y = 0$, the above system is equivalent to N identical replicas of a two dimensional deterministic model, which displays a stable limit-cycle. For $D_x \neq 0 \neq D_y$, there exists a homogeneous time-dependent solution, i.e. one in which all oscillators of the network rotate with the same phase. This homogeneous solution corresponds to the synchronised regime that of which we shall investigate the stability. The parameter ϵ controls the timescale of the Laplacian dynamics. We will specifically inspect the case of a network that is periodically rearranged in time and denote with T_s the period of the network modulation, as obtained for $\epsilon = 1$. By operating in this context, we will show that synchronisation can be eventually lost when forcing ϵ below a critical threshold. When successive swaps between two static network configurations are considered over one period T_s (as it is the case in the example addressed in the second part of the chapter), ϵ sets the frequency of the blinking. The extension to non-periodic settings is straightforward, as discussed in details in [119].

Synchronisation in fast blinking networks has been investigated in the special case of small-world networks [16]. They showed that the blinking network provides more reliable synchronisation than its static small-world counterpart. The focus of that study was to obtain rigorous bounds on the coupling strength to obtain synchronisation, whereas in this chapter we show that time-variability can induce instability, and our results hold for any kind of network, with an arbitrary time-variability of the topology.

7.3. Theoretical analysis

To proceed with the analysis we compactify the notation by introducing the $2N$-dimensional vector $\mathbf{x} = (x_1, \ldots, x_N, y_1, \ldots, y_N)^\top$. The dynamics of the system can be hence cast in the form

$$\dot{\mathbf{x}} = \mathcal{F}(\mathbf{x}) + \mathcal{L}(t/\epsilon)\mathbf{x}, \tag{7.2}$$

where $\mathcal{F}(\mathbf{x}) = (f(x_1, y_1), \ldots, f(x_N, y_N), g(x_1, y_1), \ldots, g(x_N, y_N))^\top$ and the $2N \times 2N$ block diagonal matrix $\mathcal{L}$ reads

$$\mathcal{L}(t) = \begin{pmatrix} D_x\,\mathbf{L}(t) & 0 \\ 0 & D_y\,\mathbf{L}(t) \end{pmatrix}. \tag{7.3}$$

As mentioned above, the nonlinear reaction terms, now stored in matrix $\mathcal{F}$, are chosen so as to have a stable limit-cycle in the uncoupled setting $D_x = D_y = 0$.

7.3.1. Floquet theory

The stability of the limit-cycle $(\bar{x}(t), \bar{y}(t))$ can be assessed by means of a straightforward application of the Floquet theory [132]. To this end, we focus on the two dimensional system obtained in the uncoupled limit and introduce a perturbation of the time-dependent equilibrium, namely $\delta\mathbf{x} = (x - \bar{x}, y - \bar{y})^\top$. Linearising the governing equation yields $\delta\dot{\mathbf{x}} = \mathcal{J}(t)\delta\mathbf{x}$, where $\mathcal{J}(t) = \partial_\mathbf{x}\mathcal{F}(\mathbf{x})$ is periodic of period T. Let us label with $\Phi(t)$ a fundamental matrix of the system. Then, for all t, there exists a non-singular, constant matrix $\mathbf{B}$ such that:

$$\Phi(t + T) = \Phi(t)\mathbf{B}. \tag{7.4}$$

Moreover, $\det\mathbf{B} = \exp\left[\int_0^T \operatorname{tr}\mathcal{J}(t)\,\mathrm{d}t\right]$. The matrix $\mathbf{B}$ depends in general on the choice of the fundamental matrix $\Phi(t)$. Its eigenvalues, ρ_i with $i = 1, 2$, however, do not. These are called the Floquet multipliers and yield the Floquet exponents, defined as $\mu_i = T^{-1}\ln\rho_i$. Solutions of the

examined linear system can then be written:

$$\mathbf{x}(t) = a_1 \mathbf{p_1}(t) e^{\mu_1 t} + a_2 \mathbf{p_2}(t) e^{\mu_2 t}, \tag{7.5}$$

where the $\mathbf{p_i}(t)$ functions are T-periodic, and a_i are constant coefficients set by the initial conditions. When the system is linearised about limit-cycles arising from first-order equations, one of the Floquet exponents is identically equal to zero, $\mu_1 = 0$. The latter is associated with perturbations along the longitudinal direction of the limit-cycle: these perturbations are neither amplified nor damped as the motion progresses. The other exponent, μ_2 takes instead negative real values, if the limit-cycle is stable, meaning that perturbations in the transverse direction are bound to decay in time.

7.3.2. Partial averaging theorem

We now turn to discussing the original system (7.2). The reaction parameters are set to yield a stable limit-cycle for $D_x = D_y = 0$. Furthermore, we assume the oscillators to be initially synchronised, with no relative dephasing. We then apply a small, non-homogeneous, hence node-dependent perturbation and set to explore the conditions which can yield a symmetry breaking instability of the synchronised regime, from which the oscillation death phenomenon might eventually emerge. We are in particular interested in investigating the role played by the nonautonomous network dynamics in inducing the aforementioned instability. Introduce a small inhomogeneous perturbation around the synchronous solution $\delta \mathbf{x} = (x_1 - \bar{x}, \ldots, x_N - \bar{x}, y_1 - \bar{y}, \ldots, y_N - \bar{y})^\top$, and linearise the governing equation (7.2) so as to yield

$$\delta \dot{\mathbf{x}} = [\mathcal{J}(t) + \mathcal{L}(t/\epsilon)]\delta \mathbf{x}. \tag{7.6}$$

This is a nonautonomous equation, and it is difficult to treat it analytically [72], owing in particular to the simultaneous presence of different periods. To overcome this limitation, and gain analytical insight into the problem under scrutiny, we introduce the averaged Laplacian $\langle \mathcal{L} \rangle = 1/T_s \int_0^{T_s} \mathcal{L} \, dt$ and define the following system

$$\dot{\mathbf{y}} = \mathcal{F}(\mathbf{y}) + \langle \mathcal{L} \rangle \mathbf{y}. \tag{7.7}$$

As we will rigorously show in the following, the stability of the synchronous solution of system (7.2) is eventually amenable to that of system (7.7). Stated differently, assume that an external non-homogeneous perturbation can trigger an instability in system (7.7). Then, ϵ^* exists such that the original system (7.2) is also unstable for $0 < \epsilon < \epsilon^*$. In other words, by setting ϵ sufficiently small, and thus forcing a high frequency modulation of the network Laplacian, one can yield a

loss of stability of the synchronous solution. Oscillation death can eventually emerge as a possible stationary stable attractor of the ensuing dynamics, promoted by the inherent ability of the network to adjust in time.

As a first step towards proving the results, we shall rescale time as $\tau = t/\epsilon$. Eq. (7.6) can be hence cast in the equivalent form

$$\delta\mathbf{x}' = \epsilon[\mathcal{J}(\epsilon\tau) + \mathcal{L}(\tau)]\delta\mathbf{x}, \tag{7.8}$$

where the prime denotes the derivative with respect to the new time variable τ. The *partially averaged* version of (7.8) [or alternatively the linear version of system (7.7), after time rescaling], reads $\delta\mathbf{y}' = \epsilon[\mathcal{J}(\epsilon\tau) + \langle\mathcal{L}\rangle]\delta\mathbf{y}$. In the following, we will show that $\delta\mathbf{y}(t) - \delta\mathbf{x}(t) \in \mathcal{O}(\epsilon)$ for up to a time $\tau \in \mathcal{O}(1/\epsilon)$, provided that $\delta\mathbf{y}(0) = \delta\mathbf{x}(0)$ and for $\epsilon < \epsilon^*$. This conclusion builds on a theorem that we shall prove hereafter in its full generality, and which extends the realm of applicability of the usual averaging theorem. Denote $\mathbf{x} \in \mathbb{R}^d$, and consider the following equation

$$\dot{\mathbf{x}} = \epsilon f_1(\mathbf{x}, \epsilon t) + \epsilon f_2(\mathbf{x}, t), \tag{7.9}$$

where $f_1(\mathbf{x}, t)$ is T-periodic in t, and $f_2(\mathbf{x}, t)$ is T_s-periodic in t. Notice that $f_1(\mathbf{x}, \epsilon t)$ is T/ϵ-periodic. It is assumed that f_1 and f_2 and their derivative are well behaved Lipschitz-continuous functions. Observe incidentally that Eq. (7.8) is recovered by replacing $t \mapsto \tau$, $\mathbf{x} \mapsto \delta\mathbf{x}$, $f_1(\mathbf{x}, \epsilon t) \mapsto \mathcal{J}(\epsilon\tau)\delta\mathbf{x}$, $f_2(\mathbf{x}, t) \mapsto \mathcal{L}(\tau)\delta\mathbf{x}$, and $d = 2N$.

The standard version of the averaging theorem [162] requires dealing with periodic functions, whose periods are independent of ϵ. This is obviously not the case for $f_1(\,\cdot\,, \epsilon t)$. To bypass this technical obstacle, we will adapt the proof in [162] to yield an alternative formulation of the theorem which allows for partial averaging to be performed. Define

$$u(\mathbf{x}, t) = \int_0^t \mathrm{d}s\, [f_2(\mathbf{x}, s) - \langle f_2 \rangle], \tag{7.10}$$

where $\langle f_2 \rangle = 1/T_s \int_0^{T_s} f_2(\mathbf{x}, t)\, \mathrm{d}t$ is the average of f_2 over its period. Introduce then the *near-identity* transformation

$$\mathbf{x}(t) = \mathbf{z}(t) + \epsilon u(\mathbf{z}(t), t), \tag{7.11}$$

which yields

$$\dot{\mathbf{x}} = \dot{\mathbf{z}} + \epsilon \frac{\partial u}{\partial \mathbf{z}}\dot{\mathbf{z}} + \epsilon\frac{\partial u}{\partial t}. \tag{7.12}$$

Moreover, $\partial u/\partial t\,(\mathbf{z}, t) = f_2(\mathbf{z}, t) - \langle f_2 \rangle$ by definition of u, see Eq. (7.10). Then making use of

Eq. (7.9), it is straightforward to get

$$\overbrace{\left[\mathbb{1} + \epsilon \frac{\partial u}{\partial \mathbf{z}}\right]}^{\equiv \Gamma} \dot{\mathbf{z}} = \epsilon \left[f_1(\mathbf{z} + \epsilon u, \epsilon t) + f_2(\mathbf{z} + \epsilon u, t) - f_2(\mathbf{z}, t) + \langle f_2 \rangle \right], \tag{7.13}$$

Invoking the Lipschitz-continuity of f_2 and the boundedness of u yields

$$||f_2(\mathbf{z} + \epsilon u, \epsilon t) - f_2(\mathbf{z}, \epsilon t)|| \leq L\epsilon ||u(\mathbf{z}, \epsilon t)||,$$
$$\leq L\epsilon M, \tag{7.14}$$

where L and M are positive constants. Hence

$$\Gamma \dot{\mathbf{z}} = \epsilon f_1(\mathbf{z} + \epsilon u, \epsilon t) + \epsilon \langle f_2 \rangle + \mathcal{O}(\epsilon^2),$$
$$\simeq \epsilon f_1(\mathbf{z}, \epsilon t) + \epsilon \langle f_2 \rangle. \tag{7.15}$$

We do not know in general if Γ is invertible, but the identity is and, by continuity, so is any matrix sufficiently close to it. Hence, there exists a critical value $\epsilon^* \ll 1$ such that Γ is invertible, if $0 < \epsilon < \epsilon^*$. We provide later on a self-consistent estimate for the critical threshold ϵ^*. Up to order $\mathcal{O}(\epsilon)$, we have

$$\Gamma^{-1} \simeq \left[\mathbb{1} - \epsilon \frac{\partial u}{\partial \mathbf{z}}\right]. \tag{7.16}$$

Hence finally,

$$\dot{\mathbf{z}} \simeq \epsilon \left[f_1(\mathbf{z}, \epsilon t) + \langle f_2 \rangle \right]. \tag{7.17}$$

In conclusion, system (7.9) behaves like its *partially averaged* version (7.17), for times which grow like $1/\epsilon$, when ϵ is made progressively smaller. Back to the examined model, system (7.8) stays thus close to its partially averaged version

$$\delta \mathbf{y}' = \epsilon [\mathcal{J}(\epsilon \tau) + \langle \mathcal{L} \rangle] \delta \mathbf{y}, \tag{7.18}$$

which, in terms of the original timescale t amounts to

$$\delta \dot{\mathbf{y}} = \mathcal{M}(t) \delta \mathbf{y}, \tag{7.19}$$

where $\mathcal{M}(t) = \mathcal{J}(t) + \langle \mathcal{L} \rangle$ is a T-periodic $2N \times 2N$ matrix. It is worth emphasising that systems (7.2) and (7.19) agree on times $\mathcal{O}(1)$, owing to the definition of the variable τ. Imagine conditions are set so that an externally imposed, non-homogeneous perturbation may disrupt the synchronous regime, as stemming from Eq. (7.19). Then, the same holds when the perturbation is made to act on system (7.2), the target of our analysis. The onset of instability of (7.2) can be hence rigorously assessed by direct inspection of its partially averaged counterpart (7.7), which yields the

linear problem (7.19). Patterns established at late times can be however different, the agreement between the two systems being solely established at short times.

7.3.3. Projection onto eigenbasis

System (7.19) can be conveniently studied by expanding the perturbation on the basis of the average Laplacian operator, $\langle \mathbf{L} \rangle = 1/T_s \int_0^{T_s} \mathbf{L} \, dt$ [1]. Introduce $\phi^{(\alpha)}$, such that $\sum_{j=1}^{N} \langle L \rangle_{ij} \phi_j^{(\alpha)} = \Lambda_\alpha \phi_i^{(\alpha)}$, where Λ_α stands for the eigenvalues of $\langle \mathbf{L} \rangle$ and $\alpha = 1, \ldots, N$. Note that the eigenvectors are time-independent, as the averaged network (hence, the Laplacian) is. Write then $\delta x_i(t) = \sum_{\alpha=1}^{N} c_\alpha^x(t) \phi_i^{(\alpha)}$ and $\delta y_i(t) = \sum_{\alpha=1}^{N} c_\alpha^y(t) \phi_i^{(\alpha)}$, where c_α^x and c_α^y encode the time-evolution of the linear system [11, 12, 103]. Plugging the above ansatz into equation (7.19) yields the following consistency condition:

$$\dot{\mathbf{c}}_\alpha = \mathbf{M}_\alpha(t) \mathbf{c}_\alpha, \tag{7.20}$$

where $\mathbf{c}_\alpha = (c_\alpha^x, c_\alpha^y)^\top$, and

$$\mathbf{M}_\alpha(t) = \mathbf{J}(t) + \Lambda_\alpha \begin{pmatrix} D_x & 0 \\ 0 & D_y \end{pmatrix}. \tag{7.21}$$

The fate of the perturbation is determined upon solving the above 2×2 linear system, for each Λ_α. To this end, remark that $\mathbf{M}_\alpha$ is periodic, with period T, $\forall \alpha$. Solving system (7.20) amounts therefore to computing the Floquet exponents $\mu_1^{(\alpha)}$ and $\mu_2^{(\alpha)}$, for $\alpha = 1, \ldots, N$. The dispersion relation is obtained by selecting the largest real part of $\mu_i^{(\alpha)}$, $i = 1, 2$, at fixed α [25]. For undirected networks ($A_{ij} = A_{ji}$), the Laplacian is symmetric and the Λ_α are real and non-positive [2]. For $\alpha = 1$ the largest Floquet multiplier is zero, since the model displays a stable limit-cycle in its uncoupled version ($\Lambda_1 = 0$). We then sort the indices (α) in decreasing order of the eigenvalues, so that the condition $0 = \Lambda_1 \geq \Lambda_2 \geq \ldots \geq \Lambda_N$ holds. If the dispersion relation is negative $\forall \Lambda_\alpha$ with $\alpha > 1$, the imposed perturbation fades away exponentially: the synchronous solution is therefore recovered, for both the average system (7.19), and its original analogue, in light of the above analysis, and for all ϵ. Conversely, if the dispersion relation takes positive values for some Λ_α value belonging the Laplacian eigenvalue spectrum for the given network, then the perturbation grows exponentially in time, for ϵ smaller than a critical threshold. The initial synchrony for the original system (7.2) is hence lost and patterns may emerge.

---

[1] The diagonalisability of the Laplacian matrix is a minimal requirement for the analytical treatment to hold true. This condition is trivially met when the network of couplings is assumed symmetric, as in the example worked out in the following.

[2] This condition needs to be relaxed when dealing with directed graphs. The general philosophy of the calculation remains however unchanged, at the price of some technical complication as discussed in [12].

7.4. Theoretical example and numerical results

To clarify the conclusion reached above, we shall hereafter consider an example, borrowed from [119].

7.4.1. Node dynamics

We introduce the Brusselator model, a universally accepted theoretical system for exploring the dynamics of autocatalytic reactions. This implies selecting $f(x, y) = 1 - (b+1)x + cx^2y$ and $g(x, y) = bx - cx^2y$, where b and c stand for free parameters. For $b > c + 1$, the Brusselator model displays a limit-cycle.

7.4.2. Network topology and dynamics

Following [119], we then consider two networks, made of an even number, N, of nodes arranged on a periodic ring, and label their associated adjacency matrices $\mathbf{A_1}$ and $\mathbf{A_2}$, respectively. Nodes are connected in pairs, via symmetric edges. When it comes to the network encoded in $\mathbf{A_1}$, the couples are formed by the nodes labelled with the indexes $2k - 1$ and $2k$ for $k = 1, 2, ..., N/2$ [see panel (a) in Fig. 7.1]. The network specified via the adjacency matrix $\mathbf{A_2}$ links nodes $2k$ and $2k + 1$, with the addition of nodes 1 and N [as depicted in panel (a) in Fig. 7.1]. Both networks return an identical Laplacian spectrum, namely two degenerate eigenvalues $\Lambda_1 = 0$ and $\Lambda_N = -2$, with multiplicity $N/2$. The parameters of the Brusselator are set so that the synchronised solution is stable on each network, taken independently. This is illustrated in panel (c) of Fig. 7.1, where the corresponding dispersion relation (largest real part of the Floquet multipliers vs. $-\Lambda_\alpha$) is plotted with black star symbols. Introduce now the time-varying network, specified by the adjacency matrix $\mathbf{A}(t)$, defined as:

$$\mathbf{A}(t) = \begin{cases} \mathbf{A_1} & \text{if} \quad \mathrm{mod}\,(t, T_s) \in [0, \eta[, \\ \\ \mathbf{A_2} & \text{if} \quad \mathrm{mod}\,(t, T_s) \in [\eta, 1[, \end{cases} \tag{7.22}$$

where η (resp. $1 - \eta$) is the fraction of T_s that the network spends in the configuration specified by the adjacency matrix $\mathbf{A_1}$ (resp. $\mathbf{A_2}$). The average network is hence characterised by the adjacency matrix $\langle \mathbf{A} \rangle = \eta \mathbf{A_1} + (1 - \eta)\mathbf{A_2}$, see panel (b) in Fig. 7.1.

7.4.3. Numerical results

We then set to consider the stability of the synchronised state in presence of a time-varying network, and resort to its static, averaged counterpart. The average network Laplacian has many more distinct eigenvalues, and these latter fall in a region where the largest real part of the Floquet exponents is positive, as can be appreciated in Fig. 7.1, panel (c), thus signalling the instability. The solid line stands for the dispersion relation that is eventually recovered when the couplings among oscillators extends on a continuum support and the algebraic Laplacian is replaced by the usual second order differential operator [25, 103]. Since the dynamics hosted on the average network is unstable, the synchrony of the homogeneous state can be broken on the time-varying setting, by properly modulating ϵ below a critical threshold. This amounts in turn to imposing a fast switching between the two network snapshots, as introduced above. In Fig. 7.1, panel (d), the asymptotic pattern as displayed on a time-varying network, for a sufficiently small ϵ is depicted. The nodes of the network are coloured with an appropriate code chosen so as to reflect the asymptotic value of the density displayed by the activator species x. A clear pattern is observed which testifies on the heterogeneous nature of the density distribution, following the symmetry breaking instability seeded by the inherent network dynamics. Interestingly, the equilibrium density, as displayed on each node of the collection, converges to a constant: synchronous oscillations, which define the initial homogeneous state, are self-consistently damped to yield a stationary stable, heterogeneous distribution of the concentrations. This is the oscillation death phenomenon to which we made reference above. For the sake of clarity, this effect has been here illustrated with reference to a specific case study, engineered so as to allow for an immediate understanding of the key mechanism. The result reported holds however in general and apply to other realms of investigation where time-varying network topology and nonlinear reaction terms are more complex.

To shed further light onto the dynamics of the system, we introduce the macroscopic indicator

$$S(\epsilon, t) = \frac{1}{N} \|\mathbf{x}(t) - \bar{\mathbf{x}}(t)\|^2, \tag{7.23}$$

where $\bar{\mathbf{x}}(t) = (\bar{x}, \ldots, \bar{x}, \bar{y}, \ldots, \bar{y})$. $S(\epsilon, t)$ enables us to quantify the, time-dependent, cumulative deviation between individual oscillators trajectories, and the homogeneous synchronised solution. $S(\epsilon, t)$ will rapidly converge to zero, if the synchronous state is stable. Conversely, it will take non zero, positive values, when the imposed perturbation destroys the initial synchrony. To favour an immediate reading of the output quantities, we set to measure $\langle S \rangle$, the average of $S(\epsilon, t)$, on one cycle T_s. In formulae, $\langle S \rangle = T_s^{-1} \int_t^{t+T_s} S(\epsilon, u) \, du$, where t is larger than the typical relaxation time (transient). In Fig. 7.2, main panel, $\langle S \rangle$ is plotted against ϵ, normalised to the value it takes in the limit $\epsilon \to 0$, for a choice of the parameter that corresponds to the
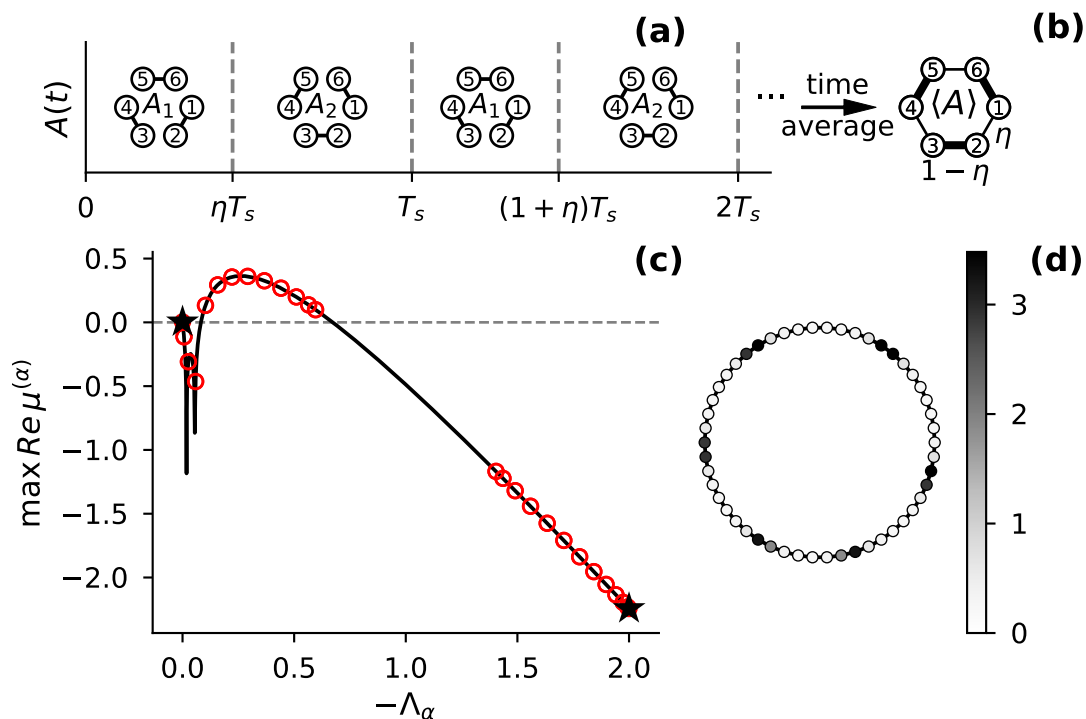
Figure 7.1.: Instability in time-varying networks. (a) Dynamics of $\mathbf{A}(t)$, as obtained by alternating two static networks with adjacency matrices $\mathbf{A_1}$ and $\mathbf{A_2}$ (see main text for a detail account of the imposed couplings), over a cycle of time duration T_s. Each network in this illustrative example is made of $N = 6$ nodes. (b) The associated time-averaged network $\langle \mathbf{A} \rangle = \eta \mathbf{A_1} + (1 - \eta) \mathbf{A_2}$. (c) Dispersion relation (max $(\mathrm{Re}\, \mu^\alpha)$ against $-\Lambda_\alpha$) obtained by assuming (i) the averaged network $\langle \mathbf{A} \rangle$ (red circles), (ii) each static network (black stars) and (iii) the continuous support case (black curve). The networks are generated according to the procedure discussed in Secs. 7.4.1 and 7.4.2, but assuming now $N = 50$. Other parameters are set to $b = 4.5$, $c = 2.5$, $D_x = 2$, $D_y = 20$, $T_s = 1$, and $\eta = 0.3$. (d) Asymptotic, stationary stable patterns, obtained for $\epsilon = 0.1 < \epsilon^*$. Shades of grey represent the value of the x variable.

dispersion relation depicted in Fig. 7.1. A clear, almost abrupt, transition is seen, for $\epsilon^* \simeq 0.25$, in qualitative agreement with the above discussed scenario. For $\epsilon < \epsilon^*$, the oscillation are turned into a stationary stable pattern, as displayed in the annexed panel. By monitoring $S(\epsilon, t)$ for a choice of ϵ below the critical threshold, one observes regular oscillations that can be traced back to the term $\bar{\mathbf{x}}$ in equation (7.23). At variance, synchronous oscillations prove robust to external perturbation when $\epsilon > \epsilon^*$: the order parameter $S(\epsilon, t)$ is identically equal to zero, the two contributions in the argument of the sum on the right hand side of equation (7.23) cancelling mutually.

To conclude the analysis, we will provide an approximate theoretical estimate of the critical threshold ϵ. The proof of the partial averaging theorem, as outlined above, assumes an invertible change of coordinates. It is therefore reasonable to quantify ϵ^* by determining the range ϵ for
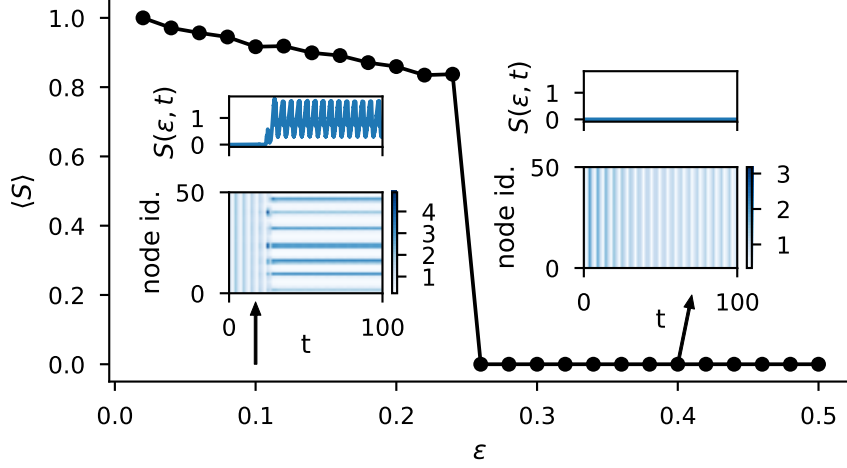
Figure 7.2.: Critical threshold ϵ^*. Average pattern amplitude, $\langle S \rangle$, as a function of ϵ, normalised to the amplitude of the pattern referred to the averaged network $\langle \mathbf{A} \rangle = \eta \mathbf{A_1} + (1 - \eta)\mathbf{A_2}$ (as formally recovered in the limit $\epsilon \to 0$). Here, $N = 50$ nodes. Other parameters are set to $b = 4.5$, $c = 2.5$, $D_x = 2$, $D_y = 20$, and $\eta = 0.3$. (Insets) Dynamics of x, on each node, over time. Shades of blue represent the value of x. (Left) for $\epsilon = 0.1$, the synchronous solution is unstable. After a transient time, oscillation death is seen, and a heterogeneous pattern develops. (Right) for $\epsilon = 0.4$, the synchronous solution is stable. $S(\epsilon, t)$ is also plotted vs. time for the two considered settings.

which the invertibility condition is matched [119]. In formulae:

$$\epsilon^* = \min\{\epsilon > 0 : \det \Gamma(\epsilon) = 0\}. \tag{7.24}$$

Using the block structure of $\partial u / \partial \mathbf{z} = \int_0^\tau [\mathcal{L}(t) - \langle \mathcal{L} \rangle] \, \mathrm{d}t$, one gets a more explicit form of the determinant

$$
\begin{aligned}
\det(\mathbb{1}_{2N} + \epsilon \partial u / \partial \mathbf{z}) = {} & \det \left(\mathbb{1}_N + \epsilon D_x \int_0^\tau [\mathbf{L}(t) - \langle \mathbf{L} \rangle] \, \mathrm{d}t \right) \\
& \times \det \left(\mathbb{1}_N + \epsilon D_y \int_0^\tau [\mathbf{L}(t) - \langle \mathbf{L} \rangle] \, \mathrm{d}t \right),
\end{aligned}
\tag{7.25}
$$

which is zero if either of the determinants is zero. A straightforward manipulation yields, for the inspected network model, the following closed expression:

$$\epsilon^* \simeq \frac{1}{\Lambda_N^{12} \eta (1 - \eta) T} \min \left[\frac{1}{D_x}, \frac{1}{D_y} \right], \tag{7.26}$$

where Λ_N^{12} stands for the maximum eigenvalue (in absolute magnitude) of the operator $(\mathbf{L_1} - \mathbf{L_2})$, with $\mathbf{L_1}$ and $\mathbf{L_2}$ being the Laplacian matrices associated to the static networks as specified by the adjacency matrices $\mathbf{A_1}$ and $\mathbf{A_2}$. Performing the calculation returns $\epsilon^* = 0.12$, a coarse approximation of the exact critical value, as determined via direct numerical integration [3].

---

[3]As an alternative for computing ϵ^*, assume T and ϵT_s are commensurable (if not, adjust the value of ϵ
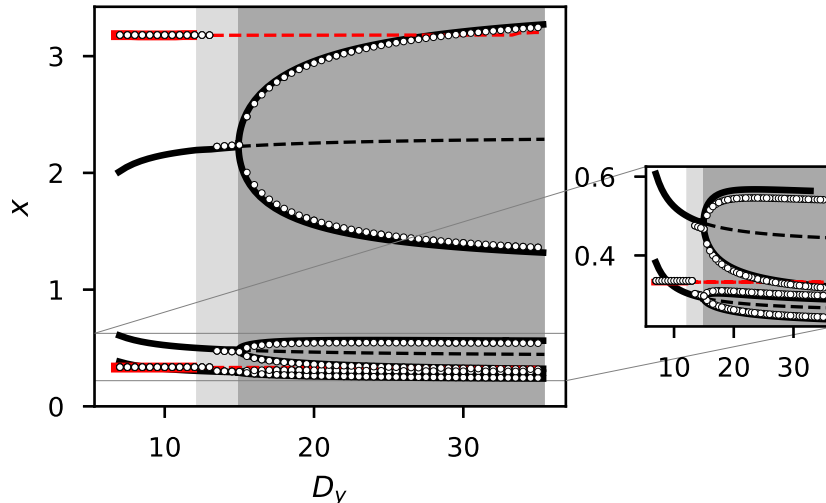
Figure 7.3.: Phase diagram for the Brusselator model coupled via time dependent pairwise exchanges, as illustrated in the caption of Fig. 7.1, with $N = 6$. The equilibrium solutions relative to species x are plotted by varying D_y, at fixed $D_x = 2$. The stability is computed for the average analogue (7.7) of model (7.1). The horizontal (red, straight) lines refer to the limit cycle: the maximum and minimum values as attained by the uncoupled oscillators, over one period, are respectively displayed. Black lines stand for the fixed points. Dashed lines refer to the unstable solutions, whereas solid lines implies stability. White circles are obtained from direct simulations of model (7.1) with $\epsilon = 0.1$ and illustrate the oscillation death phenomenon, as discussed in the main text. The panel on the right is a zoom of the lower portion of the main plot. The shaded regions are drawn to guide the reader's eye across the different regimes: synchronisation, oscillation death with 3-fixed point pattern, and oscillation death with 6-fixed point pattern correspond to the region in white, light grey, and dark grey, respectively. Notice that we chose to display a partial subset of the complete phase diagram. All stable manifolds are plotted. A limited subset of the existing unstable branches is instead shown for graphic requirements.

Finally, we shall inspect how the oscillation death phenomenon is influenced by the strength of the imposed coupling, here exemplified by the constant D_y, which we modulate when freezing D_x to a nominal value. In Fig. 7.3 different attractors, and their associated stability, are depicted, for species x, for distinct choices of the control parameter D_y. Here, the Brusselator model is assumed as the reference reaction scheme; the network of pairwise exchanges ($N = 6$), as illustrated in the caption of Fig. 7.1, is employed. The horizontal straight (red) lines refer to the limit cycle solution, and identify respectively the maximum and minimum value, as attained by the uncoupled oscillators, over one period. The solid trait marks the stable branch, while the dashed line is associated to the unstable solution. The bifurcation point is calculated analytically, from a linear stability analysis carried out for the average system (7.7). Beyond the transition

---

correspondingly) and define the common period for the reaction and diffusion parts,

$$T_c = \mathrm{LCM}(T, \epsilon T_s).$$

Compute the Floquet multipliers for the $2N \times 2N$ system which is periodic with period T_c. Repeating the above procedure for decreasing values of ϵ (and making sure T and ϵT_s are still commensurable) yields the critical ϵ, i.e. the largest ϵ for which not all μ_i's are negative.

point, when the homogeneous solution breaks apart, three stable solutions are shown to exist, corresponding to distinct values of the concentration x. These latter branches protrude inside the region where synchronous oscillations are predicted to be stable: the unstable manifolds which delineate the boundaries of the associated basins of attractions are not displayed for graphic requirements. Open (white) circles follow direct integration of model (7.1). In the simulations, ϵ is set to 0.1: the slight discrepancy between predicted and observed value of D_y (at the onset of the desynchronisation) stems from finite size corrections (the theory formally applies to the idealised setting $\epsilon \to 0$). When synchrony is lost, the system evolves towards an asymptotic state that displays oscillation death: each node is associated to a stationary stable density, which is correctly explained by resorting to the average model approximation (7.7). Increasing further the coupling strength D_y, results in a significant complexification of the phase space diagram, which considerably enrich the zoology of the emerging oscillation death patterns, as displayed in Fig. 7.3 above the supercritical pitchfork bifurcations.

7.5. Summary

In this chapter, we have considered the synchronous dynamics of a collection of nonlinear self-sustained oscillators, coupled via a generic graph. Time-variability was considered through a fast evolving network topology, in contrast with the previous chapters who considered a driving frequency with a slowly varying frequency. Here, we showed that the plasticity of the underlying network of couplings, i.e. its inherent ability to adjust in time, may seed an instability which destroys synchrony. This is in contrast with the general trend of previous chapters, where time-variability was mostly stabilising the dynamics. The system, endowed with a time-varying network of interlinked connections, behaves as its (partially) averaged analogue, provided the network dynamics is sufficiently fast. This result is formally established by proving an extended version of the celebrated averaging theorem, which allows for partial averages to be performed. Interestingly, the network driven instability materialises in asymptotic, stationary stable patterns. These latter are to be regarded as a novel evidence for the oscillation death phenomenon. In the next and last chapter, we summarise the work in this thesis, draw concluding remarks and outline possible future work.

8. Summary and conclusions

8.1. Summary

The work in this thesis aimed at combining two important ideas: synchronisation phenomena in coupled oscillator systems, and the fundamental openness of systems in nature, realised as nonautonomicity. Although synchronisation has been an active field of research in recent decades, the effect of nonautonomicity has only recently started gaining attention from the physics community. We believe that the combination of both these ingredients is key to the understanding of many real-life and man-made systems. Motivated by the modelling and understanding of living systems, theoretically and from data, this thesis investigated synchronisation and stability in nonautonomous oscillatory systems. More specifically, networks of coupled oscillators were studied, with time-varying parameters: either a time-variable driving frequency, or a time-variable network topology. Can time-variability be detrimental or beneficial to synchronisation? If so, how, why, and under which conditions? How can one deal mathematically with such nonautonomous systems, to extract meaningful physical insight? These are some of the questions that this thesis aimed to answer.

At the start, the theoretical background necessary to the understanding of the rest of the thesis was introduced. Autonomous and nonautonomous dynamical systems were introduced. Self-sustained oscillators, which serve as the dynamical base unit of all the thesis, were defined and discussed. The importance of time-variable but stable dynamics was then highlighted by the presentation of chronotaxic systems. Then, the concept of stability and its quantitative measures were discussed in details. Namely, Lyapunov exponents and Floquet exponents were introduced. Different types of Lyapunov exponents were presented, and served as the basis for a discussion of long-term and short-term stability. Numerical methods for the calculation of these exponents were presented and discussed in detail. Subsequently, synchronisation and related concepts were introduced, and illustrated for two unidirectionally coupled oscillators with fixed frequencies. Then, the relevant literature was reviewed for synchronisation in networks. Finally, the state of the art in the literature on the treatment of time-variability in coupled oscillators systems was presented, and the research questions of the thesis were then presented.

8. Summary and conclusions

As a complement to the theoretical background, a quasiperiodically driven oscillator was studied. To the best of our knowledge, this particular system has not been studied in the literature. The investigation, mostly using methods known in the literature, led to results similar to those for similar systems found in the literature. The double Arnold tongue structure was revealed via the computation of Lyapunov exponents, and subtongues of higher-order synchronisation were investigated via clustering. The system studied was an example of aperiodic yet with constant frequencies, and served to illustrate traditional approaches to modelling complex external driving in the literature, and to motivate the next chapters.

In the next three chapters – namely 4, 5, and 6 – the first main idea of the thesis was investigated: external driving with time-varying frequency, where the variability is assumed to be slow.

First, the simplest case of a system involving time-varying driving frequency was considered: a unidirectionally coupled pair of oscillators. This system generalised the canonical synchronising system consisting of a pair of unidirectionally coupled oscillators with fixed driving frequency. Moreover, it fills the gap between the latter and its corresponding noisy version. An analytical and numerical analysis of stability was provided across the parameter space – not only long-term stability but also short-term stability. This was done by means of Lyapunov exponents, as well as by the introduction of short-term LEs and by time-frequency analysis. The region of stability – where the maximum LE is negative – was shown to grow with the strength of the frequency modulation. This was explained to be caused by the birth of a new region in parameter space of intermittent synchronisation. A comparison with the noisy setting was also provided.

Second, the same system is considered and generalised to more general dynamics. A formal mathematical approach is adopted and confirms and generalises the results obtained previously. More importantly, the example is used to illustrate the mismatch that can exist between a traditional asymptotic-time analysis and a (long- but) finite-time one. The stabilisation observed previously is shown to be missed by a strictly asymptotic approach. It is also argued that in many real-life systems, and especially nonautonomous, a finite-time approach to dynamics is crucial, and sometimes even the more physically relevant one.

Third, results were generalised to a network of identical phase oscillators driven by a common time-varying-frequency driving. The stability of the synchronous solution is studied. An analytical derivation of the Lyapunov exponents – both instantaneous and long-term – is provided and confirmed by numerical results. Two cases are considered: attractive and repulsive coupling among the oscillators of the network. In the attractive case, results for the coupled pair of oscillators immediately generalise to the network: stabilisation via the enlargement of the negative LE region, and the existence of a regime of intermittent synchronisation, still hold. In the repulsive case, other phenomena can occur, as the synchronous solution is unstable when undriven. Based

on the understanding of the role of the topology and the time-variability of the driving frequency, two control strategies are suggested to stabilise the system.

Finally, the second main idea of the thesis is investigated: nonautonomicity via a time-evolving network topology. Here, contrary to the previous system, the variability is assumed to be fast. The stability of the synchronous solution is assessed. In order to do so, a extended version of the averaging theorem is proved. Then, Floquet theory is applied. It is shown that, with some tuning of the parameters, time-variability can seed an instability of the synchronous solution and yield oscillation death.

8.2. Original contributions

The original contributions of this work are listed below:

- It was shown that nonautonomous driving – as opposed to fixed-frequency driving – can stabilise the system by making the region of stability larger, for a pair of oscillators. See Figs. 4.2 for phase oscillators and Sec. 4.3 for nonlinear ones.

- The enlargement of stability due to the nonautonomous driving was compared to the case of synchronisation by noisy perturbation of the periodic driving, and shown former was shown to exhibit intermittent frequency entrainment contrary to the latter. See Sec. 4.2.5.

- A new regime of intermittent synchronisation was observed and characterised. The stabilisation phenomenon was explained by the birth and subsequent growth of the region of this intermittent regime. See Figs. 4.1 and 4.4.

- The stabilisation phenomenon was then generalised for arbitrary networks of identical phase oscillators with attractive couplings. Analytical results in terms of LEs and instantaneous LEs were provided and confirmed by numerics. The intermittent regime was also observed and described. See Sec. 6.4.1.

- The case of repulsive couplings was also investigated. The results were used to propose two control strategies to stabilise the dynamics, one in terms of changing the topology and the other in terms of varying the driving. See Sec. 6.4.2.

- For both the attractive and repulsive cases, a classification of the dynamical regimes in terms of phase dynamics, finite-time stability, and time-frequency representation was provided. This classification could prove useful to experimentalists that only have access to phase and and frequency measurements, and could thus help the inverse approach. See chapter 6.

- It was also shown that nonautonomicity in the form of time-varying network connections can induce instability and desynchronise the network. Results obtained analytically and confirmed by numerics. See chapter 7 and Fig. 7.1.

- As a result, oscillation death was shown to be induced by the time-variable network topology. This provides a new mechanism for the appearance of oscillation death, which to date has only been observed in static settings. A bifurcation diagram was computed, unveiling the structure of the heterogeneous steady state. See Fig. 7.3.

- An extended version of the acclaimed averaging theorem was proved, where a partial average can be performed over the fast-changing network topology. See Sec. 7.3.2.

Altogether, we have investigated the relationship between synchronisation and nonautonomicity for coupled oscillators. We have shown that nonautonomicity can be either beneficial or detrimental to synchronisation and stability. In order to do so, we used a finite-time approach to dynamics and stability, and in particular introduced the use of finite-time Lyapunov exponents and other finite-time methods.

8.3. Future perspectives

The study of nonautonomous oscillatory systems has only recently been attracting attention and many more questions remain open for future research. This is especially true when it comes to the modelling of living systems. Below, we list a few of these possible perspectives, some more specific and short-term, others more general and long-term.

In the first part of the thesis, a driving with a slowly varying frequency was considered. The assumption of slow variation is biologically reasonable and makes the system more mathematically tractable than the general case. For the sake of completeness, however, it would be interesting to investigate what happens in the other extreme case: fast modulation. This is the limit that was considered for the system in the last chapter. In such a scenario, we expect to be able to apply some averaging technique to investigate the dynamics.

Following a similar idea, one could consider the system in chapter 7, but this time with slowly varying topology, instead of fast. In many cases, slow variation of network links is a realistic assumption, such as in the brain. We expect such setting to exhibit intermittent behaviour, that the current use of the Floquet exponents would not capture. Such systems could need the introduction of some kind of finite-time Floquet or Lyapunov exponents. Interesting dynamics could arise in such a setting.

More generally, a question that naturally arises after all the work of this thesis: how can one treat nonautonomous systems for which the external modulation is neither slow nor fast, but at a similar timescale that of the considered system? Slow variation allows one to use an adiabatic approach, and fast variation makes it possible to use averaging techniques. The in-between, however, is not easily tractable mathematically, and yet probably exhibits rich dynamics.

In chapter 7, we observed oscillation death, induced by the time-variability in the network topology. To the best of our knowledge this is the first evidence of time-variability-induced oscillation death. So far, oscillation death was a byproduct of the study, and its structure was studied partially, but not the mechanisms behind it. Investigating such phenomenona in more detail is a potential direction for future work. One could moreover investigate whether oscillation death can ever occur due to other implementations of time-variability such as time-varying frequencies or shape of coupling function.

Indeed, apart from time-varying topology and frequencies, evidence shows that in some natural systems, the form of the coupling changes with time (without any change in the strength of the coupling) [144]. This topic is clearly related, and future research on such topics seems promising.

The motivations for the present work were the understanding of real-world systems, and in particular living systems. A next step in that direction would be to use the approach presented in this thesis to model and analyse systems based on real experimental data. A good candidate for this would be metabolic oscillations occurring in cells.

In order to do this, it might also be useful to investigate theoretically the effect of nonautonomicity in the context of networks of oscillators with distributed natural frequencies, in contrast to the identical frequencies considered here.

Finally, more generally, synchronisation in nonautonomous oscillatory systems to model living systems can clearly gain from exchanges with the out-of-equilibrium statistical physics and out-of-equilibrium thermodynamics communities. Some efforts have been made in that direction, and both fields could gain from more interaction.

Bibliography

1. ACEBRÓN J. A., BONILLA L. L., VICENTE C. J. P., RITORT F. & SPIGLER R. The Kuramoto model: A simple paradigm for synchronization phenomena. *Rev. Mod. Phys.* **77,** 137 (2005) (cited on pages 2, 26).

2. ALMENDRAL J. A. & DÍAZ-GUILERA A. Dynamical and spectral properties of complex networks. *New J. Phys.* **9,** 187 (2007) (cited on page 100).

3. ANAGNOSTOPOULOU V. & JAEGER T. Nonautonomous saddle-node bifurcations: Random and deterministic forcing. *J. Differ. Equations* **253,** 379–399 (2012) (cited on page 11).

4. ANDRZEJAK R. G., RUMMEL C., MORMANN F. & SCHINDLER K. All together now: Analogies between chimera state collapses and epileptic seizures. *Sci. Rep.* **6,** 23000 (2016) (cited on page 2).

5. ARENAS A., DÍAZ-GUILERA A., KURTHS J., MORENO Y. & ZHOU C. Synchronization in complex networks. *Phys. Rep.* **469,** 93–153 (2008) (cited on pages 2, 7, 27, 105).

6. ARNOLD V. I. *Geometrical Methods in the Theory of Ordinary Differential Equations* (Springer, New York, 1983) (cited on page 51).

7. ASHWIN P., BICK C. & BURYLKO O. Identical phase oscillator networks: bifurcations, symmetry and reversibility for generalized coupling. *Front. Appl. Math. Stat.* **2,** 7 (2016) (cited on page 29).

8. ASHWIN P., WIECZOREK S., VITOLO R. & COX P. Tipping points in open systems: bifurcation, noise-induced and rate-dependent examples in the climate system. *Phil. Trans. R. Soc. A* **370,** 1166–1184 (2012) (cited on page 11).

9. ASHWIN P., PERRYMAN C. & WIECZOREK S. Parameter shifts for nonautonomous systems in low dimension: bifurcation-and rate-induced tipping. *Nonlinearity* **30,** 2185 (2017) (cited on page 11).

10. ASHWIN P. & SWIFT J. W. The dynamics of n weakly coupled identical oscillators. *J. Nonlinear Sci.* **2,** 69–108 (1992) (cited on page 29).

11. ASLLANI M., BUSIELLO D. M., CARLETTI T., FANELLI D. & PLANCHON G. Turing patterns in multiplex networks. *Phys. Rev. E* **90,** 042814 (2014) (cited on page 111).

12. ASLLANI M., CHALLENGER J. D., PAVONE F. S., SACCONI L. & FANELLI D. The theory of pattern formation on directed networks. *Nat. Commun.* **5,** 4517 (2014) (cited on page 111).

13. ASLLANI M., EXPERT P. & CARLETTI T. A minimally invasive neurostimulation method for controlling abnormal synchronisation in the neuronal activity. *PLOS Comput. Biol.* **14,** 1–18 (2018) (cited on page 105).

14. ATSUMI Y. & NAKAO H. Persistent fluctuations in synchronization rate in globally coupled oscillators with periodic external forcing. *Phys. Rev. E* **85,** 056207 (2012) (cited on page 3).

15. BARAHONA M. & PECORA L. M. Synchronization in Small-World Systems. *Phys. Rev. Lett.* **89,** 054101 (2002) (cited on page 105).

16. BELYKH I. V., BELYKH V. N. & HASLER M. Blinking model and synchronization in small-world networks with a time-varying coupling. *Phys. D* **195,** 188–206 (2004) (cited on page 107).

17. BENETTIN G., GALGANI L., GIORGILLI A. & STRELCYN J.-M. Lyapunov Characteristic Exponents for smooth dynamical systems and for hamiltonian systems; A method for computing all of them. Part 2: Numerical application. *Meccanica* **15,** 21–30 (1980) (cited on pages 18, 39, 58).

18. BENETTIN G., GALGANI L., GIORGILLI A. & STRELCYN J.-M. Lyapunov Characteristic Exponents for smooth dynamical systems and for hamiltonian systems; a method for computing all of them. Part 1: Theory. *Meccanica* **15,** 9–20 (1980) (cited on pages 18, 39, 58).

19. BERGER A., SON D. T. & SIEGMUND S. Nonautonomous finite-time dynamics. *Discret. Contin. Dyn. Sys. B* **9,** 463 (2008) (cited on page 75).

20. BICK C., TIMME M., PAULIKAT D., RATHLEV D. & ASHWIN P. Chaos in symmetric phase oscillator networks. *Phys. Rev. Lett.* **107,** 244101 (2011) (cited on pages 3, 30).

21. BOTHA A. E. Characteristic distribution of finite-time Lyapunov exponents for chimera states. *Sci. Rep.* **6,** 29213 (2016) (cited on page 19).

22. BRAČIČ LOTRIČ M. & STEFANOVSKA A. Synchronization and modulation in the human cardiorespiratory system. *Phys. A* **283,** 451–461 (2000) (cited on pages 2, 4, 49, 71, 75).

23. BUCHSTABER V. M. & GLUTSYUK A. A. On monodromy eigenfunctions of Heun equations and boundaries of phase-lock areas in a model of overdamped Josephson effect. *Proc. Steklov Inst. Math.* **297,** 50–89 (2017) (cited on page 82).

24. BURYLKO O., KAZANOVICH Y. & BORISYUK R. Bifurcation study of phase oscillator systems with attractive and repulsive interaction. *Phys. Rev. E* **90,** 022911 (2014) (cited on page 29).

25. CHALLENGER J. D., BURIONI R. & FANELLI D. Turing-like instabilities from a limit cycle. *Phys. Rev. E* **92,** 022818 (2015) (cited on pages 105, 111, 113).

26. CHEKROUN M. D., SIMONNET E. & GHIL M. Stochastic climate dynamics: Random attractors and time-dependent invariant measures. *Phys. D* **240,** 1685–1700 (2011) (cited on page 3).

27. CHENG Y. Mean shift, mode seeking, and clustering. *IEEE Trans. Pattern Anal. Mach. Intell.* **17,** 790–799 (1995) (cited on page 42).

28. CLEMSON P. T., PETKOSKI S., STANKOVSKI T. & STEFANOVSKA A. In *Nonautonomous Dynamical Systems in the Life Sciences* 163–197 (Springer, 2013) (cited on page 9).

29. CLEMSON P. T. & STEFANOVSKA A. Discerning non-autonomous dynamics. *Phys. Rep.* **542,** 297–368 (2014) (cited on pages 4, 11, 14, 33, 90).

30. CLEMSON P. T., LANCASTER G. & STEFANOVSKA A. Reconstructing Time-Dependent Dynamics. *Proc. IEEE*, 1–17 (2015) (cited on page 14).

31. CRESSMAN J. R., ULLAH G., ZIBURKUS J., SCHIFF S. J. & BARRETO E. The influence of sodium and potassium dynamics on excitability, seizures, and the stability of persistent states: I. Single neuron dynamics. *J. Comput. Neurosci.* **26,** 159–170 (2009) (cited on page 75).

32. DATTANI J. & BARAHONA M. Stochastic models of gene transcription with upstream drives : exact solution and sample path characterization. *J. R. Soc. Interface* **14,** 20160833 (2017) (cited on page 2).

33. DE SAEDELEER B., CRUCIFIX M. & WIECZOREK S. Is the astronomical forcing a reliable and unique pacemaker for climate? A conceptual model study. *Clim. Dyn.* **40,** 273–294 (2013) (cited on pages 2, 3, 25, 32, 36, 41, 71, 75).

34. DING M., GREBOGI C. & OTT E. Dimensions Of Strange Nonchaotic Attractors. *Phys. Lett. A* **137,** 167–172 (1989) (cited on page 36).

35. DITTO W. L. *et al.* Experimental Observation of a Strange Nonchaotic Attractor. *Phys. Rev. Lett.* **65,** 533–536 (1990) (cited on pages 36, 41).

36. DRAGOMIR S. S. *Some Gronwall Type Inequalities and Applications* (Nova Science Publishers, 2003) (cited on page 81).

37. DRÓTOS G., BÓDAI T. & TÉL T. Probabilistic concepts in a changing climate: A snapshot attractor picture. *J. Climate* **28,** 3275–3288 (2015) (cited on page 3).

38. DUC L. H., CHÁVEZ J. P., SON D. T. & SIEGMUND S. Finite-time Lyapunov exponents and metabolic control coefficients for threshold detection of stimulus–response curves. *J. Biol. Dyn.* **10,** 379–394 (2016) (cited on page 19).

39. FEUDEL U., KUZNETSOV S. & PIKOVSKY A. *Strange Nonchaotic Attractors Dynamics between Order and Chaos in Quasiperiodically Forced Systems* 228 (World Scientific, Singapore, 2006) (cited on pages 19, 32, 34, 37, 41, 47).

40. FLOURAKIS M. *et al.* A conserved bicycle model for circadian clock control of membrane excitability. *Cell* **162,** 836–848 (2015) (cited on pages 2, 3, 75, 91).

41. GANDHI P., KNOBLOCH E. & BEAUME C. Dynamics of phase slips in systems with time-periodic modulation. *Phys. Rev. E* **92,** 062914 (2015) (cited on pages 25, 82).

42. GHIL M. The wind-driven ocean circulation: Applying dynamical systems theory to a climate problem. *Discrete Contin. Dyn. Syst. A* **37,** 189–228 (2017) (cited on pages 2, 3, 11, 32).

43. GHIL M., CHEKROUN M. D. & SIMONNET E. Climate dynamics and fluid mechanics: Natural variability and related uncertainties. *Phys. D* **237,** 2111–2126 (2008) (cited on page 11).

44. GIESL P. & MCMICHEN J. Determination of the area of exponential attraction in one-dimensional finite-time systems using meshless collocation. *Discret. Contin. Dyn. Sys. B* **23,** 1835–1850 (2018) (cited on page 75).

45. GLASS L. Synchronization and rhythmic processes in physiology. *Nature* **410,** 277–284 (2001) (cited on page 2).

46. GOLDBETER A. *Biochemical Oscillations and Cellular Rhythms* (Cambridge University Press, Cambridge, 1997) (cited on pages 2, 105).

47. GREBOGI C., OTT E., PELIKAN S. & YORKE J. A. Strange attractors that are not chaotic. *Phys. D* **13,** 261–268 (1984) (cited on page 36).

48. GUCKENHEIMER J. & ILYASHENKO Y. S. The duck and the devil: canards on the staircase. *Mosc. Math. J.* **1,** 27–47 (2001) (cited on pages 57, 81, 82).

49. GUSTAVSSON A.-K. *et al.* Sustained glycolytic oscillations in individual isolated yeast cells. *FEBS J.* **279,** 2837–2847 (2012) (cited on page 75).

50. HAFNER M., KOEPPL H. & GONZE D. Effect of Network Architecture on Synchronization and Entrainment Properties of the Circadian Oscillations in the Suprachiasmatic Nucleus. *PLoS Comput. Biol.* **8,** 1–16 (2012) (cited on page 2).

Bibliography

51. HAGBERG A. A., SCHULT D. A. & SWART P. J. *Exploring Network Structure, Dynamics, and Function using NetworkX* in *Proceedings of the 7th Python in Science Conference* (Pasadena, CA USA, 2008), 11–15 (cited on page 100).

52. HAKEN H. Cooperative phenomena in systems far from thermal equilibrium and in nonphysical systems. *Rev. Mod. Phys.* **47,** 67–121 (1975) (cited on page 1).

53. HALLER G. Finding finite-time invariant manifolds in two-dimensional velocity fields. *Chaos* **10,** 99–108 (2000) (cited on page 75).

54. HALLER G. Lagrangian Coherent Structures. *Annu. Rev. Fluid Mech.* **47,** 137–162 (2015) (cited on pages 19, 75).

55. HALLER G. & YUAN G. Lagrangian coherent structures and mixing in two-dimensional turbulence. *Phys. D* **147,** 352 –370 (2000) (cited on pages 3, 19, 75).

56. HEAGY J. & DITTO W. L. Dynamics of a Two-Frequency Parametrically Driven Duffing Oscillator. *J. Nonlinear Sci.* **1,** 423–455 (1991) (cited on pages 36, 37).

57. HOLME P. Modern temporal network theory: a colloquium. *Eur. Phys. J. Bs* **88,** 234 (2015) (cited on pages 4, 27, 30).

58. HOLME P. & SARAMÄKI J. Temporal networks. *Phys. Rep.* **519,** 97–125 (2012) (cited on pages 4, 27, 30).

59. HONG H. & STROGATZ S. H. Conformists and contrarians in a Kuramoto model with identical natural frequencies. *Phys. Rev. E* **84,** 46202 (2011) (cited on page 29).

60. HOU Z. & XIN H. Oscillator death on small-world networks. *Phys. Rev. E* **68,** 055103 (2003) (cited on page 105).

61. HRAMOV A. E., KORONOVSKII A. A., PONOMARENKO V. I. & PROKHOROV M. D. Detecting synchronization of self-sustained oscillators by external driving with varying frequency. *Phys. Rev. E* **73,** 026208 (2006) (cited on pages 49, 71).

62. IATSENKO D. *et al.* Evolution of Cardio-Respiratory Interactions with Age. *Phil. Trans. R. Soc. Lond. A* **371,** 20110622 (2013) (cited on page 2).

63. ILYASHENKO Y. S., RYZHOV D. A. & FILIMONOV D. A. Phase-lock effect for equations modeling resistively shunted Josephson junctions and for their perturbations. *Funct. Anal. Appl.* **45,** 192 (2011) (cited on pages 82, 84, 85, 88).

64. IVIĆ S., MRŠA HABER I. & LEGOVIĆ T. Lagrangian coherent structures in the Rijeka Bay current field. *Acta Adriatica* **58,** 373–389 (2017) (cited on pages 19, 75).

65. JENSEN R. V. Synchronization of driven nonlinear oscillators. *Am. J. Phys.* **70,** 607–619 (2002) (cited on pages 25, 54, 55, 57, 72, 80, 82, 94).

66. JIMÉNEZ-MARTÍN M., RODRÍGUEZ-LAGUNA J., D'HUYS O., de la RUBIA J. & KORUTCHEVA E. Synchronization of fluctuating delay-coupled chaotic networks. *Phys. Rev. E* **95,** 052210 (2017) (cited on page 27).

67. KAPITANIAK T. Distribution of Transient Lyapunov Exponents in of Quasiperiodically Forced Systems. *Prog. Theor. Phys.* **93,** 831–833 (1995) (cited on page 37).

68. KARRASCH D. Linearization of hyperbolic finite-time processes. *J. Differential Equations* **254,** 256–282 (2013) (cited on page 75).

69. KASZÁS B., FEUDEL U. & TÉL T. Leaking in history space: A way to analyze systems subjected to arbitrary driving. *Chaos* **28,** 033612 (2018) (cited on page 75).

70. KIM C., LEE E. K. & TALKNER P. Numerical method for solving stochastic differential equations with dichotomous noise. *Phys. Rev. E* **73,** 026101 (2006) (cited on page 64).

71. KIM M.-Y., ROY R., ARON J. L., CARR T. W. & SCHWARTZ I. B. Scaling Behavior of Laser Population Dynamics with Time-Delayed Coupling: Theory and Experiment. *Phys. Rev. Lett.* **94,** 088101 (2005) (cited on page 105).

72. KLOEDEN P. E. & RASMUSSEN M. *Nonautonomous Dynamical Systems* (American Mathematical Society, Providence, 2011) (cited on pages 3, 7, 10, 11, 34, 49, 75, 108).

73. KLOEDEN P. E. & PÖTZSCHE C. *Nonautonomous dynamical systems in the life sciences* 3–39 (Springer, 2013) (cited on pages 3, 11, 75).

74. KO T.-W. & ERMENTROUT G. B. Partially locked states in coupled oscillators due to inhomogeneous coupling. *Phys. Rev. E* **78,** 16203 (2008) (cited on pages 29, 100).

75. KORI H., KURAMOTO Y., JAIN S., KISS I. & HUDSON J. L. Clustering in globally coupled oscillators near a Hopf bifurcation: theory and experiments. *Phys. Rev. E* **89,** 62906 (2014) (cited on page 29).

76. KORI H. & MIKHAILOV A. S. Strong effects of network architecture in the entrainment of coupled oscillator systems. *Phys. Rev. E* **74,** 66115 (2006) (cited on page 30).

77. KORI H. & MIKHAILOV A. S. Entrainment of randomly coupled oscillator networks by a pacemaker. *Phys. Rev. Lett.* **93,** 254101 (2004) (cited on page 30).

78. KOSESKA A., VOLKOV E. & KURTHS J. Oscillation quenching mechanisms: Amplitude vs. oscillation death. *Phys. Rep.* **531,** 173–199 (2013) (cited on page 105).

79. KUMAR P., PRASAD A. & GHOSH R. Stable phase-locking of an external-cavity diode laser subjected to external optical injection. *J. Phys. B* **41,** 135402 (2008) (cited on page 105).

80. KURAMOTO Y. *Self-entrainment of a population of coupled non-linear oscillators Title* in *International symposium on mathematical problems in theoretical physics* (Kyoto, 1975), 420–422 (cited on page 2).

81. KURAMOTO Y. *Chemical oscillations, waves, and turbulence* (Springer-Verlag, Tokyo, 1984) (cited on pages 26, 105).

82. KURAMOTO Y. & BATTOGTOKH D. Coexistence of coherence and incoherence in nonlocally coupled phase oscillators. *Nonlinear Phenom. Complex Systems* **5,** 380–385 (2002) (cited on pages 29, 100).

83. KUREBAYASHI W., SHIRASAKA S. & NAKAO H. Phase reduction method for strongly perturbed limit cycle oscillators. *Phys. Rev. Lett.* **111,** 214101 (2013) (cited on pages 13, 80).

84. KUREBAYASHI W., SHIRASAKA S. & NAKAO H. A criterion for timescale decomposition of external inputs for generalized phase reduction of limit-cycle oscillators. *NOLTA* **6,** 171–180 (2015) (cited on pages 13, 80).

85. LANCASTER G., SUPRUNENKO Y. F., JENKINS K. & STEFANOVSKA A. Modelling chronotaxicity of cellular energy metabolism to facilitate the identification of altered metabolic states. *Sci. Rep.* **6,** 29584 (2016) (cited on pages 2–4, 14, 49, 71, 75).

86. Lancaster G., Clemson P. T., Suprunenko Y. F., Stankovski T. & Stefanovska A. Detecting chronotaxic systems from single-variable time series with separable amplitude and phase. *Entropy* **17,** 4413–4438 (2015) (cited on page 14).

87. Langa J. A., Robinson J. C. & Suárez A. Stability, instability, and bifurcation phenomena in non-autonomous differential equations. *Nonlinearity* **15,** 887 (2002) (cited on page 11).

88. Lehahn Y., d'Ovidio F., Lévy M. & Heifetz E. Stirring of the northeast Atlantic spring bloom: A Lagrangian analysis based on multisatellite data. *J. Geophys. Res. C* **112** (2007) (cited on pages 19, 75).

89. Lekien F., Shadden S. C. & Marsden J. E. Lagrangian coherent structures in *n*-dimensional systems. *J. Math. Phys.* **48,** 065404 (2007) (cited on page 75).

90. Leloup J.-C., Gonze D. & Goldbeter A. Limit Cycle Models for Circadian Rhythms based on Transcriptional Regulation in Drosophila and Neurospora. *J. Biol. Rhythms* **14,** 433–448 (1999) (cited on page 2).

91. Lucas M., Fanelli D., Carletti T. & Petit J. Desynchronization induced by time-varying network. *Europhys. Lett.* **121,** 50008 (2018).

92. Lucas M., Newman J. & Stefanovska A. Stabilization of dynamics of oscillatory systems by nonautonomous perturbation. *Phys. Rev. E* **97,** 042209 (2018).

93. Lucas M., Fanelli D. & Stefanovska A. Nonautonomous driving induces stability in network of identical oscillators. *Phys. Rev. E* **99,** 012309 (2019).

94. Lyapunov A. M. The general problem of the stability of motion. *Int. J. Control* **55,** 531–534 (1992) (cited on page 75).

95. Malicet D. Random walks on Homeo(S^1). *Commun. Math. Phys.* **356,** 1083–1116 (2017) (cited on page 64).

96. Mañé R. In *Dynamical systems and turbulence, Warwick 1980* 230–242 (Springer, 1981) (cited on page 17).

97. Mantegna R. N. & Spagnolo B. Noise enhanced stability in an unstable system. *Phys. Rev. Lett.* **76,** 563–566 (1996) (cited on pages 64, 71).

98. McGuinness M., Hong Y., Galletly D. & Larsen P. Arnold tongues in human cardiorespiratory systems. *Chaos* **14,** 1–6 (2004) (cited on pages 2, 4, 71).

99. Moon W. & Wettlaufer J. S. A Stochastic Dynamical Model of Arctic Sea Ice. *J. Climate* **30,** 5119–5140 (2017) (cited on page 75).

100. Moorcroft R. L. & Fielding S. M. Criteria for shear banding in time-dependent flows of complex fluids. *Phys. Rev. Lett.* **110,** 086001 (2013) (cited on pages 3, 19, 75).

101. Mormann F., Lehnertz K., David P. & Elger C. E. Mean phase coherence as a measure for phase synchronization and its application to the EEG of epilepsy patients. *Phys. D* **144,** 358–369 (2000) (cited on page 2).

102. Nadini M. *et al.* Epidemic spreading in modular time-varying networks. *Sci. Rep.* **8,** 2352 (2018) (cited on page 30).

103. Nakao H. & Mikhailov A. S. Turing patterns in network-organized activator–inhibitor systems. *Nat. Phys.* **6,** 544 (2010) (cited on pages 105, 111, 113).

104. Nakao H. Phase reduction approach to synchronisation of nonlinear oscillators. *Contemp. Phys.* **57,** 188–214 (2016) (cited on page 13).

105. NAKAO H., YASUI S., OTA M., ARAI K. & KAWAMURA Y. Phase reduction and synchronization of a network of coupled dynamical elements exhibiting collective oscillations. *Chaos* **28,** 045103 (2018) (cited on page 13).

106. NEWMAN J. Necessary and sufficient conditions for stable synchronization in random dynamical systems. *Ergod. Theory Dyn. Syst.*, 1–19 (2017) (cited on pages 64, 71).

107. NEWMAN J., LUCAS M. & STEFANOVSKA A. *Limitations of the asymptotic approach to dynamics* submitted, preprint at arXiv:1810.04071. (2018) (cited on page 81).

108. NEWMAN M. *Networks* 2nd (Oxford university press, Oxford, UK, 2018) (cited on pages 25, 27).

109. NICOLIS G. & PRIGOGINE I. *Self-organization in nonequilibrium systems* (Wiley, New York, 1977) (cited on pages 1, 105).

110. OROSZ G., MOEHLIS J. & ASHWIN P. Designing the dynamics of globally coupled oscillators. *Prog. Theor. Phys.* **122,** 611–630 (2009) (cited on page 29).

111. OSELEDETS V. I. A multiplicative ergodic theorem. Characteristic Ljapunov, exponents of dynamical systems. *Tr. Mosk. Mat. Obs.* **19,** 179–210 (1968) (cited on page 16).

112. OTT E. & ANTONSEN T. M. Low dimensional behavior of large systems of globally coupled oscillators. *Chaos* **18,** 37113 (2008) (cited on pages 26, 30).

113. OTT W. & YORKE J. A. When Lyapunov exponents fail to exist. *Phys. Rev. E* **78,** 056203 (2008) (cited on page 16).

114. PANAGGIO M. J. & ABRAMS D. M. Chimera states: coexistence of coherence and incoherence in networks of coupled oscillators. *Nonlinearity* **28,** R67 (2015) (cited on pages 29, 100).

115. PARK Y. & ERMENTROUT G. B. Weakly coupled oscillators in a slowly varying world. *J. Comput. Neurosci.* **40,** 269–281 (2016) (cited on pages 13, 80).

116. PECORA L. M. & CARROLL T. L. Master stability functions for synchronized coupled systems. *Phys. Rev. Lett.* **80,** 2109 (1998) (cited on page 28).

117. PERRA N. *et al.* Random walks and search in time-varying networks. *Phys. Rev. Lett.* **109,** 238701 (2012) (cited on page 30).

118. PERRYMAN C & WIECZOREK S. Adapting to a changing environment: non-obvious thresholds in multi-scale systems. *Proc. R. Soc. A* **470,** 1–15 (2014) (cited on pages 3, 75).

119. PETIT J., LAUWENS B., FANELLI D. & CARLETTI T. Theory of Turing Patterns on Time Varying Networks. *Phys. Rev. Lett.* **119,** 148301 (2017) (cited on pages 27, 30, 105, 106, 112, 115).

120. PETKOSKI S. & STEFANOVSKA A. Kuramoto model with time-varying parameters. *Phys. Rev. E* **86,** 046212 (2012) (cited on page 30).

121. PFEUTY B., MATO G., GOLOMB D. & HANSEL D. Electrical synapses and synchrony: the role of intrinsic currents. *J. Neurosci.* **23,** 6280–6294 (2003) (cited on page 3).

122. PIETRAS B. & DAFFERTSHOFER A. Ott-Antonsen attractiveness for parameter-dependent oscillatory systems. *Chaos* **26,** 103101 (2016) (cited on page 30).

123. PIKOVSKII A. S. Synchronization and stochastization of array of self-excited oscillators by external noise. *Radiophys. Quantum Electron.* **27,** 390–395 (1984) (cited on pages 53, 64, 71).

124. PIKOVSKY A. & FEUDEL U. Characterizing strange nonchaotic attractors. *Chaos* **5,** 253–260 (1995) (cited on pages 19, 37).

125. PIKOVSKY A. & POLITI A. *Lyapunov Exponents: A Tool to Explore Complex Dynamics* (Cambridge University Press, Cambridge, UK, 2016) (cited on pages 7, 15, 17, 18, 20, 21, 50).

126. PIKOVSKY A. & ROSENBLUM M. Dynamics of globally coupled oscillators: Progress and perspectives. *Chaos* **25,** 97616 (2015) (cited on page 28).

127. PIKOVSKY A., ROSENBLUM M. & KURTHS J. *Synchronization: A Universal Concept in Nonlinear Sciences* (Cambridge University Press, Cambridge, UK, 2003) (cited on pages 7, 12, 14, 25, 41, 51, 53, 62–65, 71, 92, 93, 96, 105).

128. POINCARÉ H. Mémoire sur les courbes définies par une équation différentielle. *J. Math. Pures Appl.* (1881) (cited on page 75).

129. PRASAD A., NANDI A. & RAMASWAMY R. Aperiodic Nonchaotic Attractors, Strange And Otherwise. *Int. J. of Bifurcat. and Chaos* **17,** 3397–3407 (2007) (cited on page 36).

130. PRASAD A. & NEGI S. S. Strange nonchaotic attractors. *Int. J. of Bifurcat. and Chaos* **11,** 291–309 (2001) (cited on page 36).

131. PRASAD A. & RAMASWAMY R. Characteristic distributions of finite-time Lyapunov exponents. *Phys. Rev. E* **60,** 2761–2766 (1999) (cited on pages 19, 37).

132. R. G. *Nonlinear ordinary differential equations* (Blackwell, Oxford, 1990) (cited on pages 20, 107).

133. RADICCHI F. & MEYER-ORTMANNS H. Entrainment of coupled oscillators on regular networks by pacemakers. *Phys. Rev. E* **73,** 036218 (2006) (cited on page 30).

134. RAMOS A. G. *et al.* Lagrangian coherent structure assisted path planning for transoceanic autonomous underwater vehicle missions. *Sci. Rep.* **8,** 4575 (2018) (cited on pages 3, 19, 75).

135. RASMUSSEN M. Finite-time attractivity and bifurcation for nonautonomous differential equations. *Differential Equations and Dynam. Systems* **18,** 57–78 (2010) (cited on page 75).

136. RODRIGUES F. A., PERON T. K. D. M., JI P. & KURTHS J. The Kuramoto model in complex networks. *Phys. Rep.* **610,** 1–98 (2016) (cited on pages 2, 7, 27).

137. ROMEIRAS F. J., GREBOGI C. & OTT E. Multifractal properties of snapshot attractors of random maps. *Phys. Rev. A* **41,** 784 (1990) (cited on page 11).

138. SCHRÖDINGER E. *What Is Life?* (Cambridge University Press, Cambridge, 1944) (cited on page 1).

139. SERKIN V. N., HASEGAWA A. & BELYAEVA T. L. Nonautonomous solitons in external potentials. *Phys. Rev. Lett.* **98,** 074102 (2007) (cited on page 75).

140. SHADDEN S. C., DABIRI J. O. & MARSDEN J. E. Lagrangian analysis of fluid transport in empirical vortex ring flows. *Phys. Fluids* **18,** 047105 (2006) (cited on pages 19, 75).

141. SHUAI J. W. & WONG K. W. Nonchaotic attractors with highly fluctuating finite-time Lyapunov exponents. *Phys. Rev. E* **57,** 5332–5336 (1998) (cited on pages 19, 37).

142. STANKOVSKI T., PEREIRA T., MCCLINTOCK P. V. E. & STEFANOVSKA A. Coupling functions: universal insights into dynamical interaction mechanisms. *Rev. Mod. Phys.* **89,** 045001 (2017) (cited on pages 4, 29, 90).

143. STANKOVSKI T. *et al.* Alterations in the coupling functions between cortical and cardio-respiratory oscillations due to anaesthesia with propofol and sevoflurane. *Phil. Trans. R. Soc. A* **374,** 20150186 (2016) (cited on page 2).

144. STANKOVSKI T. Time-varying coupling functions: dynamical inference and cause of synchronization transitions. *Phys. Rev. E* **95,** 022206 (2017) (cited on page 122).

145. STRATONOVICH R. L. *Topics In the Theory of Random Noise* (Gordon and Breach, New York, 1967) (cited on page 71).

146. STROGATZ S. H. *Sync: The emerging science of spontaneous order* (Penguin UK, 2004) (cited on pages 1, 7, 51, 105).

147. STROGATZ S. H. *Nonlinear Dynamics and Chaos: with Applications to Physics, Biology, Chemistry, and Engineering* 2nd (Westview Press, Boulder, 2014) (cited on pages 2, 7, 9).

148. SUGITANI Y., KONISHI K. & HARA N. *Amplitude Death in Oscillators Network with a Fast Time-Varying Network Topology* in *Nonlinear Dynamics of Electronic Systems: 22nd International Conference, NDES 2014, Albena, Bulgaria, July 4-6, 2014. Proceedings* **438** (2014), 219 (cited on page 106).

149. SUPRUNENKO Y. F., CLEMSON P. T. & STEFANOVSKA A. Chronotaxic systems: a new class of self-sustained nonautonomous oscillators. *Phys. Rev. Lett.* **111,** 024101 (2013) (cited on pages 2, 4, 9, 11, 14, 25, 49, 71, 72).

150. SUPRUNENKO Y. F., CLEMSON P. T. & STEFANOVSKA A. Chronotaxic systems with separable amplitude and phase dynamics. *Phys. Rev. E* **89,** 012922 (2014) (cited on pages 4, 14, 25, 49, 72).

151. SUPRUNENKO Y. F. & STEFANOVSKA A. Generalized Chronotaxic Systems: Time-dependent oscillatory dynamics stable under continuous perturbation. *Phys. Rev. E* **90,** 32921 (2014) (cited on pages 4, 14, 25, 49, 72, 73).

152. TAKENS F. In *Dynamical systems and turbulence, Warwick 1980* 366–381 (Springer, 1981) (cited on page 17).

153. TASS P. *et al.* Detection of *n:m* Phase Locking from Noisy Data: Application to Magnetoencephalography. *Phys. Rev. Lett.* **81,** 3291–3294 (1998) (cited on pages 2, 4, 71).

154. TEW KAI E. *et al.* Top marine predators track Lagrangian coherent structures. *PNAS* **106,** 8245–8250 (2009) (cited on pages 3, 19, 75).

155. TOENJES R. & BLASIUS B. Perturbation analysis of complete synchronization in networks of phase oscillators. *Phys. Rev. E* **80,** 026202 (2009) (cited on page 92).

156. TÖGER J. *et al.* Vortex Ring Formation in the Left Ventricle of the Heart: Analysis by 4D Flow MRI and Lagrangian Coherent Structures. *Ann. Biomed. Eng.* **40,** 2652–2662 (2012) (cited on pages 19, 75).

157. TÖNJES R., MASUDA N. & KORI H. Synchronization transition of identical phase oscillators in a directed small-world network. *Chaos* **20,** 33108 (2010) (cited on page 29).

158. TORAL R., MIRASSO C. R., HERNÁNDEZ-GARCIA E. & PIRO O. Analytical and numerical studies of noise-induced synchronization of chaotic systems. *Chaos* **11,** 665–673 (2001) (cited on pages 53, 64).

159. TURING A. M. The chemical basis of morphogenesis. *Philos. Trans. Royal Soc. B* **237,** 37–72 (1952) (cited on page 105).

160. USHIO M. *et al.* Fluctuating interaction network and time-varying stability of a natural fish community. *Nature* **554,** 360 (2018) (cited on pages 3, 75).

161. Varela F., Lachaux J.-P., Rodriguez E. & Martinerie J. The brainweb: Phase synchronization and large-scale integration. *Nat. Rev. Neurosci.* **2,** 229–239 (2001) (cited on pages 2, 4, 71).

162. Verhulst F. *Nonlinear differential equations and dynamical systems* (Springer Science & Business Media, 1990) (cited on page 109).

163. Wang N., Ramirez U., Flores F. & Datta-Barua S. Lagrangian coherent structures in the thermosphere: Predictive transport barriers. *Geophys. Res. Lett.* **44,** 4549–4557 (2017) (cited on pages 3, 19, 75).

164. Watanabe S. & Strogatz S. H. Integrability of a globally coupled oscillator array. *Phys. Rev. Lett.* **70,** 2391 (1993) (cited on pages 27, 28).

165. Watanabe S. & Strogatz S. H. Constants of motion for superconducting Josephson arrays. *Phys. D* **74,** 197–253 (1994) (cited on page 27).

166. Winfree A. *The Geometry of Biological Time* (Springer, New York, 1980) (cited on page 2).

167. Wolf A., Swift J. B., Swinney H. L. & Vastano J. A. Determining Lyapunov exponents from a time series. *Phys. D* **16,** 285–317 (1985) (cited on page 17).

168. Yuan D. *et al.* Periodic synchronization in a system of coupled phase oscillators with attractive and repulsive interactions. *Front. Phys.* **13,** 130504 (2018) (cited on page 29).

169. Zou W., Wang X.-G., Zhao Q. & Zhan M. Oscillation death in coupled oscillators. *Front. Phys. China* **4,** 97 (2009) (cited on page 105).